MODELLING OF FLOW AND HEAT TRANSPORT IN VERTICAL LOOP GROUND HEAT EXCHANGERS

By

Christopher G. Cvetkovski

A Thesis

Submitted to the Faculty of Graduate Studies

through the Department of Civil and Environmental Engineering

in Partial Fulfillment of the Requirements for

the Degree of Master of Applied Science

at the University of Windsor

Windsor, Ontario, Canada

2014

© 2014 Christopher G. Cvetkovski

UMI Number: 1562212

UMI
Dissertation Publishing

ProQuest®

Modelling of Flow and Heat Transport in Vertical Loop Ground Heat Exchangers

by

Christopher G. Cvetkovski

APPROVED BY:

_____

J. Yang

Department of Earth and Environmental Sciences

_____

R. Carriveau

Department of Civil and Environmental Engineering

_____

D.S-K. Ting, Co-Advisor

Department of Mechanical, Automotive and Materials Engineering

_____

T. Bolisetti, Advisor

Department of Civil and Environmental Engineering

April 14, 2014

DECLARATION OF CO-AUTHORSHIP / PREVIOUS PUBLICATION

I. Co-Authorship Declaration

I hereby declare that this thesis incorporates material that is result of joint research, as follows:

The collaboration is covered in Chapter 2 of the thesis. This chapter incorporates the outcome of a joint research with Ms. Seyyedeh Hoda Mozaffari and Dr. Stanley Reitsma under the supervision of Dr. Tirupati Bolisetti and Dr. David S-K. Ting. In all cases the key ideas, primary contributions, data analysis and interpretations were performed by the author and the contributions of the co-authors were primarily review and general education on Ground Source Heat Pumps and Computational Fluid Dynamics.

I am aware of the University of Windsor Senate Policy on Authorship and I certify that I have properly acknowledged the contribution of other researchers to my thesis, and have obtained written permission from each of the co-author(s) to include the above material(s) in my thesis.

I certify that, with the above qualification, this thesis, and the research to which it refers, is the product of my own work.

II. Declaration of Previous Publication

This thesis includes 3 original papers that have been previously published or submitted/to be submitted for publication in peer reviewed journals as indicated and 3 original papers that are planned to be submitted to the journals as indicated:

Thesis Chapter	Publication Title/Citation	Publication Status
Chapter 2	C. G. Cvetkovski, S. H. Mozaffari, S. Reitsma, T. Bolisetti, and D. S. K. Ting, "On Fluid Flow and Heat Transfer in a Pipe With a U-Bend," in *ASME 2013 Heat Transfer Summer Conference Proceedings: Heat Transfer in Energy Systems; Thermophysical Properties; Theory and Fundamental Research in Heat Transfer*, Minneapolis, MN, 2013, vol. 1, p. 10.	Published
Chapter 3	Heat Transfer in a U-Bend Pipe: Dean Number versus Reynolds Number, C. G. Cvetkovski, S. Reitsma, T. Bolisetti, and D. S. K. Ting	Under Review by Journal of Energy and Buildings

Chapter 4	On Secondary Flow Structures in Coaxial Pipe with an End Cap, C. G. Cvetkovski, S. Reitsma, T. Bolisetti, and D. S. K. Ting	To Be Submitted to The International Journal of Heat and Fluid Flow
Chapter 5	The Effects of Inner Pipe Offset on Coaxial Ground Source Heat Exchangers, C. G. Cvetkovski, S. Reitsma, T. Bolisetti, and D. S. K. Ting	To Be Submitted to The Journal of Geothermics
Chapter 6	Single U-Bend vs. Coaxial Ground Exchanger Loops, C. G. Cvetkovski, S. Reitsma, T. Bolisetti, and D. S. K. Ting	Submitted to The ASHRAE Trade Journal

I certify that I have obtained a written permission from the copyright owner(s) to include the above published material(s) in my thesis. I certify that the above material describes work completed during my registration as graduate student at the University of Windsor.

I declare that, to the best of my knowledge, my thesis does not infringe upon anyone's copyright nor violate any proprietary rights and that any ideas, techniques, quotations, or any other material from the work of other people included in my thesis, published or otherwise, are fully acknowledged in accordance with the standard referencing practices. Furthermore, to the extent that I have included copyrighted material that surpasses the bounds of fair dealing within the meaning of the Canada Copyright Act, I certify that I have obtained a written permission from the copyright owner(s) to include such material(s) in my thesis.

I declare that this is a true copy of my thesis, including any final revisions, as approved by my thesis committee and the Graduate Studies office, and that this thesis has not been submitted for a higher degree to any other University or Institution.

iv

ABSTRACT

The performance of ground source heat pumps relies greatly on the heat transfer efficiency throughout the ground loop configuration. Vertical ground loops can employ a U-Bend or a Coaxial pipe configuration which generates vortical structures and turbulence, enhancing the heat transfer process. For the U-Bend, the Dean Number (radius of curvature) and the Reynolds Number (inlet velocity) are tested. For the Coaxial, the inner pipe offset, and the Reynolds Number (inlet velocity) are tested for improved configurations. For the U-Bend, it was found the Reynolds Number dominates. In the Coaxial system, it was found that inner pipe offset destroys the heat flux of the system. Comparing the two systems, the Coaxial pipe shows both lower pressure loss and increased heat flux at equivalent inlet flow rates.

DEDICATION

I dedicate this thesis to my beautiful girlfriend, Jandark Jajo, my family, friends and colleagues for their support and aid. Thanks, heavenly Father.

ACKNOWLEDGEMENTS

TABLE OF CONTENTS

LIST OF FIGURES

CHAPTER 1: INTRODUCTION

CHAPTER 2: ON FLUID FLOW AND HEAT TRANSFER IN A PIPE WITH A U-BEND

CHAPTER 3: HEAT TRANSFER IN A U-BEND PIPE: DEAN NUMBER VERSUS REYNOLDS NUMBER

CHAPTER 4: ON SECONDARY FLOW STRUCTURES IN COAXIAL PIPE WITH AN END CAP

CHAPTER 5: THE EFFECTS OF INNER PIPE OFFSET ON COAXIAL GROUND SOURCE HEAT EXCHANGERS

CHAPTER 6: SINGLE U-BEND VERSUS COAXIAL GROUND EXCHANGER LOOPS

LIST OF TABLES

CHAPTER 2: ON FLUID FLOW AND HEAT TRANSFER IN A PIPE WITH A U-BEND

CHAPTER 3: HEAT TRANSFER IN A U-BEND PIPE: DEAN NUMBER VERSUS REYNOLDS NUMBER

CHAPTER 4: ON SECONDARY FLOW STRUCTURES IN COAXIAL PIPE WITH AN END CAP

CHAPTER 5: THE EFFECTS OF INNER PIPE OFFSET ON COAXIAL GROUND SOURCE HEAT EXCHANGERS

CHAPTER 6: SINGLE U-BEND VERSUS COAXIAL GROUND EXCHANGER LOOPS

NOMENCLATURE

C_{des} Detached Eddy Simulation Constant

C_p Specific heat capacity, J kg^{-1} K^{-1}

C_μ Eddy Viscosity Constant

d Distance to nearest wall, m

D Diameter, mm

Dn Dean Number

F_{ecc} Eccentricity Factor, Degree of offset (0 is no offset, 1 is inner pipe in contact with outer pipe)

G Görtler Number

G_b Generation of Turbulent Kinetic Energy due to Buoyancy, J kg^{-1}

G_{k1} Generation of Turbulent Kinetic Energy due to Mean Velocity, J kg^{-1}

g Gravitational Acceleration, m s^{-2}

k Thermal conductivity, W m^{-1} K^{-1}

k_1 Turbulent Kinetic Energy, J kg^{-1}

L Length of Pipe, m

l_{des} Length Scale for Detached Eddy Simulation, m

n   Number of Diameters

r   Radius of pipe, m

R_l Characteristic linear dimension perpendicular to the axis of rotation, m

Rc   Radius of curvature, mm

Re   Reynolds Number

S_{k1} Turbulent Kinetic Energy Source Term, J kg^{-1}

S_ε Dissipation Rate Source Term, J kg^{-1} s^{-1}

T   Temperature, K

Ta   Taylor Number

t_p Thickness of the Pipe Wall, m

Ue   External velocity, m s^{-1}

V   Velocity, m s^{-1}

y+   Dimensionless wall distance

Y_k Dissipation Rate of k

Y_M Partial Dissipation Rate due to Fluctuating Dilation of Compressible Turbulence

GREEK SYMBOLS:

Δ Change

ε Dissipation Rate, J kg^{-1} s^{-1}

μ Dynamic Viscosity, Pa s

μ_t Eddy Viscosity, Pa s

Ω Vorticity, s^{-1}

A   Thermal diffusivity, m^2 s

θ Momentum thickness, m

δ Curvature parameter (r/Rc)

ν Kinematic viscosity, m^2 s^{-1}

ξ Inner Pipe Offset, m

ρ Density, kg m^{-3}

φ Radial position around bend, degrees

SUBSCRIPTS:

cur Curved Section Property of Pipe

in   Inlet/Inner Pipe Property

out Outlet/Outer Pipe Property

st   Straight Section Property of Pipe

wall Complete Wall Property

x,y,z Directional modifiers

CHAPTER 1

INTRODUCTION

1.0 OVERVIEW

Geothermal energy is not new; however, serious widespread implementation of this green technology has been increasing in recent years, especially in Canada. The principle is quite simple. The earth has a very large but not necessarily infinite thermal energy reserve emanating from the core. This thermal energy can be extracted and used in various applications. These applications include electricity generation, space heating and cooling and hot springs. The application possible depends entirely on the value of the local ground temperature. Electricity generation can exist only in areas of high ground temperatures where steam can be generated to turn turbines. Ground source heat pumps can be installed in any temperature zone [1].

Ground source heat pumps (GHSPs) are a technology that is used to supply heat or absorb unwanted heat from a building. In the summer the GSHP is used to absorb heat from the building and deposit it into the earth and in the winter the GSHP is used to gather heat energy from the earth and supply it to the building. The principle is quite simple. The complete system itself consists of the building ductwork, the heat pump and the ground loop (ground heat exchanger). The ground heat exchanger acts a pre-heating or pre-cooling unit for the heat pump (water-air) to efficiently raise or lower the temperature to the desired value. The efficiency of this system depends greatly on the

1

efficiency of these three parts [2]. In this thesis the final component, the ground loop or ground heat exchanger will be the focus.

The ground loop is a series of pipes in which a working fluid, typically water or a heat transfer fluid such as a water-glycol mix is used. These pipe loops are typically categorized into vertical and horizontal systems. Vertical systems consist of the pipe loop's orientated vertically installed in boreholes dug 75 to 150 mm wide by 100 - 200 m deep. Horizontal systems consist of a pipe loop generally parallel with the ground surface installed in trenches only 1 to 2 m deep. In general the choice between the two systems is dependent on the available space. Horizontal systems are generally easier and less expensive to install, where vertical systems, needing deep boreholes to be installed are much more expensive, although more efficient, i.e. less total pipe length. Vertical systems because of their nature can be installed in many more places than a horizontal system because of the required surface land area [3].

Vertical systems are the focus of this work as it will impact many more people [4]. As stated earlier, the efficiency of the ground loop is paramount, thus increasing the efficiency of the ground loop can save thousands off the cost of installation. This can be done by changing the makeup of the vertical pipe configuration. The most-common pipe loop configuration for a vertical GSHP is a U-Bend. A U-Bend is the configuration that consists of two straight pipe legs connected by a U-Bend shape at the bottom. That is the flow will leave the surface through a downward pipe, be redirected by a U-Bend, 180° bend, into a return pipe back to the surface. A relatively new technology for pipe loop configurations is called a Coaxial system. This system consists of two pipes (one installed within another, concentric to each other) with an end cap that will redirect the flow from

2

the delivery pipe, inner pipe, to the return pipe, the outer annulus. The U-Bend and the Coaxial system are shown in Figure 1.1.
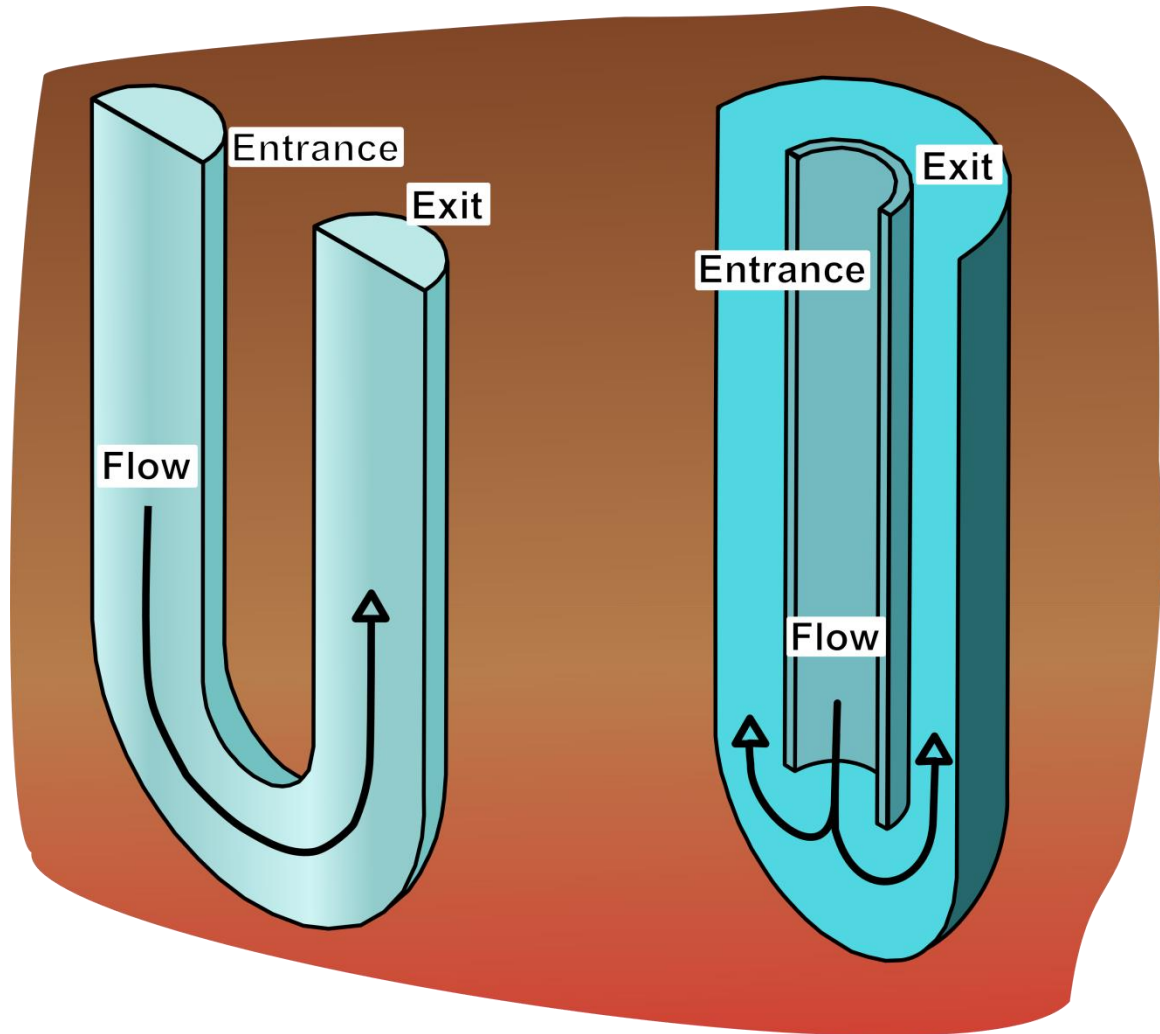
Figure 1.1: U-Bend (left) and Coaxial (right) Ground Loop (not-to-scale)

In both these systems there are improvements that can be made. For example, in the U-Bend, what is the ideal flow rate, the ideal radius of curvature of the U-Bend, the ideal turbulence level? In the Coaxial, what is the ideal flow rate, inner pipe offset and

3

associated turbulence level? In both of these cases, as optimizing heat transfer is the primary goal, turbulence will play a huge role as is associated relationship with heat transfer rates is strong [5]. Finally their comparative performance in equal scenarios with respect to heat transfer and other operational metrics is important to determine. In all, the work included in this thesis focuses on the behaviour of the fluid internal to the pipe and uses constant heat sources to simulate the ground. This assumption is used to focus the CFD model on the flow behaviour as it was determined to be very influential in the performance of the system.

2.0 ONTARIO CENTRES OF EXCELLENCE CONTRACT WITH GEOSOURCE ENERGY INC.

This work is tied to an industrial contract through the Ontario Centres of Excellence. The research partner is Geosource Energy Inc. whose goals in the contract were to develop further understanding of the U-Bend and the Coaxial systems. They requested research in the area of key design parameters and optimization of their design focus. That is, should they focus on flow rate, velocity, pipe loop configuration, etc. The key milestones of this contract that were completed because of this work are that of the U-Bend parametric study, parametric Coaxial study, and a comparative study of a sample U-Bend and a Coaxial system.

3.0 METHODOLOGY

To accomplish the above goals and objectives the following method was employed. First a numerical model was built and validated with the U-Bend system, after

4

which the parametric study was completed, Chapter 2 and 3. During the computational calculations similar models were employed for the Coaxial system. For which limited experimental works were completed to validate the CFD model. Following proper realization of the inherent physics, the parametric study was completed, Chapter 4 and 5. Lastly, the two systems themselves were simulated with equal grounds for comparison purposes, Chapter 6. There is some information repeated among the Chapters as they are formatted for Journal submission and items like the validation and computational models are duplicated.

REFERENCES

[1]   A. Capozza, "Design of borehole heat exchangers for ground-source heat pumps: A literature review, methodology comparison and analysis on the penalty temperature," *Energy & Buildings*, vol. 55, pp. 369–379, Dec. 2012.

[2]   G. Florides and S. Kalogirou, "Ground heat exchangers—A review of systems, models and applications," *Renewable Energy*, vol. 32, no. 15, pp. 2461–2478, Dec. 2007.

[3]   H. Benli, "A performance comparison between a horizontal source and a vertical source heat pump systems for a greenhouse heating in the mild climate Elaziğ, Turkey," *Applied Thermal Engineering*, vol. 50, no. 1, pp. 197–206, Jan. 2013.

[4]   H. Zeng, N. Diao, and Z. Fang, "Heat transfer analysis of boreholes in vertical ground heat exchangers," *International Journal of Heat and Mass Transfer*, vol. 46, no. 23, pp. 4467–4481, Nov. 2003.

[5]   W. Kays, M. Crawford, and B. Weigand, *Convective Heat and Mass Transfer*, 4th ed. McGraw-Hill, 2005.

CHAPTER 2[1]

ON FLUID FLOW AND HEAT TRANSFER IN A PIPE WITH A U-BEND[2]

Christopher George Cvetkovski[a], Seyyedeh Hoda Mozaffari[b], Stanley Reitsma[c], Tirupati Bolisetti[a], David S-K. Ting[b] [3]

[a] Department of Civil and Environmental Engineering, University of Windsor, Windsor, Ontario, Canada

[b] Department of Mechanical, Materials and Automotive Engineering, University of Windsor, Windsor, Ontario, Canada

[c] Geosource Energy Inc., 1508 Hwy 54, Caledonia, Ontario, Canada

---

[1] This chapter incorporates the outcome of a joint research with Ms. Seyyedeh Hoda Mozaffari and Dr. Stanley Reitsma under the supervision of Dr. Tirupati Bolisetti and Dr. David S-K. Ting. In all cases the key ideas, primary contributions, data analysis and interpretations were performed by the author and the contributions of the co-author were primarily review and education on software implementation.

[2] Copyright © ASME

[3] Corresponding author. 401 Sunset Avenue, Windsor, Ontario, Canada, N9B 3P4 Telephone: 519-253-3000 ext. 2599 Email: dting@uwindsor.ca

1.0 INTRODUCTION

Geothermal energy is a green energy that has been gaining momentum in recent years. This technology uses the ground as a heat source or heat sink, for supplying free heat or rejecting unwanted heat, depending on the season of the year. They are generally classified into two main types based on the orientation of the ground heat exchanger. These are the vertical ground source heat pump and the horizontal ground source heat pump. Vertical ground source heat pumps are more versatile compared to their horizontal counterparts [1]. Unlike horizontal or helical configurations the land area requirement for vertical systems is minimal and many can be installed in what is known as a field for applications that require a large thermal capacity. Vertical ground source heat pumps utilize a pipe inserted into a borehole of a relatively small radius, ~150 mm, for boreholes that can reach 200+ m depths. The most common pipe configuration consists of a downward pipe, the U-Bend and the return pipe. The efficiency of these systems revolves around the total amount of heat transferred versus the length of the pipe needed, and to some extent, the required pumping. The U-Bend creates vortices and serves to benefit the system when the proper setup is constructed.

In general, there are three types of vortices that exist in flows through curved domains. These three types of vortices, sometimes referred to as instabilities, are the Taylor-Couette (Eqn. 1), Görtler (Eqn. 2) and Dean (Eqn. 3) vortices [2]. The Taylor-Couette vortices can be generated by two Coaxial cylinders with at least one of them rotating. Vortices appear when the Taylor Number, the ratio of the centrifugal to the viscous forces, is above 1,700. It is a function of Ω, the characteristic angular velocity,

8

R_l, the characteristic perpendicular linear dimension to the rotation axis, and the kinematic viscosity, ν. The Görtler vortices occur only in the boundary layer at the outer concave wall of the curved domain at which longitudinal vortices develop above the critical Görtler Number, the ratio of the centrifugal to viscous forces. The Görtler Number is a function of the external velocity of the flow U_e, the momentum thickness θ, the kinematic viscosity ν, and the radius of curvature of the wall, R_c. The Dean Vortex phenomenon is similar to the Taylor-Couette in that it is perpendicular to the walls but the Dean instabilities are primarily driven by the pressure gradients of the flow field. Like the other instabilities, a critical Dean Number for the channel geometry exists, above which these vortices form and below which they do not [3]. The Dean Number is a function of the Reynolds Number, Re, and the curvature parameter, δ. The curvature parameter is the radius of the pipe divided by the radius of curvature of the bend. The critical Dean Number as it relates to the longitudinal streamwise velocity of the channel has two solution paths and thus, the CFD modeller must be careful when determining the critical Dean Number for the flow. Vortices as they relate to heat transfer have been studied in the past to improve heat transfer.

$$Ta = \frac{4\Omega^2 R_l^4}{v^2} \qquad (1)$$

$$G = \frac{U_e\theta}{v}\left(\frac{\theta}{R_c}\right)^{\frac{1}{2}} \qquad (2)$$

$$Dn = Re\delta^{\frac{1}{2}} \qquad (3)$$

For the geothermal application of ground source heat pumps improvements to the heat transfer process will only benefit the entire system, making it more efficient and

attractive for general use. The parameters easily controlled in this application would be the curvature of the U-Bend and the velocity of the water flowing through the pipe. This leads to changes primarily in the Reynolds (Eqn. 4, where D is the diameter in mm) and Dean Numbers [4].

$$Re = \frac{\rho V \left(\frac{D}{1000}\right)}{\mu} \qquad (4)$$

The Reynolds Number is controlled by the channels cross sectional geometry and the flow velocity. The Reynolds Number is used to classify the flow between either laminar or turbulent. When the Reynolds Number is lower than approximately 2,000, the flow is classified as being laminar and when it is higher than 5,000 the flow is fully turbulent. Between 2,000 and 5,000 the flow is generally referred to as the transitional phase where the entire flow domain cannot be classified one way or the other but for specific zones in the fluid either laminar or turbulent behavior may exist but not both. The velocity of the flow, and by extension the Reynolds Number, will affect the resident time of the fluid in the system. This is an important phenomenon in the geothermal industry as the time the working fluid stays exposed to the heat source or heat sink increases the more efficient the heat transfer will be given the length constraint.

This paper will detail a numerical approach to investigate the effects of Reynolds and Dean Numbers on the fluid flow and heat transfer in a pipe with a U-Bend. The simulated results will be verified based on limited existing experimental data in the literature. The numerical analysis will be performed using FLUENT. FLUENT is a

versatile and reliable software which allows the user to change multiple parameters very easily, and when properly applied, can generate accurate results of complex flows such as the one under consideration here [5].

2.0 NUMERICAL FORMULATION

The numerical model was set up using the commercially available software package provided by ANSYS Inc. The default modeller and meshing program was used and FLUENT was the solver. Transient analysis was performed with a two hour simulation period of 120 steps of 60 seconds each and Detached Eddy Simulation was the turbulence model selected based on literature review [6]–[8]. Second order implicit formulation was employed for the transient analysis.

The realizable k-ε model takes the following form as found commonly in the literature [7]. Equations 5 and 6 show the main equations for the transportable variables, the turbulent kinetic energy, k_1, and the dissipation rate, ε, respectively.

$$
\frac{\partial}{\partial t}(\rho k_1) + \frac{\partial}{\partial x_j}(\rho k_1 u_j)
$$
$$
= \frac{\partial}{\partial x_j}\left[\left(\mu + \frac{\mu_t}{\sigma_{k_1}}\right)\left(\frac{\partial k_1}{\partial x_j}\right)\right] + G_{k_1} + G_b - \rho\epsilon - Y_M + S_{k_1} \tag{5}
$$

$$
\frac{\partial}{\partial t}(\rho\epsilon) + \frac{\partial}{\partial x_j}(\rho\epsilon u_j)
$$
$$
= \frac{\partial}{\partial x_j}\left[\left(\mu + \frac{\mu_t}{\sigma_\epsilon}\right)\left(\frac{\partial\epsilon}{\partial x_j}\right)\right] + \rho C_1 S\epsilon - \rho C_2\left(\frac{\epsilon^2}{k_1 + \sqrt{(\nu\epsilon)}}\right) \tag{6}
$$
$$
+ C_{1\epsilon}\frac{\epsilon}{k_1}C_{3\epsilon}G_b + S_\epsilon
$$

where,

$$
\mu_t = \frac{\rho C_\mu k^2}{\epsilon} \tag{7}
$$

11

$$C_\mu = \frac{1}{A_0 + \dfrac{A_8 k U^*}{\epsilon}} \tag{8}$$

Here G_{k1} is the generation of the turbulence kinetic energy due to the mean velocity gradients, G_b is the generation of the turbulence kinetic energy due to buoyancy, Y_M is the contribution of the fluctuating dilation in compressible turbulence to the overall dissipation rate and S_{k1} and S_ϵ are the source terms.

There are two main differences between the realizable k-ε and the standard k-ε model. First the eddy viscosity, μ_t, calculated in Equation 7, is not based on a constant C_μ; which in the standard k-ε model is typically assumed to be equal to 0.09. Instead, C_μ is calculated via Equation 8; i.e., it is a function of the mean strain and rotation rates, turbulence fields and the angular velocity of the system rotation.

Detached Eddy Simulation further provides modifications to the traditional realizable k-ε model [5]. First, the dissipation term, Y_k, shown in Equation 9, is modified to account for a new wall distance, l_{des}, shown in Equation 12. This is to preserve the RANS computation mode throughout the boundary layer [9].

$$Y_k = \frac{\rho k^{\frac{3}{2}}}{l_{des}} \tag{9}$$

$$l_{rke} = \frac{k^{\frac{3}{2}}}{\epsilon} \tag{10}$$

$$l_{les} = C_{des}\Delta \tag{11}$$

12

$$l_{des} = l_{rke} - f_d \max(0, l_{rke} - C_{des}\Delta) \qquad (12)$$

where $C_{des} = 0.61$.

The numerical model consisted of the geometry as shown in Figure 2.1. There is a straight section of an 1828 mm upstream pipe, an 180° U-Tube bend of varying curvature, and a 508 mm downstream return pipe. The diameter of the numerical model was chosen to be 44.45 mm as typical U-Tubes in the geothermal industry are of this dimension. To save computational resources only half of the pipe was modeled and the symmetry boundary condition was taken advantage of. The inlet boundary was set as a uniform velocity inlet with a constant temperature of 285 K. The velocity will be kept at 0.5 m/s during the mesh independence study. The outlet was set as an outflow with a flow rating of one, i.e., all the fluid is exiting across this boundary. The pipe wall was set to be a stationary non slip entity with a constant temperature of 300 K. The thermal properties of the materials used in the model are given in Table 2.1.
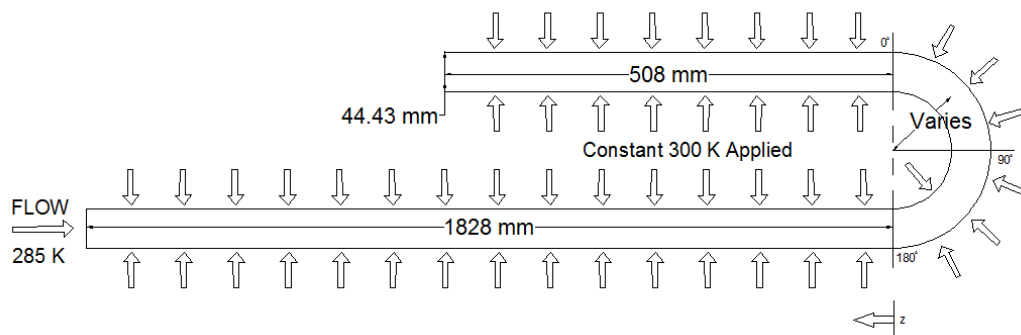
Figure 2.1: Geometrical Configuration of Numerical Model

13

Table 2.1: Material Thermal Properties

Material	ρ (kg m^{-3})	C_p (J kg^{-1} K^{-1})	k (W m^{-1} K^{-1})	μ (Pa s)
Water	998.2	4182	0.6	1.003e-3
Acrylic	1180	1470	0.19	N/A

From the literature review of these types of problems the following solution methods and discretization processes were chosen. The SIMPLE, Semi-Implicit Method for Pressure-Linked Equations, algorithm was selected for the pressure-velocity coupling [10], [11]. The Bounded Central Differencing was selected for the momentum discretization as it is the default for Detached Eddy Simulation in FLUENT. PRESTO!, Pressure Staggering Option, was selected as the pressure interpolation scheme because of its well documented accuracy for flow in curved domains [12]. The gradient is based on the least squares cell, the turbulent viscosity uses the first order upwind equations, and the energy are modeled via second order upwind equations. All flow parameters are relaxed with a factor of 0.75 [11], [13].

A desktop and the SHARCNET, Shared Hierarchical Academic Research Computing Network, Supercomputer system for Canadian researchers were utilized to perform the calculations. The desktop primarily performed the smaller simulations where the larger simulations requiring more resources were reserved for SHARCNET. The desktop was an HP with an Intel Core i7-2600 with 8GB of RAM and an Intel HD Integrated Graphics card. The SHARCNET visualization system used was an HP Linux node Intel Xeon processor with 50 GB of RAM. The GPU is a dual ATI FirePro V9800 configuration.

14

This visualization was used for meshing purposes with the FLUENT solver operations reserved for the computational nodes of varying processing cores and memory sizes.

3.0 NUMERICAL VERIFICATION

The meshing was done on a half-pipe model to take advantage of the symmetry characteristics of the flow and free up computational resources for a finer cell density. Eight meshes of varying densities were computed and the y^+ at the 180° radial position of the U-Bend is plotted in Figure 2.2. The y^+ value is the dimensionless wall distance. It defines the law of the wall and is used when classifying the wall sublayers and the mesh densities for use in computational fluid dynamics. FLUENT uses a hybrid wall function approach when the y^+ is much larger than 30 [5].
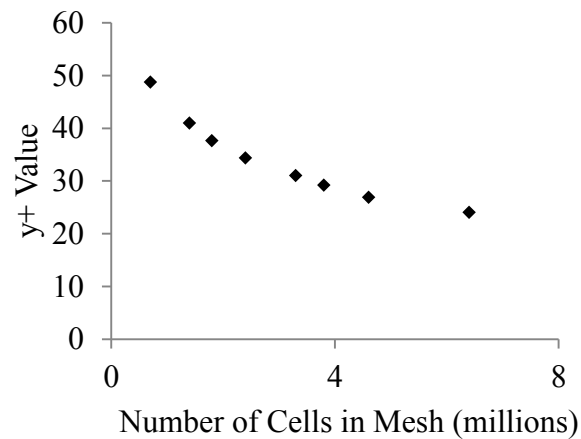
Figure 2.2: y+ Values at Outer Wall of Varying Mesh Densities

15

For meshes with a y^+ that is significant less than 30 this model is invalid because the mesh becomes too fine for the hybrid wall function to be invoked and yet too coarse for the near wall effects to be realized. The model can be used if the y^+ value is less than one, but the memory resources needed to generate such a fine mesh throughout the large simulation domain was not available. Thus, the mesh that produced a y^+ of around 30 was chosen. The helical velocity across the center of the end of the U-Bend is plotted in Figure 2.3. The helical velocity is mathematically the integrated scalar product of the velocity and vorticity fields of the flow. Any vortex having a non-zero axial component for the velocity will have a non-zero helicity and therefore is a helical structure. The magnitude of the helical velocity provides a numerical realization of the strength and size of the vortical structures, no matter if they are Taylor, Görtler, Dean, streamwise in the boundary layers or free shear flows [14]. We see that the results of the mesh with a y^+ of 30, 3.3 million cells, do not vary from the results of that from a mesh of a slightly larger y^+ value, such as the mesh with 3.8 million cells. However, when the y^+ drops below 30, as in the mesh with 2.4 million cells, the solution changes drastically because the wall function approach of FLUENT is not introduced into the problem. Thus, the 3.3 million cell mesh was selected.
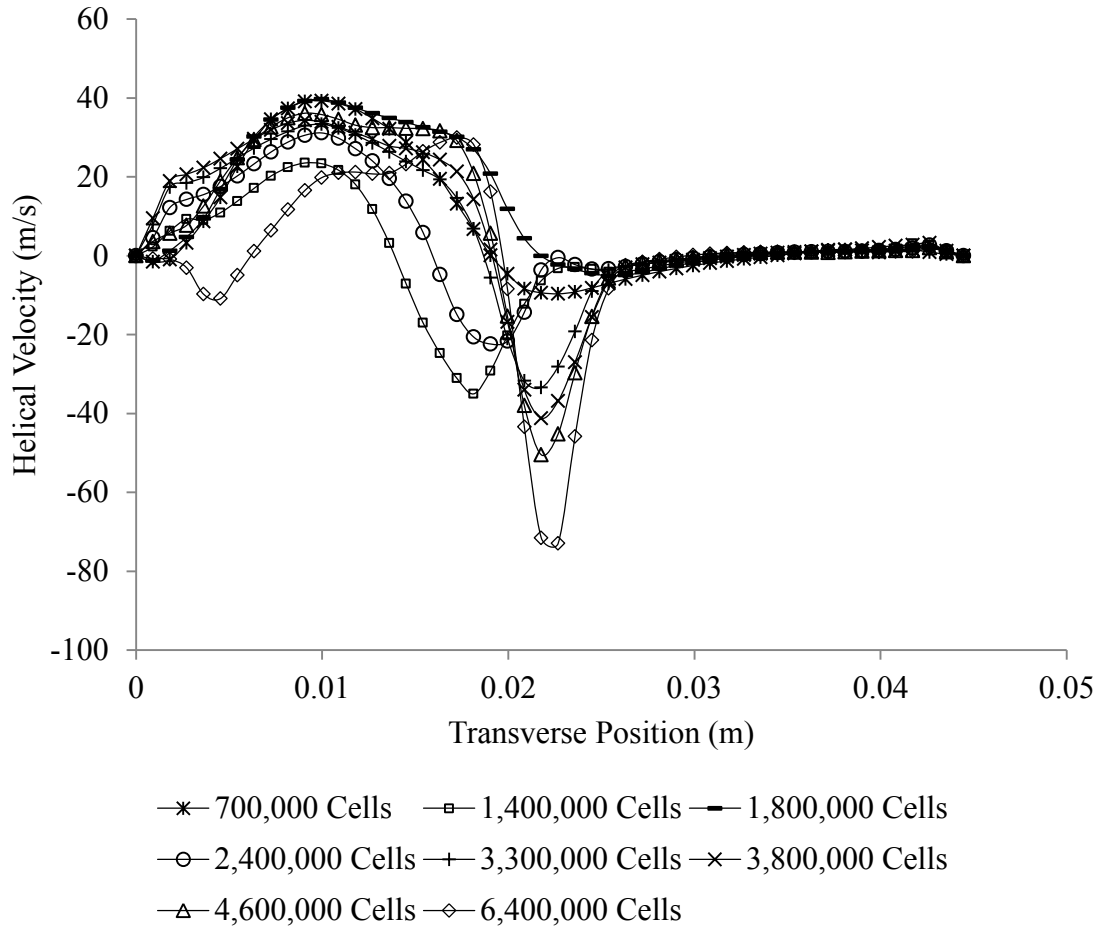
Figure 2.3: Helical Velocity of Varying Mesh Densities at Z = 0 of Return Pipe

The mean velocity contours from the experiment conducted by Sudo et al. [15] are shown in Figure 2.4. The experiment was conducted at a Reynolds Number of 6.0×10^4, this along with a pipe diameter of 104 mm and radius of curvature of 208 mm gives a Dean Number of 4.2×10^3. We used FLUENT to model the same conditions tested by Sudo et al [15]. The simulated velocity profiles are shown in Figure 2.5. In both cases, the pipe is placed on a horizontal plane.

17
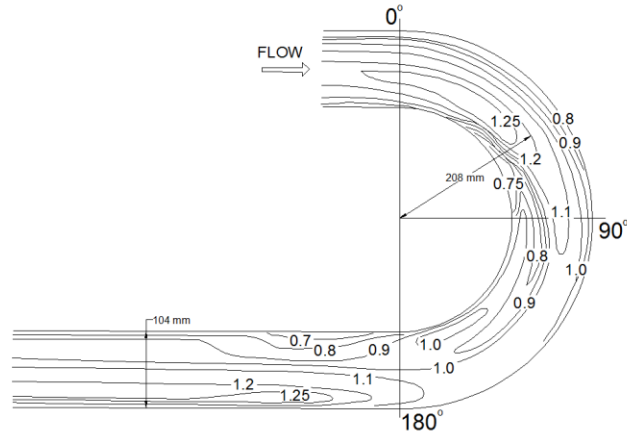
Figure 2.4: Experimental Velocity Contours [15]
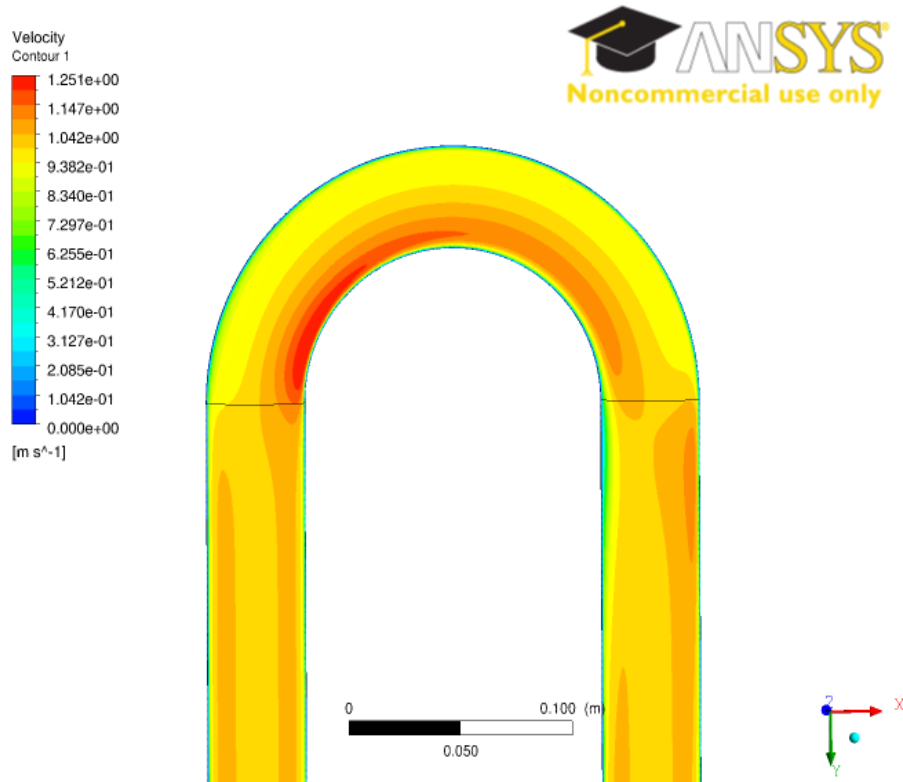
Figure 2.5: Streamwise Velocity of Numerical Model, Sudo et al. [15] Geometry Replica

18

The two figures are rotated such that the flow enters on the left in and exits from the right. The area of particular interest is the second half of the U-Bend, where the experimental and simulated velocity contours are very similar. During the model development process we have also utilized the results of Kaul [16] and Sugiyama and Hitomi [17] for validation.

4.0 RESULTS AND DISCUSSIONS

For a flow through a U-Bend, two large vortical structures often referred to as Dean vortices are typically formed. These vortices are generated by the sharp curvature and the resulting change in the streamwise velocity into a transverse one at the U-Bend [18]. Beyond the critical Dean Number, two smaller counter rotating vortices also appear [19]. There is not much work on how this critical number affects the heat transfer, or what happens to the effectiveness of heat convection when the Dean Number is below, at, and above it.

Figure 2.6 shows the variation in the flow structures with changes in the Dean Number. Water enters the pipe at a uniform velocity from the top left (the entrance is out of view), and exits through the right (the exit is also out of view). The Reynolds Number is fixed at 250 while the Dean Number was altered from 100 to 150, and then to 200 by increasing the curvature. The figure shows moderate changes in the vorticity, mostly after the U-Bend at Dn = 100. The vorticity magnitude appears to be slightly more intense at Dn = 150, and the activities seem to stay closer to the bend. At Dn of 200, the vorticity is most intense, with significant increase before the bend, and it also spreads farthest downstream.
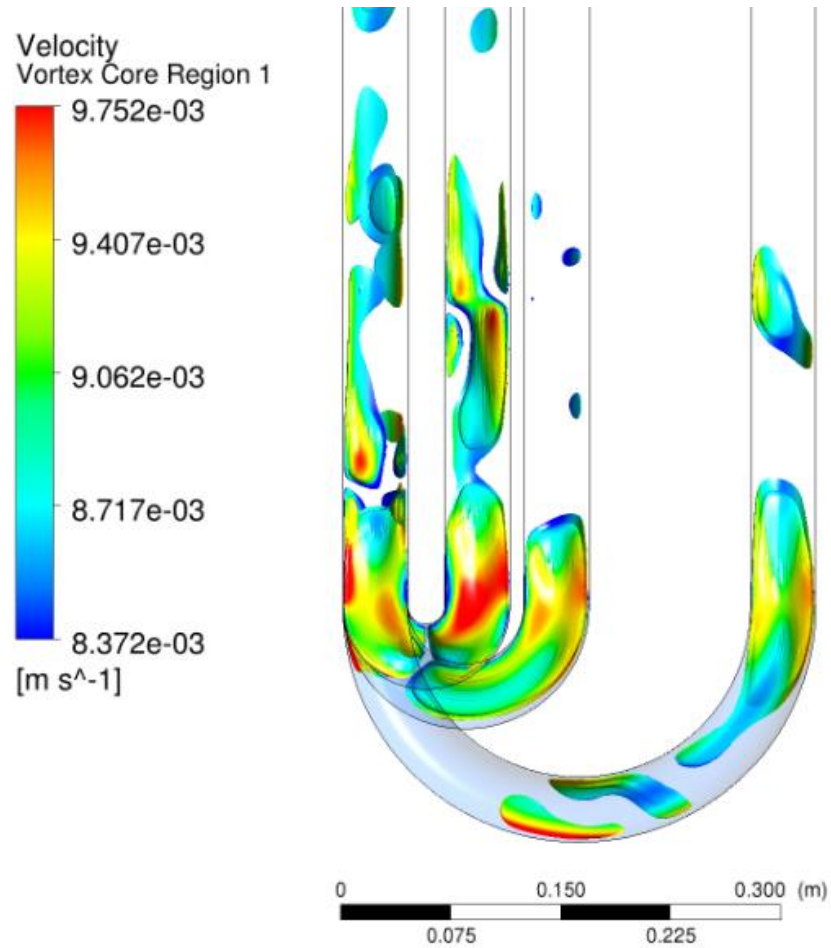
Figure 2.6: Vortical Structures of U-Bend at Re = 250

Ground source heat pumps generally operate with a much greater curvature at the U-Bend and a much lower velocity than the conditions considered above. Therefore, in the following section the effects of Re and Dn on the flow and heat transfer in a pipe with a U-Bend are investigated for conditions of interest in geothermal applications. As a first

approximation, we assume the pipe wall to be at a fixed and uniform temperature of 300 K with 285 K water entering the pipe at a uniform velocity.

4.1 TEST CONDITIONS

In practical ground source heat pump applications the flow rate is small at around 1.6 m^3 s^{-1} [20]. For the 44.45 mm diameter pipe under study, this flow rate implies a mean velocity of 0.29 m s^{-1}. Thus, the uniform inlet velocity was varied from 0.05 m s^{-1} to 1.3 m s^{-1} to enable the scrutinization of Re and Dn on the fluid flow and heat transfer. It is a known fact that the convection heat transfer coefficient increases with increasing Re (flow turbulence). On the other hand, the resident time over which heat is being transferred from the hot wall to the cold water decreases with increasing velocity (Re). These countering effects are further complicated by the intriguing Dean Number effect, posting an interesting engineering optimization challenge. This study aims at taking a first step toward overcoming this challenge by varying Re and Dn as summarized in Tables 2.2 and 2.3.

For the first case, the inlet velocity was changed from 0.05 to 1.3 m s^{-1}, resulting in Re altering from 2,212 to 57,508, and Dn varying from 2,206 to 57,347, as depicted in Table 2.2. The corresponding effect is a decrease in the mean temperature of the outgoing water as illustrated in Figure 2.7. The more than 5°C drop in temperature is substantial, considering the fact that there is only a 15°C difference between the incoming water and the wall, and that the total length of the pipe under investigation is only about 2.4 m. The total heat exchange from wall to water should be increased with increasing flow velocity and/or Re, but since the total water mass flow rate is also increased, it is reasonable that

21

the outlet water temperature decreases. In other words, for the studied conditions, the shortening of the resident time associated with increasing velocity has a dominating effect in reducing the heat transfer over the enhancement of the convective heat transfer coefficient with increasing Re and Dn.
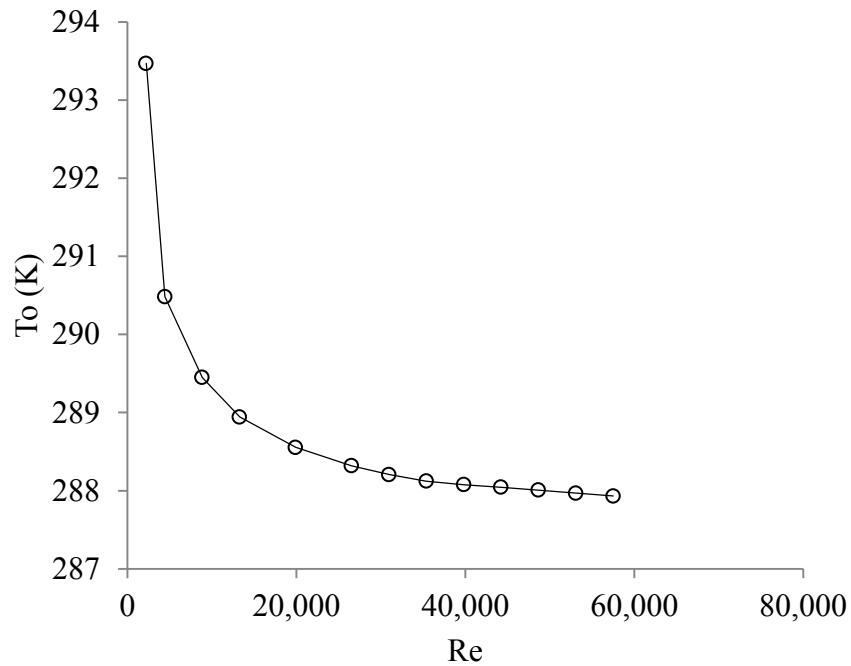
Figure 2.7: Temperature versus Reynolds Number at Outlet

22

Table 2.2: Velocity Variation Data

Rc (mm)	D (mm)	V_i (m s^{-1})	Re	Dn
22.35	44.45	0.05	2,212	2,206
22.35	44.45	0.1	4,424	4,412
22.35	44.45	0.2	8,847	8,822
22.35	44.45	0.3	13,271	13,234
22.35	44.45	0.45	19,907	19,851
22.35	44.45	0.6	26,542	26,468
22.35	44.45	0.7	30,966	30,879
22.35	44.45	0.8	35,390	35,291
22.35	44.45	0.9	39,814	39,703
22.35	44.45	1	44,237	44,113
22.35	44.45	1.1	48,661	48,525
22.35	44.45	1.2	53,085	52,936
22.35	44.45	1.3	57,508	57,347

To focus on the role of Dean Number, we fixed Re at 44,237 and reduced the curvature to vary Dn from 44,113 to 28,555 as summarized in Table 2.3. All these values are significantly larger than the critical Dean Number proposed by Bolinder [19]. When changing the radius of curvature the total length of the pipe varied slightly, and this tends to increase the resident time of the water in the pipe. Thus, for the purpose of consistency, the temperatures were normalized to a length of 2.4 m, removing any changes caused by resident time. In other words, only the effect of Dean Number is portrayed in Figure 2.8. It is clear that over the range of conditions considered, the mean outgoing water temperature increases with Dn. In other words, an increase in Dn in this range resulted in a significant enhancement of the heat transfer rate.

23
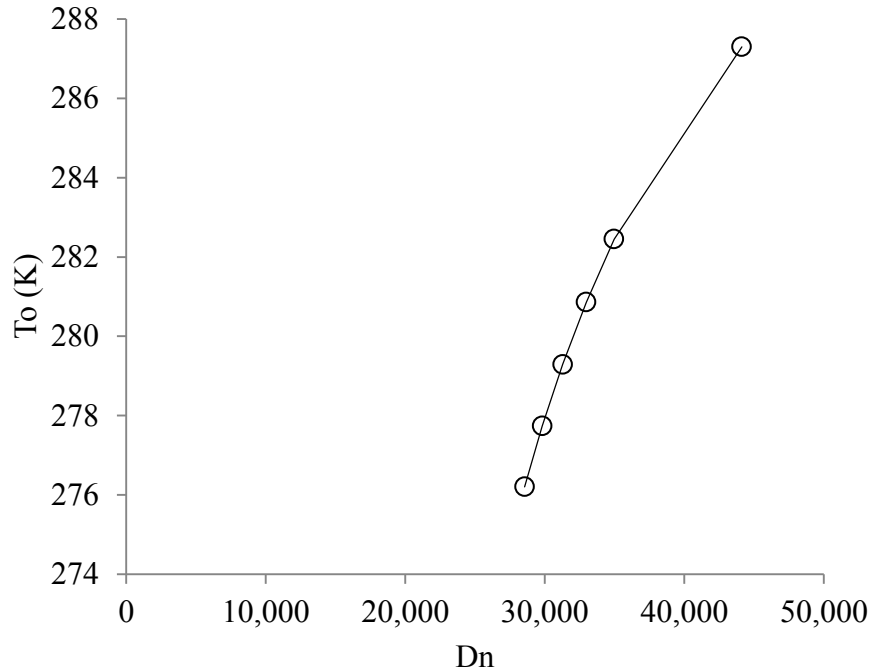
Figure 2.8: Outlet Temperature versus Dean Number for Reynolds Number of 44,237

Table 2.3: Curvature Change Data

Rc (mm)	D (mm)	Re	Dn
22.35	44.45	44,237	44,113
35.56	44.45	44,237	34,972
40.01	44.45	44,237	32,970
44.45	44.45	44,237	31,280
48.90	44.45	44,237	29,823
53.34	44.45	44,237	28,555

When comparing the results portrayed in Figure 2.7 (Table 2.2) with those in Figure 2.8 (Table 2.3), we note that the effectiveness of heat transfer in the pipe with the U-Bend decreases with reduction in the fluid resident time, in spite of expected augmentation

24

associated with increasing Re and Dn. With fixed resident time and Re, increasing Dn resulted in substantial augmentation of the rate of heat transfer as shown in Figure 2.8.

Another factor to consider when looking at the overall system efficiency is the pressure drop. The pressure drop values of Table 2.4 are plotted in Figure 2.9. We see that, as expected, the pressure drop does indeed increase as the Dean Number increases. For the studied system the trend is asymptotic, i.e., the increase in pressure drop with increasing Dean Number decreases at larger Dean Numbers. Over the range of conditions considered, the difference between the largest and smallest pressure drop values is only about 3%. For a full size system, however, this 3% increase may be of significant practical importance in terms of pump size and pumping costs. Thus, we should try to minimize the pressure drop while balancing the thermal performance and the overall cost of operation.

Table 2.4: Pressure Drop for Re = 44,237

Rc (mm)	Dn	Pressure Drop (kPa)
40.01	32,970	1.139
44.45	31,280	1.137
48.9	29,823	1.131
53.34	28,555	1.111
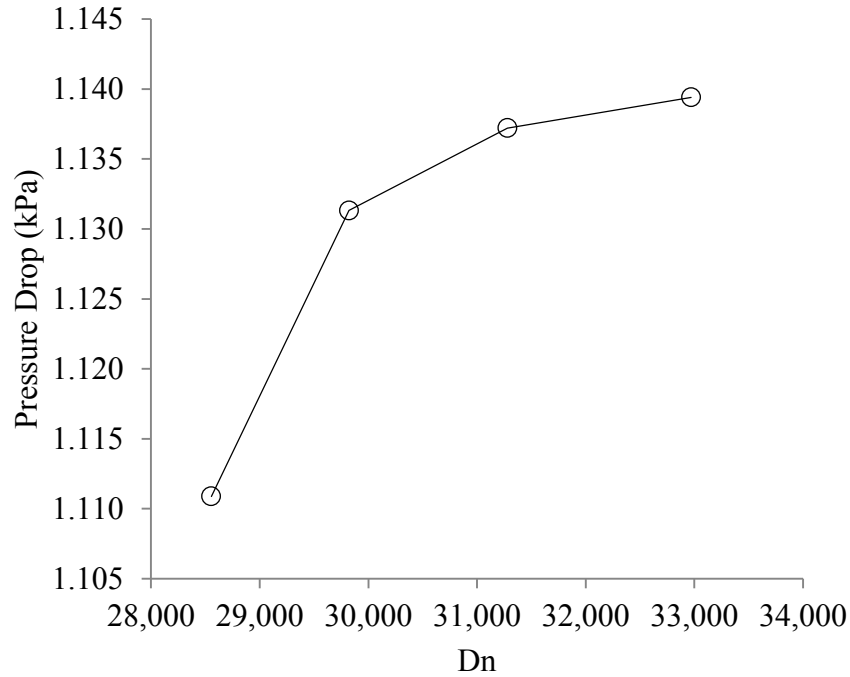
Figure 2.9: Pressure Drop versus Dean Number for Reynolds Number of 44,237

Let us take a closer look at the case with the lowest Re and the smallest Dn considered. This is when the velocity is 0.05 m s^{-1} and the radius of curvature is 53.34 mm or 1.2 times the diameter of the pipe; see Table 2.2. The geometry is shown in Figure 2.10. The velocity contours of the U-Bend for this case are detailed in Figure 2.11. The helical velocity of the flow as the flow approaches and leaves the U-Bend are depicted in Figure 2.12 (a-d).

26
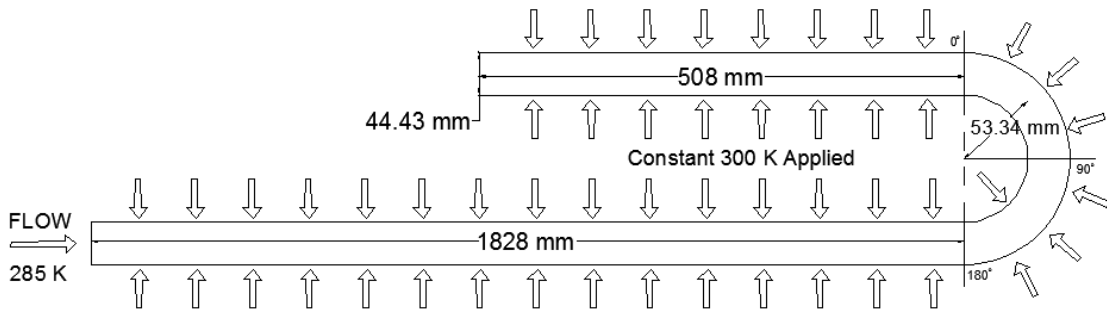
Figure 2.10: Geometric Model with R_c = 22.35 mm
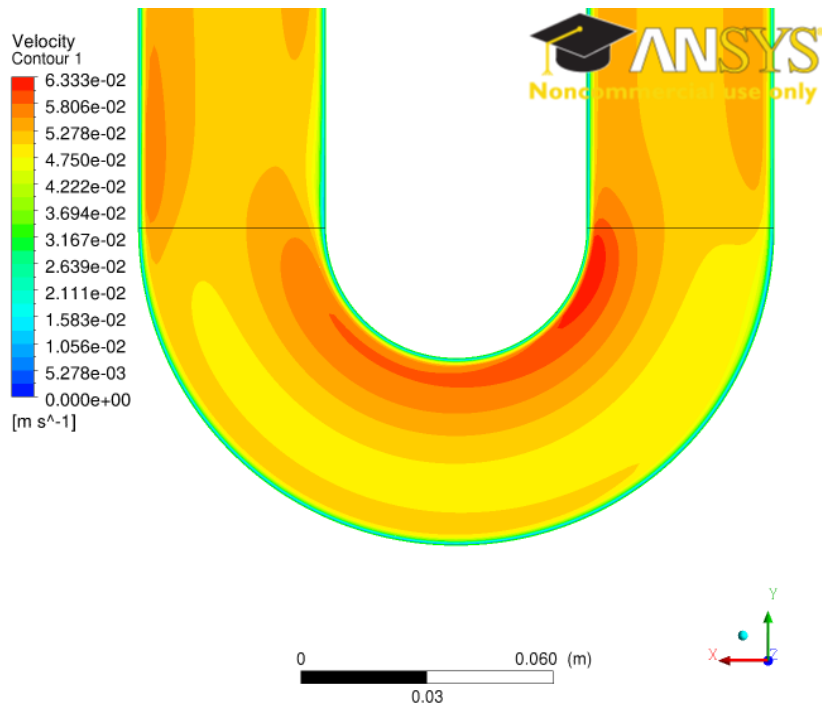
Figure 2.11: Velocity Contours, V = 0.05 m/s and R_c = 53.34 mm

27
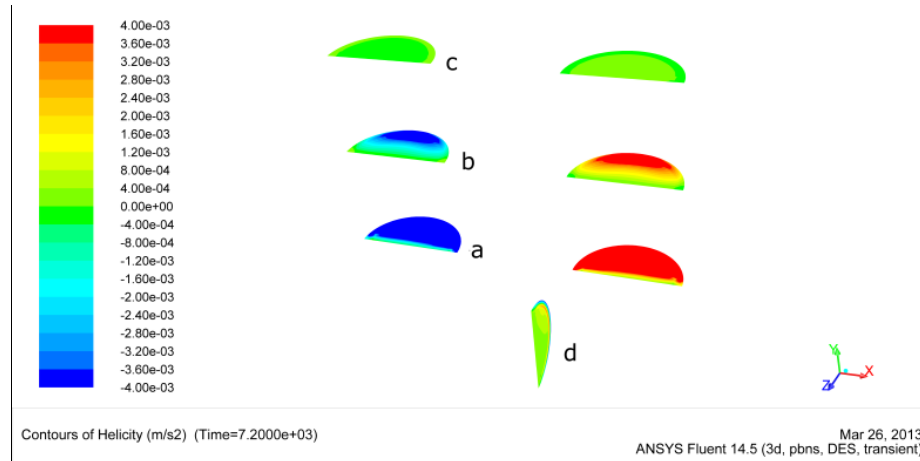
Figure 2.12: Helical Velocity at (a) 0D Down/Up Stream of Bend, (b) 1D Down/Up Stream of Bend, (c) 2D Down/Up Stream of Bend, (d) $\varphi = 90^{\circ}$ of Bend

The surface heat transfer coefficient of this pipe configuration is shown in Figure 2.13. The contours show that along the inner wall, the coefficient reaches a maxima at $\varphi = 0$, and subsequently, a minima at $\varphi = 180^{\circ}$. It is interesting to note that both these maximum and minimum heat transfer coefficient points fall unto the high velocity region as depicted in Figure 2.11. The heat transfer coefficient along the outer wall through the bend is high over a relatively large extent, indicating that the Dean's vortices are scouring away the heat rather effectively. The corresponding values of helical velocity at particular cross sections are depicted in Figure 2.12. We can see that the helical structures start forming before $\varphi = 90^{\circ}$ and last about a diameter or two downstream of $\varphi = 180^{\circ}$.

28

Contours of Surface Heat Transfer Coef. (w/m2-k) (Time=7.2000e+03) Mar 20, 2013
ANSYS Fluent 14.5 (3d, pbns, DES, transient)
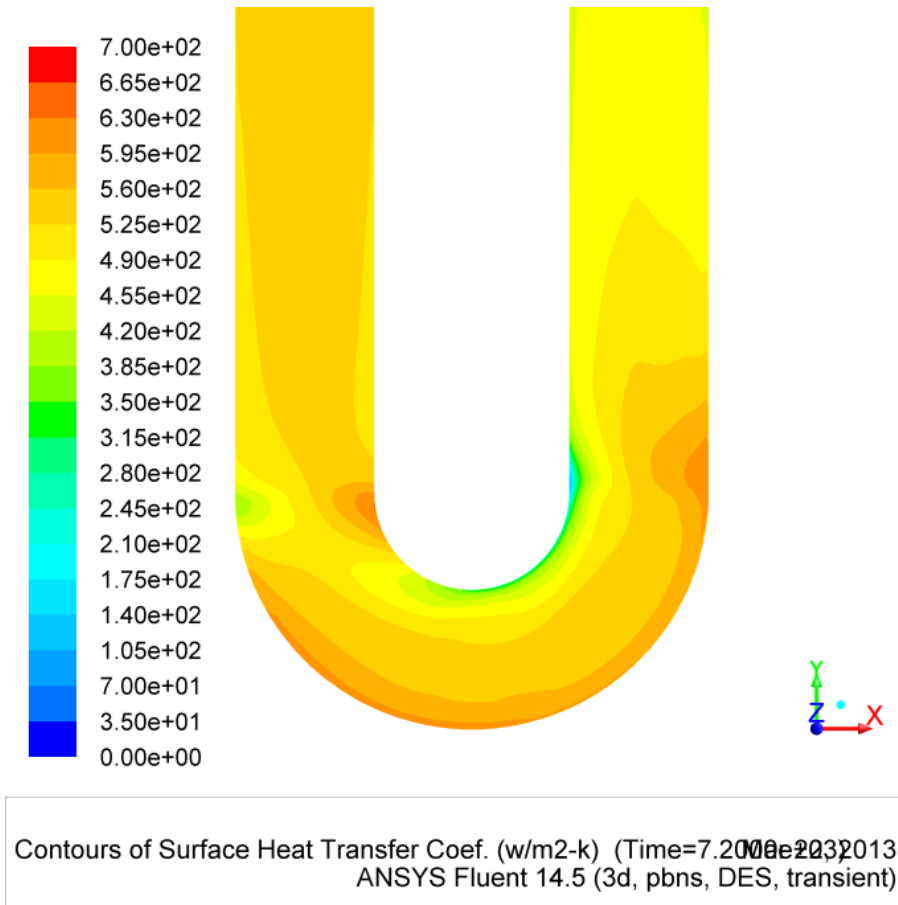
Figure 2.13: Surface Heat Transfer Coefficient

Figure 2.14 depicts the vortical magnitude across the plane of symmetry of the pipe. It is clear that the U-Bend generates the flow turbulence, i.e., the vorticity magnitude is significantly enhanced. This is especially true along the wall of the U-Bend; see 2.15 – 2.17. The high vorticity region along the outer wall region corroborates well with the high heat transfer region as depicted in Figure 2.13; even though this outer high vorticity region is narrower than that along the inner wall around the U-Bend. These high vorticity high heat transfer regions are closed associated with the two large symmetrical kidney

29

shaped Dean's vortices, which form along the wall from the outer to the inner portion of the bend, intensifying as they cross the midway point.
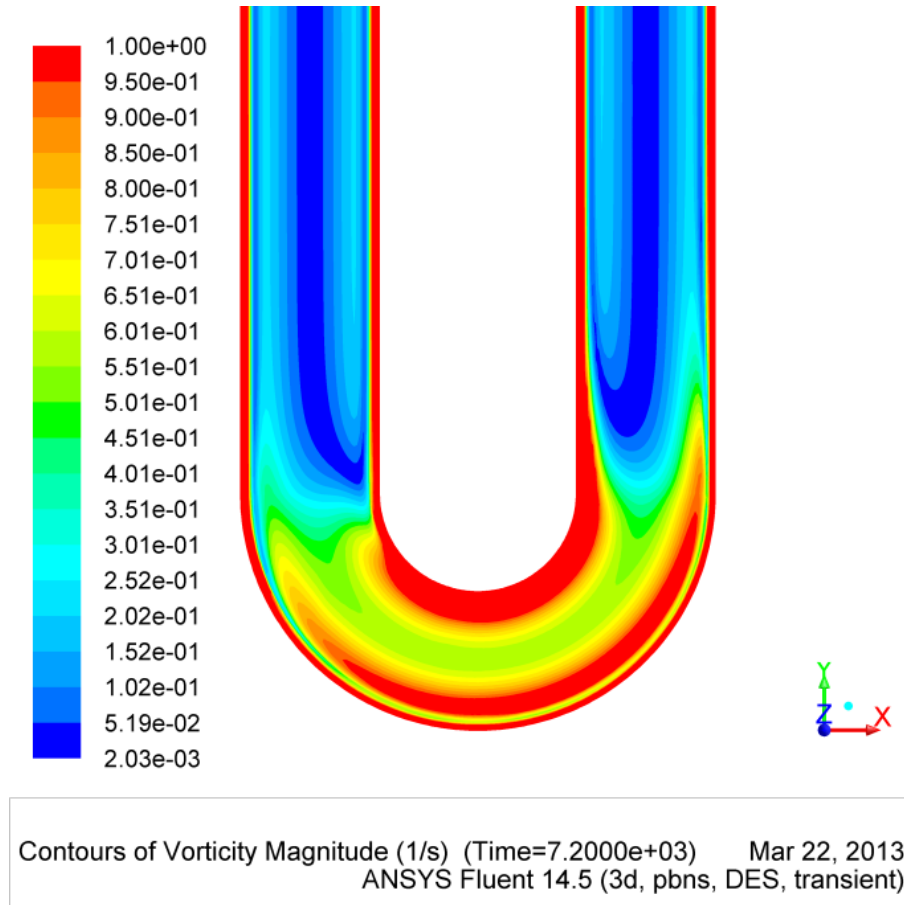
Figure 2.14: Vortical Magnitude across Plane of Symmetry
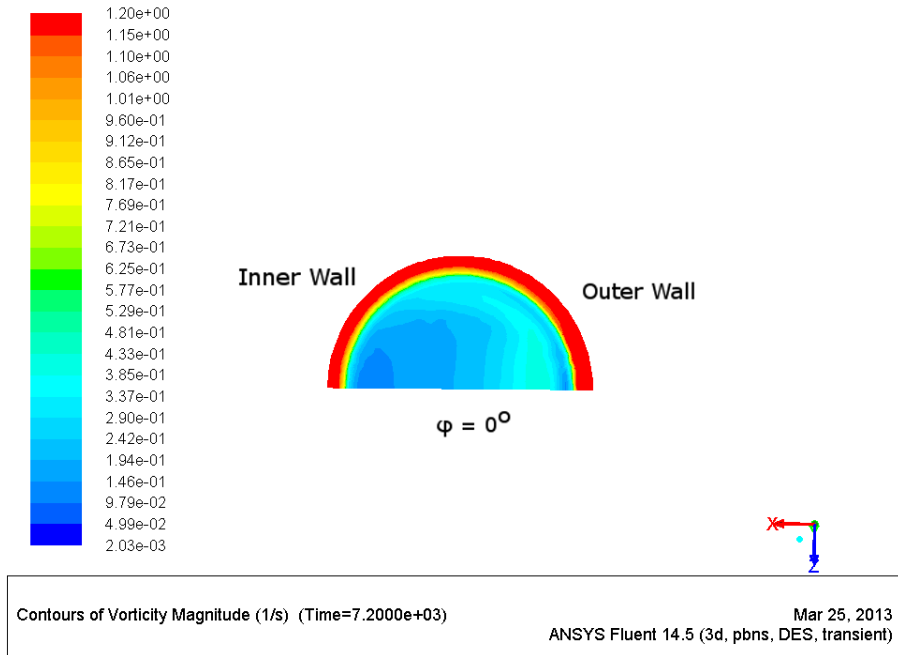
Figure 2.15: Vorticity Magnitude at φ = 0°
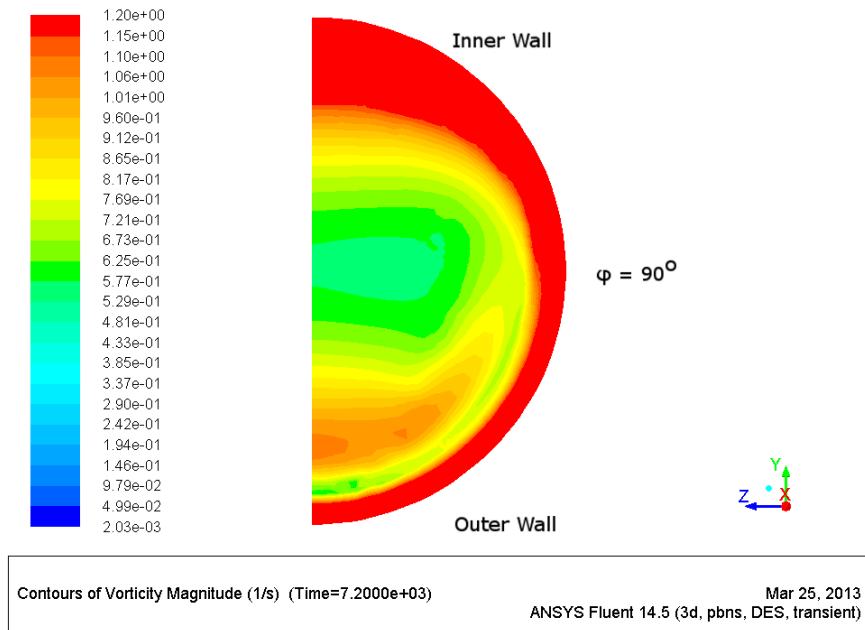
Figure 2.16: Vorticity Magnitude at φ = 180°

31
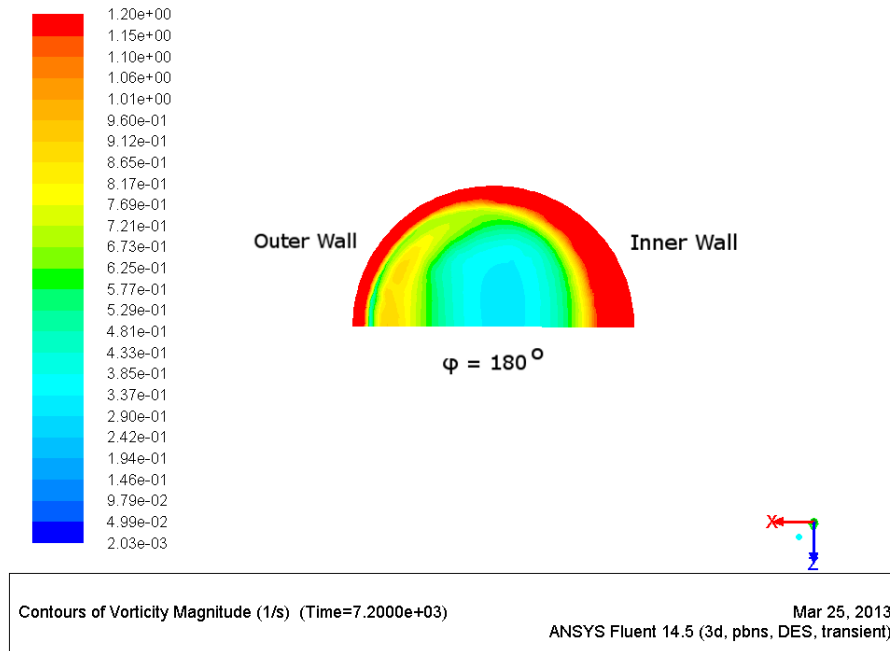
Figure 2.17: Vorticity Magnitude at $\varphi = 90^{o}$

5.0 CONCLUSION

Ground source heat pump's main purpose is to transfer heat to or from the earth through the use of a heat transferring fluid. The most common geometry for the ground heat exchanger is similar to that of a very long pipe with a U-Bend. It is found that in addition to redirecting the flow back up to the surface, the U-Bend generates Dean's vortices. These Dean's vortices have been found to enhance the heat transfer significantly, especially around the U-Bend and shortly after it. Increasing the velocity tends to decrease the resident time for heat transfer, and hence, it can lead to a reduction in outgoing fluid temperature in spite of increases in both Re and Dn.

32

ACKNOWLEDGEMENTS

www.manaraa.com

REFERENCES

[1]   G. Florides and S. Kalogirou, "Ground heat exchangers—A review of systems, models and applications," *Renewable Energy*, vol. 32, no. 15, pp. 2461–2478, Dec. 2007.

[2]   P. Hall, "Taylor—Gortler vortices in fully developed or boundary-layer flows: linear theory," *Journal of Fluid Mechanics*, vol. 124, pp. 475–494, 1982.

[3]   S. A. Berger, L. Talbot, and L. S. Yao, "Flow in curved pipes," *Annual Review of Fluid Mechanics*, vol. 15, no. 1, pp. 461–512, 1983.

[4]   J. Eustice, "Flow of water in curved pipes," *Proceedings of the Royal Society A: Mathematical, Physical and Engineering Sciences*, vol. 84, no. 568, pp. 107–118, Jul. 1910.

[5]   ANSYS Inc., *Fluent Theory Guide*. ANSYS, Inc., 2009.

[6]   J-S. Seo, J-K. Shin, Y-D. Choi, and J.-C. Lee, "Detached eddy simulation of a developing turbulent flow in a 270 curved duct," *Transactions of the Korean Society of Mechanical Engineers B*, vol. 32, no. 6, pp. 471–478, Jun. 2008.

[7]   T. H. Shih, W. W. Liou, A. Shabbir, Z. Yang, and J. Zhu, "A new k-ε eddy viscosity for high Reynolds Number turbulent flows - model development and validation," National Aeronautics and Space Administration, TM-106721, 1994.

[8]   R. Friedrich, B. Geurts, and O. Métais, *Direct and large-eddy simulation*, 5th ed. Kluwer Academic Publishers, 2004.

[9]   M. Strelets, *Detached eddy simulation of massively separated flows*. American
        Institute of Aeronautics & Astronautics, 2001.

[10]   S. V. Patankar and D. B. Spalding, "A calculation procedure for heat, mass and
        momentum transfer in three-dimensional parabolic flows," *International Journal
        of Heat and Mass Transfer*, vol. 15, no. 10, pp. 1787–1806, 1972.

[11]   S. V. Patankar, *Numerical Heat Transfer and Fluid Flow*. Taylor & Francis
        Group, 1980.

[12]   S. Muntean, A. Ruprecht, and R. Susan-Resiga, "A numerical investigation of the
        3d swirling flow in a pipe with constant diameter. part 1: inviscid computation,"
        in *Proceedings of the Workshop on Vortex Dominated Flows-Achievements and
        Open Problems*, 2005, pp. 77–86.

[13]   C. Hirsch, *Numerical Computation of Internal and External Flows: The
        Fundamentals of Computational Fluid Dynamics*. Butterworth-Heinemann, 2007.

[14]   H. K. Moffatt and A. Tsinober, "Helicity in laminar and turbulent flow," *Annual
        review of fluid mechanics*, vol. 24, no. 1, pp. 281–312, 1992.

[15]   K. Sudo, "Experimental investigation on turbulent flow through a circular-
        sectioned 180° bend," *Experiments in Fluids*, vol. 28, no. 1, pp. 0051–0057, 2000.

[16]   U. Kaul, "Turbulent flow in a 180 bend: modeling and computations," *NASA
        Contractor Report 4141*, p. 50, 1989.

[17]   H. Sugiyama and D. Hitomi, "Numerical analysis of developing turbulent flow in a 180° bend tube by an algebraic Reynolds stress model," *International Journal for Numerical Methods in Fluids*, vol. 47, no. 12, pp. 1431–1449, 2005.

[18]   O. Boiron, V. Deplano, and R. Pelissier, "Experimental and numerical studies on the starting effect on the secondary flow in a bend," *Journal of Fluid Mechanics*, vol. 574, pp. 109–129, 2007.

[19]   C. J. Bolinder, "First- and higher-order effects of curvature and torsion on the flow in a helical rectangular duct," *Journal of Fluid Mechanics*, vol. 314, pp. 113–138, 1996.

[20]   A. Bagdanavicius and N. Jenkins, "Power requirements of ground source heat pumps in a residential area," *Applied Energy*, vol. 102, pp. 591–600, Feb. 2013.

CHAPTER 3

HEAT TRANSFER IN A U-BEND PIPE: DEAN NUMBER VERSUS REYNOLDS NUMBER

1.0 INTRODUCTION

Ground source heat pumps (GSHPs) are a means to extract or reject energy from or to the earth for heating and cooling purposes. A typical GSHP system, as shown in Figure 3.1, consists of a reversible heat pump, the building ductwork and the ground loop. The heat pump acts as a reversible vapor-compression refrigeration loop [1], [2] so that the system can be reversed for the different seasonal modes. A pump delivers a pretreated working fluid to affect the heating or cooling of the indoor building environments [3]. A group of ground source heat pumps can be linked together to form a geothermal energy field where each system works in parallel to manage thermal requirement for large buildings. There are many types of ground source heat pumps available to the consumer and each has its own advantages and disadvantages. Vertical ground source heat pumps are the most common and they employ a vertical pipe loop underground as opposed to a horizontal or helical configuration [4]. These vertical pipe loops can often reach depths of 100 m. With the relatively constant ground temperature [5]–[7], the vertical ground loops provide an advantage with a more predictable performance in the heat transfer process [8], [9]. Since these vertical systems go straight into the earth they require boreholes to be dug to the length that is required. The cost of this digging exponentially rises with the depth resulting in tens of thousands being spent on the installation. Overestimation and rough modelling of the systems size and

37

performance are the cause of the large capital needed [4]. Thus there is a strong need to better understand the heat transfer between the working fluid, the pipe wall and the surrounding environment under different conditions. Currently the models that are employed in design and GSHP software are analytical and approximate [10], [11]. Since the detailed flow structures and turbulence within the loops can have a significant effect on the rate of heat transfer, they should be properly included and simulated using computational and numerical methods [12]–[14].
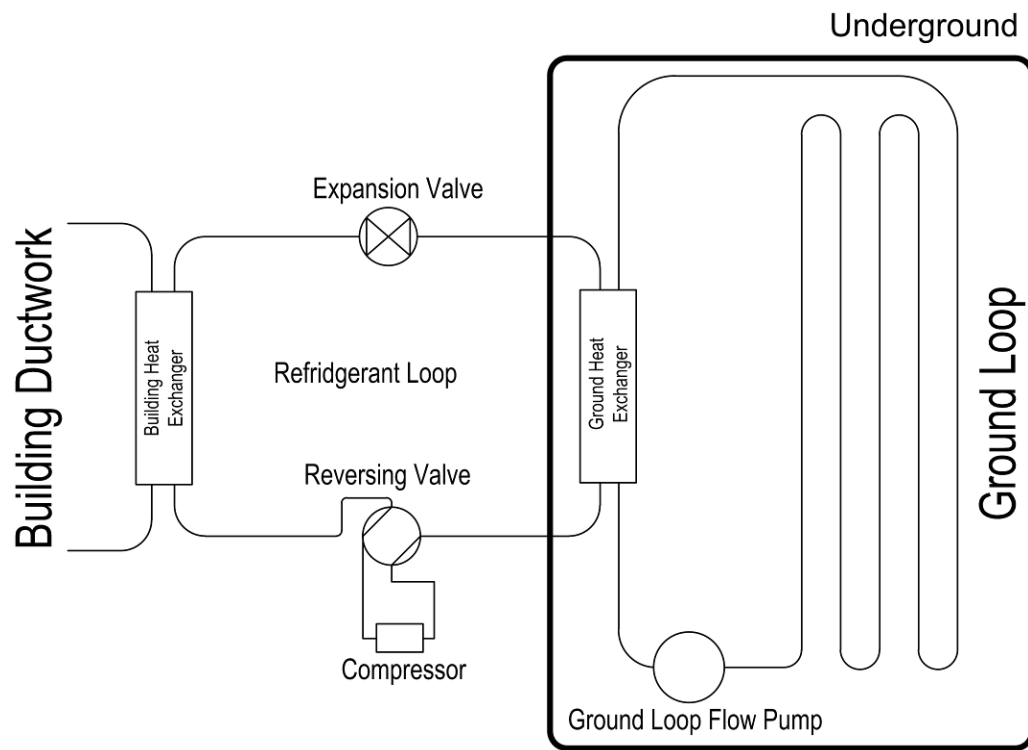
Figure 3.1: Typical Ground Source Heat Pump System

In vertical pipe loop setups, there exists a U-Bend section of pipe that returns the working fluid back to the surface. This U-Bend can generate secondary flows called the Dean vortices in addition to flow turbulence which are known to enhance heat transfer [16]–[21]. The Dean Number is the product of the Reynolds Number (Re) and the square root of the radius of the pipe (r) over the bend's radius of curvature (Rc) and can be expressed as:

$$Dn = Re\sqrt{\frac{r}{Rc}} \qquad (1)$$

In pipe flow, such as that encountered in ground source heat pumps, the heat transfer between the wall and the fluid is predominately convective. The bottleneck of the heat transfer is the inner boundary layer, where a no-slip condition implies conduction behaviour. This bottleneck is more significant when the flow is laminar. Promoting flow turbulence reduces the bottleneck and enhances the convection process [22], [23]. Over the narrow range of temperatures involved in low temperature geothermal processes, the fluid properties such as the Prandtl number remain relatively unchanged. As such the convective heat transfer is primarily a function of the Reynolds Number in a straight pipe. For a pipe with a U-Bend, the effect imposed by the Dean Number also becomes important.

Florides and Kalogirou reviewed the current state of ground source heat pumps up until 2006 [10]. The general conclusions included increasing GSHP performance with increased flow velocity when using smaller pipes and the line source model is the

39

standard analytical approach for evaluating the characteristics of the borehole. However, it does not comment on the analytical models' accuracy with respect to the much more detailed numerical methods, such as the finite volume techniques used in this study. More recently Philippe et al. [11] investigated the three main analytical models (infinite line source, infinite cylindrical model, and finite line source) and tested the validity ranges for maximum accuracy. The infinite line source model which applies Lord Kelvin's heat source equations to GSHPs was developed in 1948 by Ingersoll and Plass [18]. The infinite long line is at the centre of the borehole and the borehole material is neglected, that is, the heat transfer is gathered from soil characteristics. The assumption that the borehole has negligible effects is problematic especially with large borehole radii [11].

Ingersoll et al. in 1954 [19], [20] proposed the infinite cylindrical model which imposes a constant rate of heat transfer at the borehole wall, rather than at the centre. The borehole of infinite length is solved numerically by integrating the model from zero to infinity with a constant far field temperature. Eskilson [21] extended this model to finite length and used a virtual line of equal length that extended above the surface to account for the surface behaviour. Also, the basis of this model is that the line is, instead of being a continuous source of heat, is a series of point sources. This increases the accuracy when the effects of the edge of the borehole and soil formation are important [11].

Shin et al. [22] studied the relationship of heat transfer and turbulent flows for square ducts. They found that the turbulence inherent in the system enhances the heat transfer efficiency, and the temperature distribution is relatively uniform except around the 90 degree bend. Di Liberto and Ciofalo [15] investigated the heat transfer in a straight pipe, a slightly curved, and a severely curved pipe. It is found that both the flow velocity

40

and the heat flux are the highest at the outside wall. The scope of this work is somewhat limited by the range of curvature and length of the straight portion of the pipe relevant to GSHP.

This study aims at improving our understanding of the in-pipe mechanisms affecting the ground source heat pump performance. To do so, a systematic parametric study concerning the effects of the Dean Number and the Reynolds Number on the heating and cooling modes is conducted using FLUENT.

2.0 MATHEMATICAL FORMULATION

Numerical turbulence modelling is chosen in this study because it has the ability to look at more details than that of analytical models. Detached Eddy Simulation models (DES) is chosen because Large Eddy Simulation (LES) tends to underperform at the boundary layers of which are very influential in the type of flow considered here. At the boundary layers DES utilizes a switch in the algorithm that changes the equations to a RANS model, in the boundary layer [25]–[27].

With DES, the option for the RANS model to be used for the boundary layer is available in the algorithm. The choice for the RANS model completely depends on the flow situation. The realizable k-ε model was selected for the RANS model to be used in the DES [28]. The realizable k-ε model takes the following form [26]. In this modified realizable k-ε model there are two transportable variables, that is, variables that are modelled and then carried through the mesh to solve for the rest of the parameters such as velocity, pressure and vorticity. The first variable is the turbulent kinetic energy, k_1, and is the kinetic energy associated with the turbulent eddies in the flow. The second variable

41

is the dissipation rate, ε, and is the rate at which the turbulent kinetic energy is dissipated into thermal energy internal to the flow. The transportable variables, the turbulent kinetic energy, k_1, and the dissipation rate, ε, respectively are [12]:

$$\frac{\partial}{\partial t}(\rho k_1) + \frac{\partial}{\partial x_j}(\rho k_1 u_j)$$
$$= \frac{\partial}{\partial x_j}\left[\left(\mu + \frac{\mu_t}{\sigma_{k_1}}\right)\left(\frac{\partial k_1}{\partial x_j}\right)\right] + G_{k_1} + G_b - \rho\epsilon - Y_M + S_{k_1} \tag{2}$$

$$\frac{\partial}{\partial t}(\rho\epsilon) + \frac{\partial}{\partial x_j}(\rho\epsilon u_j)$$
$$= \frac{\partial}{\partial x_j}\left[\left(\mu + \frac{\mu_t}{\sigma_\epsilon}\right)\left(\frac{\partial \epsilon}{\partial x_j}\right)\right] + \rho C_1 S\epsilon - \rho C_2\left(\frac{\epsilon^2}{k_1 + \sqrt{(v\epsilon)}}\right)$$
$$+ C_{1\epsilon}\frac{\epsilon}{k_1}C_{3\epsilon}G_b + S_\epsilon \tag{3}$$

where,

$$\mu_t = \frac{\rho C_\mu k_1^2}{\epsilon} \tag{4}$$

$$C_\mu = \frac{1}{A_0 + \frac{A_8 k U^*}{\epsilon}} \tag{5}$$

Here G_{k1} is the generation of the turbulence kinetic energy due to the mean velocity gradients, G_b is the generation of the turbulence kinetic energy due to buoyancy (forces induced by gravity and the gradient of density between the materials), Y_M is the contribution of the fluctuating dilation in compressible turbulence to the overall dissipation rate and S_{k1} and S_ε are the source terms.

There are two main differences between the realizable k-ε and the standard k-ε model. The standard k-ε model usually assumes the value of C_μ to be 0.09 whereas the

42

realizable variant calculates the constant based on Equation 5 above. The eddy viscosity, μ_t calculated in Equation 4 is then based on this new constant, C_μ.

To preserve the RANS computation mode throughout the boundary layer DES further provides modifications to the traditional realizable k-ε model [12]. The dissipation term, Y_k, shown in Equation 6, is modified to account for a new wall distance, l_{des}, shown in Equation 9. This new wall distance is the switch that serves as the criterion for using a LES approach or a RANS approach to modelling that particular volume of fluid.

$$Y_k = \frac{\rho k_1^{\frac{3}{2}}}{l_{des}} \qquad (6)$$

$$l_{rke} = \frac{k_1^{\frac{3}{2}}}{\epsilon} \qquad (7)$$

$$l_{les} = C_{des}\Delta \qquad (8)$$

$$l_{des} = l_{rke} - f_d \max(0, l_{rke} - C_{des}\Delta) \qquad (9)$$

where C_{des} = 0.61 (the mathematical constant associated with DES).

3.0 MODEL SETUP AND COMPUTATIONAL FRAMEWORK

Shown in Table 3.1 are the individual test cases for this study as well as some critical parameters that differentiate the cases. The pipe studied in all test cases is fixed at a length of 1.9 m with varying straight pipe lengths proceeding and succeeding the U-Bend. The varying pipe length is needed to accommodate the changing curved pipe section with altering Dean Number. The wall temperature is selected to be fixed at 300 K

43

and the inlet temperature is varied to create the desired temperature difference. The uniform inlet velocity was set based on the Reynolds Number. The diameter of the pipe is fixed at 0.0254 m and water is considered to be the working fluid. Since the Dean Number is a function of the pipe radius, bend curvature radius and Reynolds Number, and the Reynolds Number and pipe radius are fixed for the different test cases the radius of curvature is changed as summarized in Table 3.2, i.e. the higher the Dean Number the smaller the radius of curvature. The straight pipe length is checked to ensure proper development length for the flow to become fully developed before entering the U bend. Based on the radius of curvature the curved pipe length is calculated for normalization purposes. The flow time is also deduced for these same purposes. The numerical model consisted of the geometry as shown in Figure 3.2. Uniform velocity enters the flow domain and is exposed to non-slip wall entities held at a constant temperature. The flow is directed through the U-bend of varying curvature and exits through the outlet downstream of the bend. The uniform inlet was assumed to have no turbulence (turbulence intensity = zero). The outlet was set as an outflow with a flow rating of one, i.e., all the fluid is exiting across this boundary. To save computational resources only half of the pipe was modeled and the symmetry boundary condition was taken advantage of.

From the literature review of similar geometry and flow condition simulations the following solution methods and discretization processes were chosen. The Semi-Implicit Method for Pressure-Linked Equations (SIMPLE) algorithm was selected for the pressure-velocity coupling [24], [25]. The Bounded Central Differencing, the default for DES, was selected for the momentum discretization. Pressure Staggering Option

44

(PRESTO!), was selected as the pressure interpolation scheme because of its well documented accuracy for flow in curved domains [24]. The gradient is based on the Green-Gauss cell method and the turbulent viscosity and energy equations use the second order upwind equations. All flow parameters are relaxed with a factor of 0.75 [4].

In the present study, the Reynolds Numbers, Dean Numbers, and temperature differences are independently varied to examine the effects of these three key parameters on the performance of heat transfer. Two Reynolds Numbers are strategically chosen to cover the critical points at which the flow changes from laminar to transitional and transitional to turbulent as shown in Table 3.1. The Dean Numbers are limited by practicality and are chosen to elucidate the Dean Vorticity effect on the heat transfer process. Both heating and cooling modes are studied. These are compared with the isothermal case with no heat transfer, i.e. $\Delta T = 0$.

FLUENT has proven to be very flexible and accurate for many flow conditions and hence, is chosen for this study [12]. SHARCNET, the Shared Hierarchical Academic Research Computing Network, provided not only the computing power but also allowed for simulations to complete in a timely manner while allowing long simulation times. The Linux based nodes utilized were either AMD Opterons at 2.2 GHz clock speeds or Intel Xeons at 2.6 GHz clock speeds with 32GB of memory available per node. Meshing and analysis were reserved for "visualization nodes." These are a group of Linux based servers dedicated for generating dense meshes and the viewing of large result files.

Shown in Table 3.2 are the individual test cases for this study as well as some critical parameters that differentiate the cases. The wall temperature is selected to be

45

fixed at 300 K and the inlet temperature is varied to create the desired temperature difference. The uniform inlet velocity was set based on the Reynolds Number. The diameter of the pipe is fixed at 0.0254 m and water is the working fluid. Since the Dean Number is a function of the pipe radius, bend curvature radius and Reynolds Number, and the Reynolds Number and pipe radius are fixed for the different test cases the radius of curvature is changed as summarized in Table 3.2, i.e. the higher the Dean Number the smaller the radius of curvature. The straight pipe length is checked to ensure proper development length for the flow to become fully developed before entering the U bend. Based on the radius of curvature the curved pipe length is calculated for normalization purposes. The flow time is also deduced for these same purposes. The numerical model consisted of the geometry as shown in Figure 3.2. Uniform velocity enters the flow domain and is exposed to non-slip wall entities held at a constant temperature. The flow is directed through the U-bend of varying curvature and exits through the outlet downstream of the bend. The uniform inlet was assumed to have no turbulence (turbulence intensity = zero). The outlet was set as an outflow with a flow rating of one, i.e., all the fluid is exiting across this boundary. To save computational resources only half of the pipe was modeled and the symmetry boundary condition was taken advantage of.

Table 3.1: Parameter Combination Matrix

Re	Dn	ΔT (K)
2,000	1,500	-25 (Heating)
5,000	1,750	0
	2,000	25 (Cooling)

46
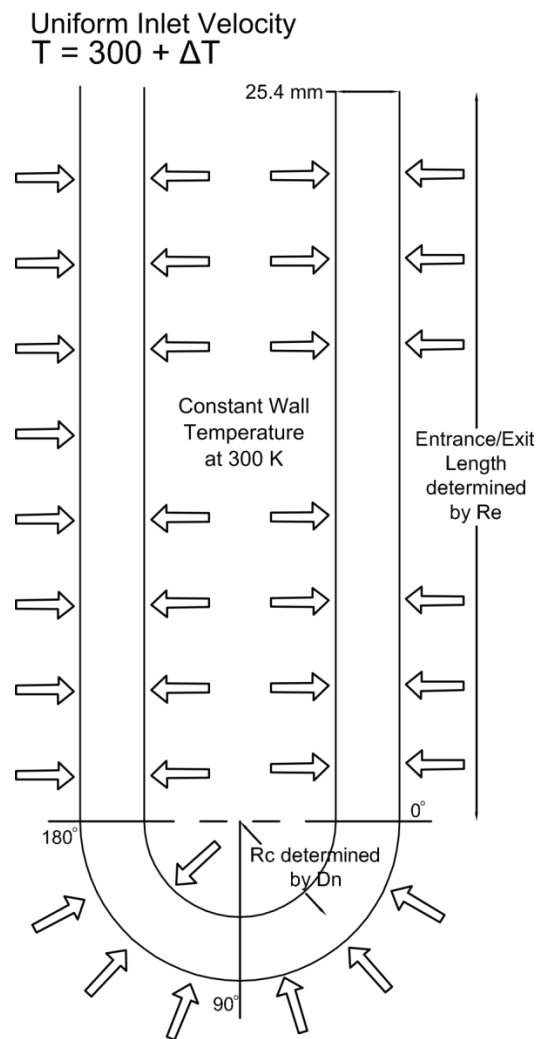
Figure 3.2: Schematic of the Borehole Exchanger with U-Bend

Table 3.2: Test Cases

Case No.	Re	Dn	T_{in} (K)	V_{in} (m s^{-1})	Rc (m)	Length$_{st}$ (m)	Length$_{cur}$ (m)
1	2,000	1,500	275	7.91E-02	2.26E-02	0.880	0.14
2	2,000	1,500	300	7.91E-02	2.26E-02	0.880	0.14
3	2,000	1,500	325	7.91E-02	2.26E-02	0.880	0.14
4	2,000	1,750	275	7.91E-02	1.66E-02	0.902	0.10
5	2,000	1,750	300	7.91E-02	1.66E-02	0.902	0.10
6	2,000	1,750	325	7.91E-02	1.66E-02	0.902	0.10
7	2,000	2,000	275	7.91E-02	1.27E-02	0.915	0.08
8	2,000	2,000	300	7.91E-02	1.27E-02	0.915	0.08
9	2,000	2,000	325	7.91E-02	1.27E-02	0.915	0.08
10	5,000	1,500	275	1.98E-01	1.41E-01	0.508	0.89
11	5,000	1,500	300	1.98E-01	1.41E-01	0.508	0.89
12	5,000	1,500	325	1.98E-01	1.41E-01	0.508	0.89
13	5,000	1,750	275	1.98E-01	1.04E-01	0.626	0.65
14	5,000	1,750	300	1.98E-01	1.04E-01	0.626	0.65
15	5,000	1,750	325	1.98E-01	1.04E-01	0.626	0.65
16	5,000	2,000	275	1.98E-01	7.94E-02	0.702	0.50
17	5,000	2,000	300	1.98E-01	7.94E-02	0.702	0.50
18	5,000	2,000	325	1.98E-01	7.94E-02	0.702	0.50

Length$_{st}$ = Straight Pipe Length, Length$_{cur}$ = Curved Pipe Length

From the literature review of similar geometry and flow condition simulations the following solution methods and discretization processes were chosen. The Semi-Implicit Method for Pressure-Linked Equations (SIMPLE) algorithm was selected for the pressure-velocity coupling [26], [27]. The Bounded Central Differencing, the default for DES, was selected for the momentum discretization. Pressure Staggering Option (PRESTO!), was selected as the pressure interpolation scheme because of its well documented accuracy for flow in curved domains [26]. The gradient is based on the Green-Gauss cell method and the turbulent viscosity and energy equations use the second order upwind equations. All flow parameters are relaxed with a factor of 0.75 [12].

48

FLUENT has proven to be very flexible and accurate for many flow conditions and hence, is chosen for this study [12]. SHARCNET, the Shared Hierarchical Academic Research Computing Network, provided not only the computing power but also allowed for simulations to complete in a timely manner while allowing long simulation times. The Linux based nodes utilized were either AMD Opterons at 2.2 GHz clock speeds or Intel Xeons at 2.6 GHz clock speeds with 32GB of memory available per node. Meshing and analysis were reserved for "visualization nodes." These are a group of Linux based servers dedicated for generating dense meshes and the viewing of large result files.

4.0 VERIFICATION AND VALIDATION

Verification and validation are two important steps in any mathematical modeling study. During the verification process, the model is tested to check if the governing equations are solved correctly; whereas, the validation ensures proper realization of the involved physics. To verify and validate the numerical model chosen, a two-step process was utilized. First the model was run with varying mesh densities on an identical geometry to obtain a completely independent solution. Then the appropriate mesh density for our numerical computer model was used on an existing experiment conducted by Sudo et al. [29] to ensure accuracy and efficiency in the calculations.

First, the mesh independence consisted of generating a progressively denser mesh until the average relative error of the results converges to less than 1%. Figure 3.3 shows the variation of the velocity magnitude across the centerline of the U-Bend for the meshes generated in the study. The mesh was refined from 1×10^{-8} (Mesh 1) to 1×10^{-20} (Mesh 4). The relative error between Mesh 3 (1×10^{-15}) and the much finer Mesh 4 was only

49

0.8%. Thus, Mesh 3 is deemed adequate as far as accuracy is concern and yet does not drain an unnecessarily large amount of computational resources.
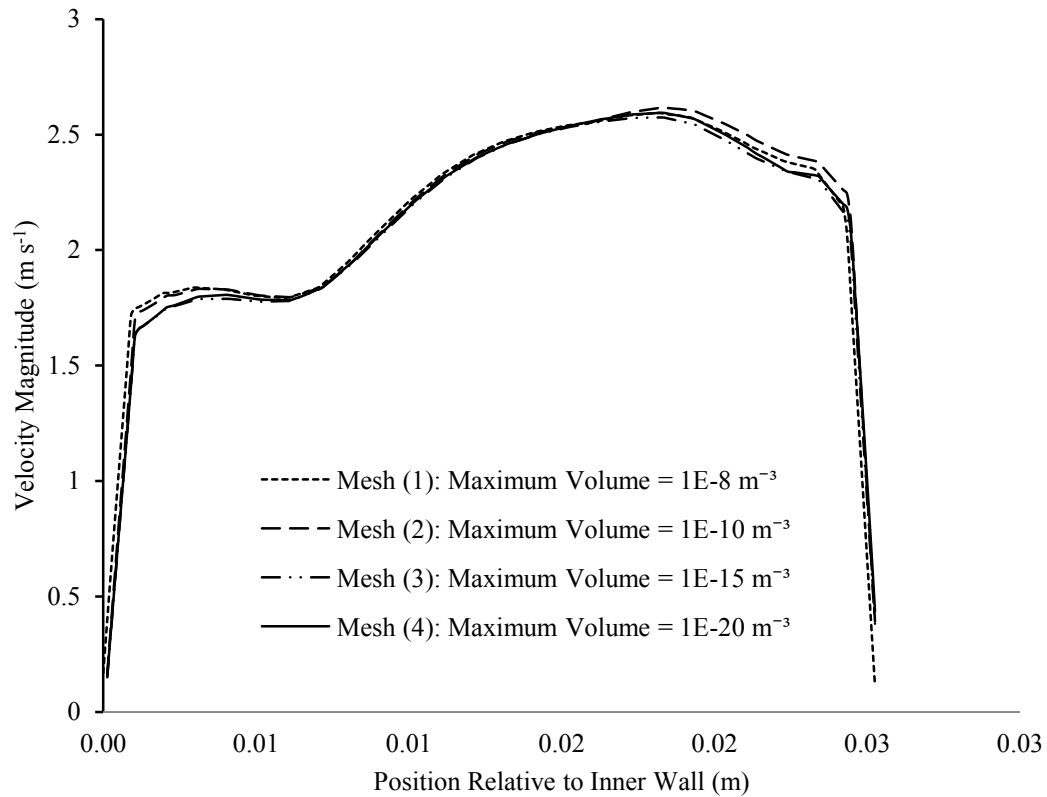
Figure 3.3: Variation of Velocity Magnitude across Centerline at $\Phi = 90^{\circ}$ Of U-Bend with Varying Mesh Densities

A requirement of DES is that the grid size must be smaller than the length scale for the flow domain. The turbulence length scale will be used as the criterion for the maximum size of the grid cells [25]–[27]. The turbulence length scale for the pipes in this

simulation is equal to 7% of the hydraulic diameter (0.0254 m). This is because FLUENT uses a turbulence length scale based on the mixing length rather than the traditional formulation [12]. In other words, the maximum grid size is 9 x 10^{-5} m which is significantly smaller than 1.8 x 10^{-3} m (the turbulence length scale).

In the second stage, to validate the accuracy of the computation, a geometry matching the isothermal air flow experiment conducted by Sudo et al. [29] was generated. The model setup of Sudo et al. consisted of a fan blowing air into the U-Bend arrangement with a pipe diameter of 104 mm. The air would travel through the first straight portion of the duct that was one hundred diameters long, the U-Bend's radius of curvature was two diameters and the exiting straight length portion was forty diameters. The Reynolds Number of the flow was 6.0 x 10^4 which resulted in a mean velocity of 8.7 m/s. The air would exit the second straight portion into the atmosphere. The results of the experiment are compared to that of the numerical model to ensure the results and trends of the CFD run simulation are reasonably correct. Figure 3.4 shows the experimental results for the relative velocity magnitude of Sudo et al. [29] and the same contours for the CFD model. The relative velocity of the flow is the local velocity of the region over the initial inlet velocity of the system. The areas that peak at 1.25 of the inlet flow exist in the same regions for the numerical work. Good agreement was determined to exist and along with the proven models for this type of flow and FLUENT's consistency in mathematical calculations it was decided to run the cases on SHARCNET.
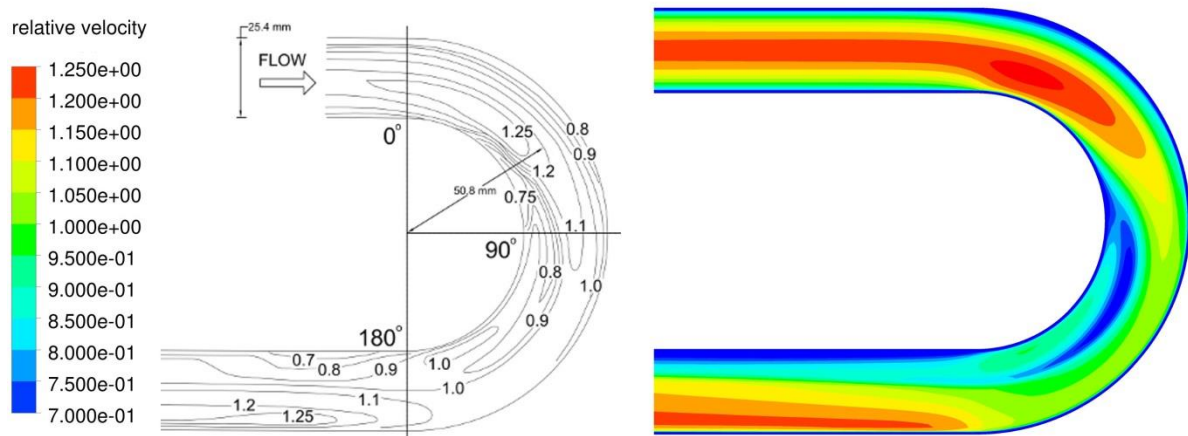
Figure 3.4: Experimental/Numerical Velocity Contours, Sudo et al. [29], Re = 60,000, Dn = 30,000, ΔT = 0

For the above simulations, modelling the turbulent flow is much more difficult than the heat transfer process. For turbulent flows there are countless CFD models and modifications to those models that produce varied results. In FLUENT, heat transfer analysis is relatively straight forward for simple heat transfer scenarios such as the one in this study. Simple convection applied between the wall and the fluid where the wall is a constant heat source is modelled along with the validated turbulence model.

5.0 RESULTS AND DISCUSSION

In the following sections, results from the many cases studied will be presented in the order of the isothermal case, the heating mode and the cooling mode. The isothermal case is included to isolate the turbulence generation from the geometry and the heat transfer process. The heating and cooling modes are included as they are the main

52

operation modes of ground source heat pumps. Within these three sections two Reynolds Numbers and three Dean Numbers are tested. Two Reynolds Numbers are strategically chosen to cover the critical points at which the flow changes from laminar to transitional and transitional to turbulent as shown in Table 3.1. The Dean Numbers are limited by practicality and chosen to reveal the Dean Vorticity effect in curved pipes.

5.1 ISOTHERMAL CASE, ΔT = 0 K

The isothermal case is the base case. As it is isothermal, there will be no temperature included in the system effectively removing thermal effects. It is valuable because it portrays the effect of straight, and, more importantly, the curved section on the flow characteristics such as flow turbulence and vortical structures. It also serves as a reference to elucidate the possible added effect of thermal energy gradient on these flow characteristics. In the previous section we have simulated such a case for validation purposes.

5.1.1 TRANSITIONAL FLOW WITH VARYING DEAN NUMBER, ΔT = 0 K

Transitional flow occurs when the Reynolds Number is around 2,000. Three Dean Numbers (Dn) that were tested at this level are, 1,500, 1,750, and 2,000. Figure 3.5(a) shows the contours of the flow on the plane of symmetry in the simulation. A clear pattern of increasing intensity as the flow passes through the U-Bend is observed. This turbulence intensity is defined as the local root-mean square turbulence normalized by the uniform inlet velocity. The increase in turbulence in and after the U-Bend is due to the

53

increasing centrifugal force experienced by the fluid due to the Dean phenomenon. The Dean Vortex structures develop from water moving from the inner onto the outer wall regions along the diameter and back around the circumference of the pipe. The maximum turbulence intensity occurs in the recirculating zone. It manifests itself farther downstream of the U-Bend as Dn increases with the maximum reaching 40% when Dn = 2,000 and Re = 2,000. At larger Re of 5,000 two recirculating zones appear, one at the beginning of the U-Bend and the other at the end of the U-Bend. These result in two high turbulence intensity regions as shown in Figure 3.5(b). These two high turbulence regions will have more mixing and more turbulent activity leading to better thermal energy transfer. These two regions are regions of interest as their existence and transformation over the Reynolds Number will be vital in enhancing the heat transfer process.
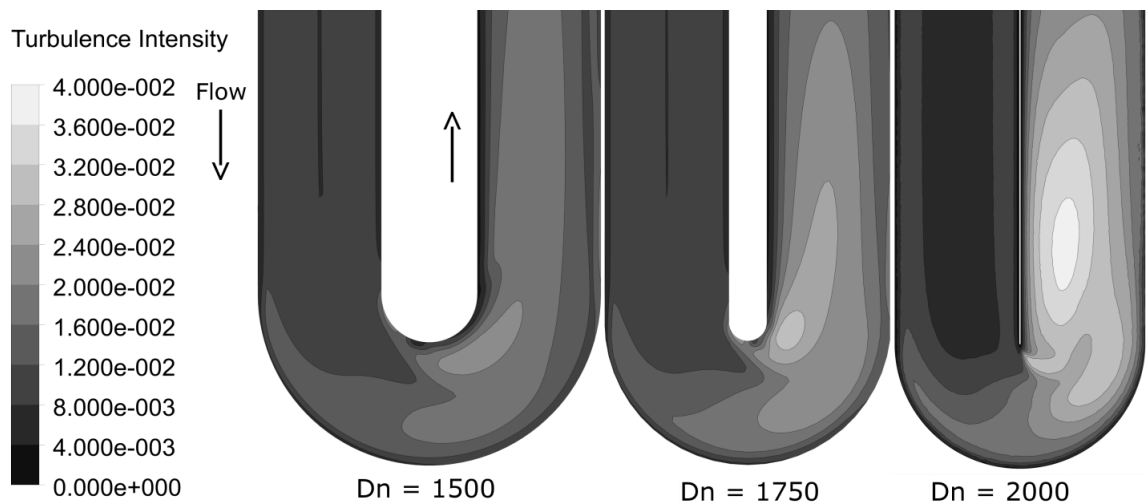
Figure 3.5(a): Contours Map of Turbulence Intensity; Re = 2,000 and $\Delta T = 0$
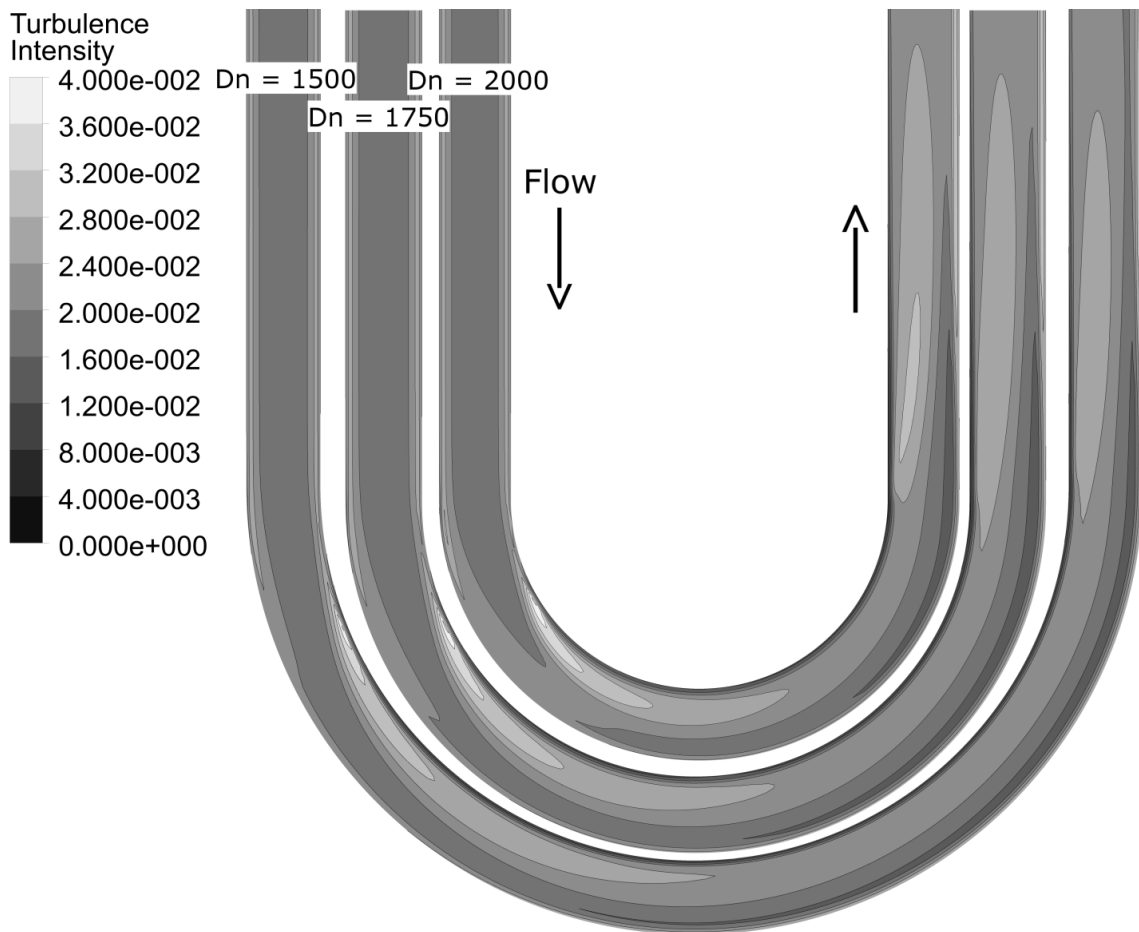
Figure 3.5(b): Contours Map of Turbulence Intensity; Re = 5,000 and $\Delta T = 0$

Figure 3.6 shows the contours of the velocity pattern as it evolves from the inlet of the U-Bend to the outlet. The contours show how the flow progresses to the outer wall from the centrifugal forces and how the recirculating zone increases in size as the flow

progresses further in the U-Bend. This region corresponds with the region of high turbulence intensity.

| $\varphi = 0°$ | $\varphi = 45°$ | $\varphi = 90°$ | $\varphi = 135°$ | $\varphi = 180°$ |
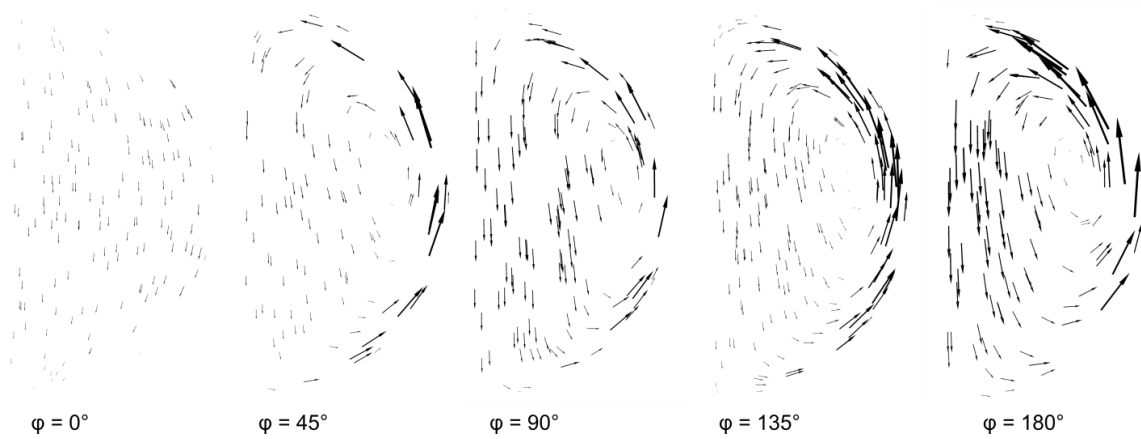
Figure 3.6: Arrow Plot of Velocity in and Around the U-Bend Region for Re = 5,000, Dn = 1,500 and $\Delta T = 0$

5.2 HEATING MODE, ΔT = -25 K

As there are two operating modes in ground source heat pumps, it is important to understand flow and heat transfer under these two unique situations and isolate the thermal gradient's effect on the turbulence and Dean Vortex generation, and/or vice versa. The heating mode in this study will be defined as when the fluid inlet temperature is 275 K and the wall temperature is 300 K. Low turbulence cases will be tested with all three accompanying Dean Numbers.

5.2.1 LOW TURBULENCE WITH VARYING DEAN NUMBER, ΔT = -25 K

Figure 3.7 shows the surface heat transfer coefficient from the wall to the water at low flow turbulence (Re = 5,000). There are two main areas of high coefficients in these cases, the inner wall at approximately the 90º radial position and more dominantly around the outer wall area at slightly downstream of the 180º position. The pattern to note is that these areas increase in size and magnitude as the Dean Number increases. The structure at the 180º radial position is present because of the Dean Number, after the Dean Vortex structures form they work to scour away the heat from the outer wall. At this Reynolds Number, the organised Dean vortices create smaller turbulent eddies that are effective in convecting away the thermal energy from the warm wall, enabling more energy to be transferred per unit area. Note that the underlying turbulence contours for this heating mode is similar to the isothermal case shown in Figure 3.5(b). While the highest turbulence levels correspond to the recirculating zones near the inner wall at approximately 90° and just after 180° (Figure 3.5(b)), the highest heat flux corresponds to the outer wall just downstream of 180°.
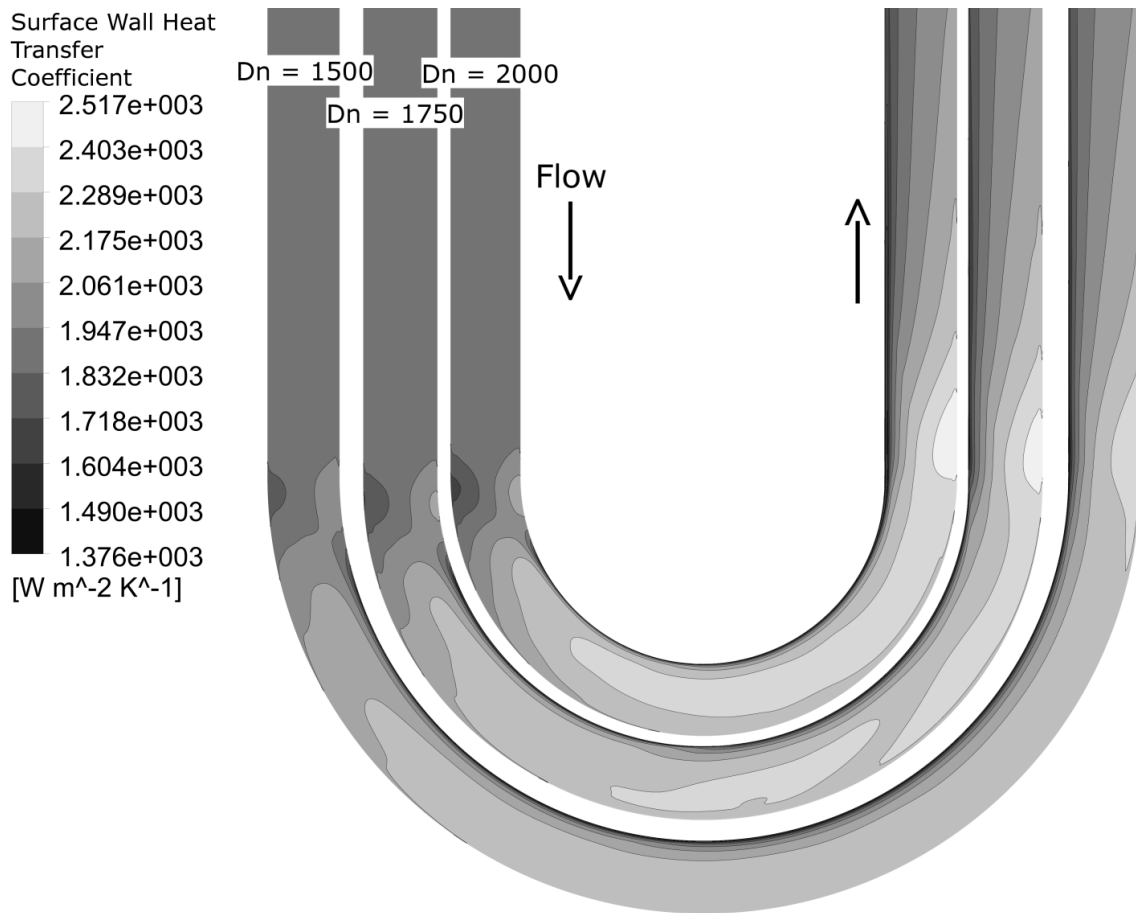
Figure 3.7: Contours Map of Surface Wall Heat Transfer Coefficients; Re = 5,000 and

ΔT = -25 K

5.3 COOLING MODE, ΔT = 25 K

Similar to the heating mode, the cooling mode is also important in this application of geothermal energy. This mode is defined in this study as when the fluid inlet temperature is 325 K and the wall temperature is 300 K. As with the heating mode tests, this heat transfer process will be tested with the low turbulence mode and all three accompanying Dean Numbers, when forced convection dominants.

58

5.3.1 LOW TURBULENCE WITH VARYING DEAN NUMBER, ΔT = 25 K

As in the heating mode, the heat transfer process was analysed at low turbulence flow regime with three Dean Numbers. Comparisons are drawn between the cooling mode, heating mode and the isothermal case. Figure 3.8 shows the surface heat transfer coefficient from the wall to the fluid for this case. As can be seen in the figure when compared to Figure 3.7 it is seen that the regions of higher heat transfer for both cooling and heating are literally identical. In other words, since the flow is relatively faster, the corresponding natural convection which is expected to behave differently for heating and cooling modes, is negligible, in comparison to the prevailing forced convection. This is useful as design for enhanced heat transfer based on Dn and Re will be the same for both operating modes of GSHPs.
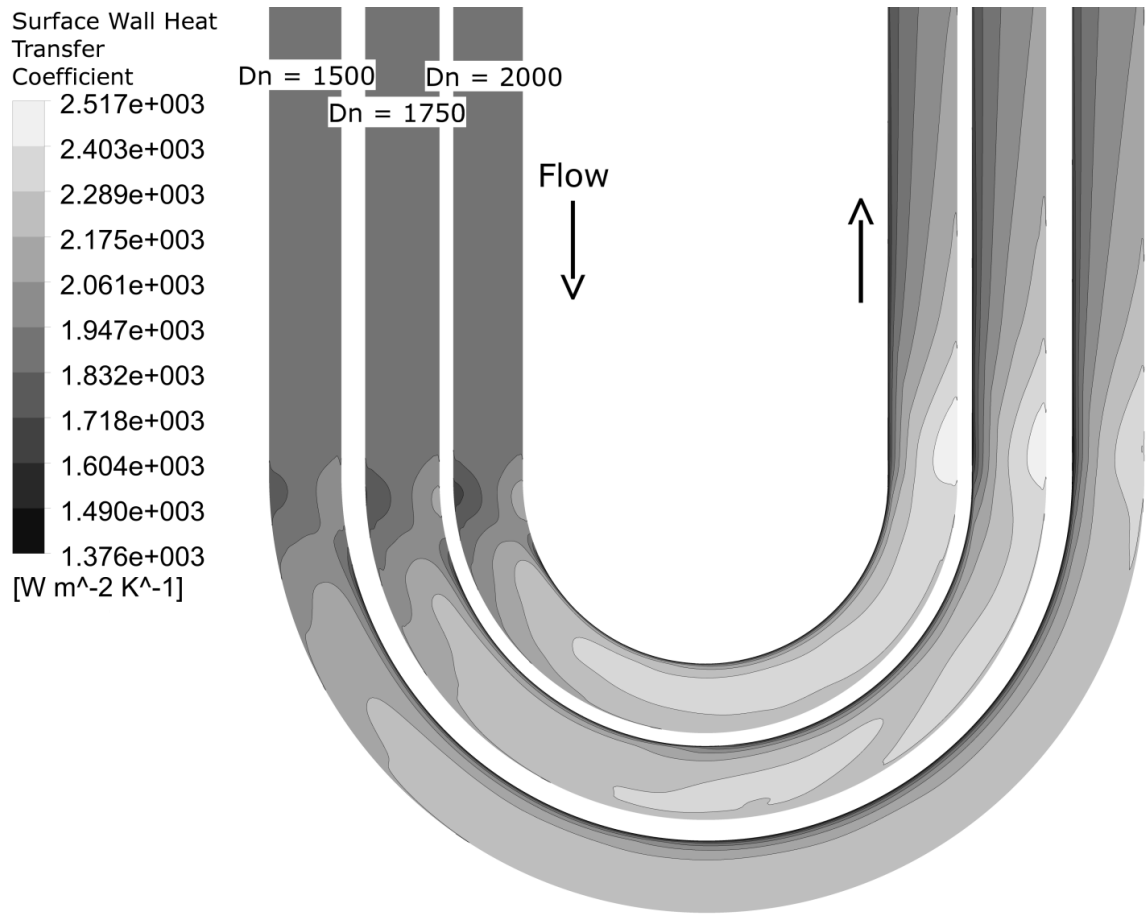
Figure 3.8: Contours Map of Surface Wall Heat Transfer Coefficients; Re = 5,000 and

$\Delta T = 25$ K

5.4 DIFFERENTIATING CURVED PIPE AND STRAIGHT PIPE EFFECTS

The total length of the pipe is kept constant in all the cases of this study. The changing Dean Numbers will ultimately change the length of curved pipe, i.e. the higher the Dean Number the smaller the radius of curvature thus smaller curved section within one level of the Reynolds Number. The straight pipe portion then becomes the

complement length to bring the total length to 1.9 m. The details of these lengths can be found in Table 3.2.

Figure 3.9 shows the heat flux through the wall for the cooling and heating modes for the three selected Dean Numbers and two Reynolds Numbers. The average total wall heat flux is an average of the heat through the whole straight-curved-straight pipe system while the average curved wall heat flux is simply that corresponds to the U-Bend. As expected the heat flux for the cooling and heating modes is the same as it is mainly a function of the temperature gradient, for this predominantly convective heat transfer. For Re = 2,000, both the average total wall heat flux and the average curved wall heat flux decrease with increasing Dean Number. Note that this decrease is more significant in the curved pipe region because as the U-Bend section (volume) decreases with increasing Dean Number, it tends to encompass mostly the recirculating fluid which is neither located next to the heat source nor effective in scouring thermal energy from it. In other words, the creation of laminar recirculating zones alone is not good as far as effective convection heat transfer is concern, as laminar flow increases the conduction bottleneck.
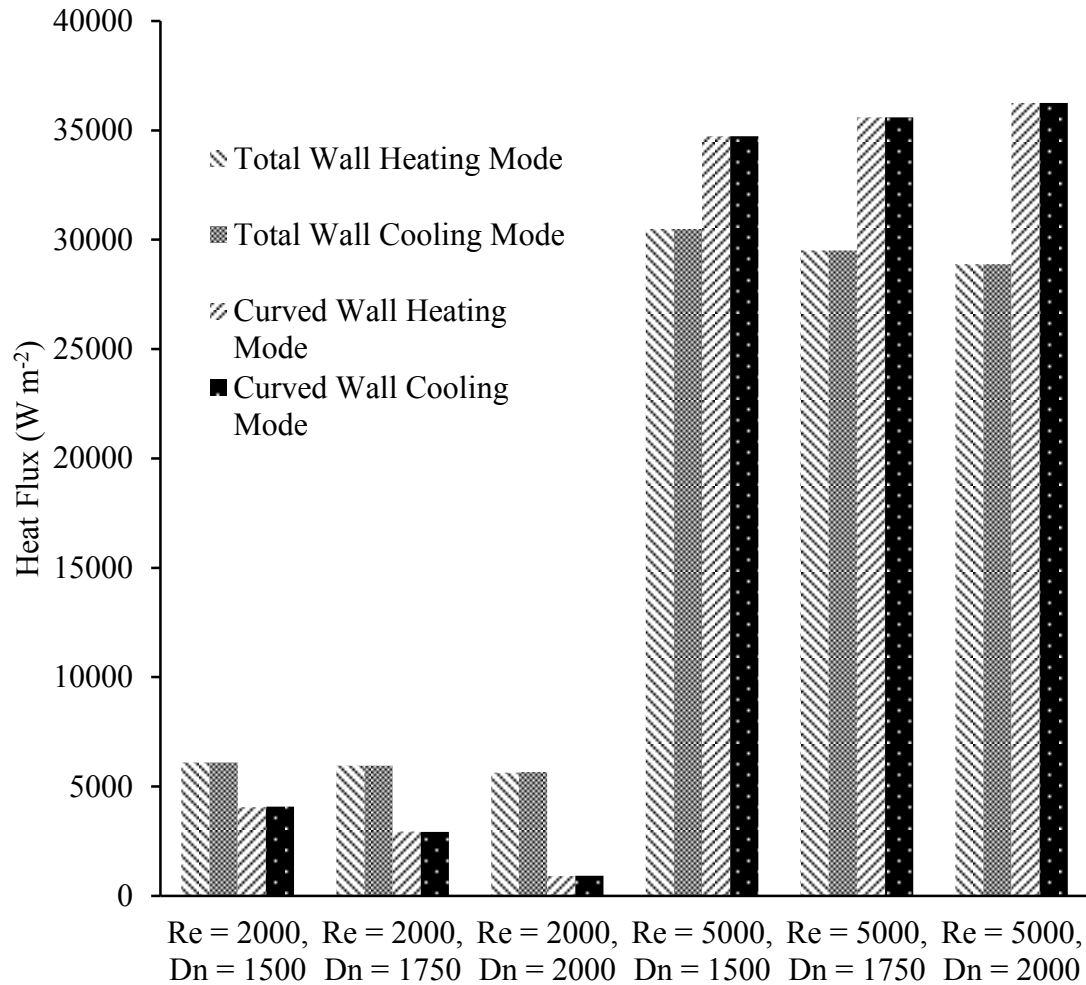
Figure 3.9: Average Wall Heat Flux for the Curved and Total Wall Sections of All Test Cases with ΔT, Cooling Mode (Heat Flux from Fluid to Wall, ΔT = 25 K), Heating Mode (Heat Flux from Wall to Fluid, ΔT = -25 K)

The average total heat flux for Re = 5,000 decreases with increasing Dean Number, whereas in the curved pipe section the heat flux increases with the Dean Number. This indicates that the Dean Number is very important when enhancing heat flux in turbulent pipe flow. The slight decrease in the average total heat flux is partly due

62

to an extension of the straight pipe section, which is relatively ineffective in transferring heat, in keeping the total length fixed at 1.9 m. In geothermal practise, however, there would not be a decrease as the total length is on the order of 100 m; that is, a change in the curved section would not result in a noticeable change in the length of the straight sections.

The average heat flux in the curved section decreases with increasing Dean Number at the transitional Reynolds Number (Re = 2,000). On the other hand, it increases with Dean Number at the low turbulence Reynolds Number (Re = 5,000). More importantly, the corresponding average heat flux jumps by a factor of approximately five when increasing the Reynolds Number from 2,000 to 5,000. The total heat transfer rate is graphed in Figure 3.10. Only the results corresponding to the heating mode are plotted, recalling from Figure 3.9 that other than the sign reversal there is no difference in the heat transfer whether the heat is absorbed or rejected from the fluid. The trend of these values will give an indication of how the Dean Number affects the total wall heat flux of the fixed length system independent of the length that the curved section has as a result of the Dean Number. Unlike Figure 3.9, which indicates a reduction of wall heat flux with increasing Dean Number; increasing trends from Figure 3.10 show that if the length of the curved pipe was equal among all Dean Numbers, i.e. spiraling of the curved section, then the heat flux of the system would increase as a result of increased Dean Numbers. Essentially, this metric provided an explanation as to what would happen if the U-Bend spiraled around at the strong curvature to an equivalent length along all test cases.
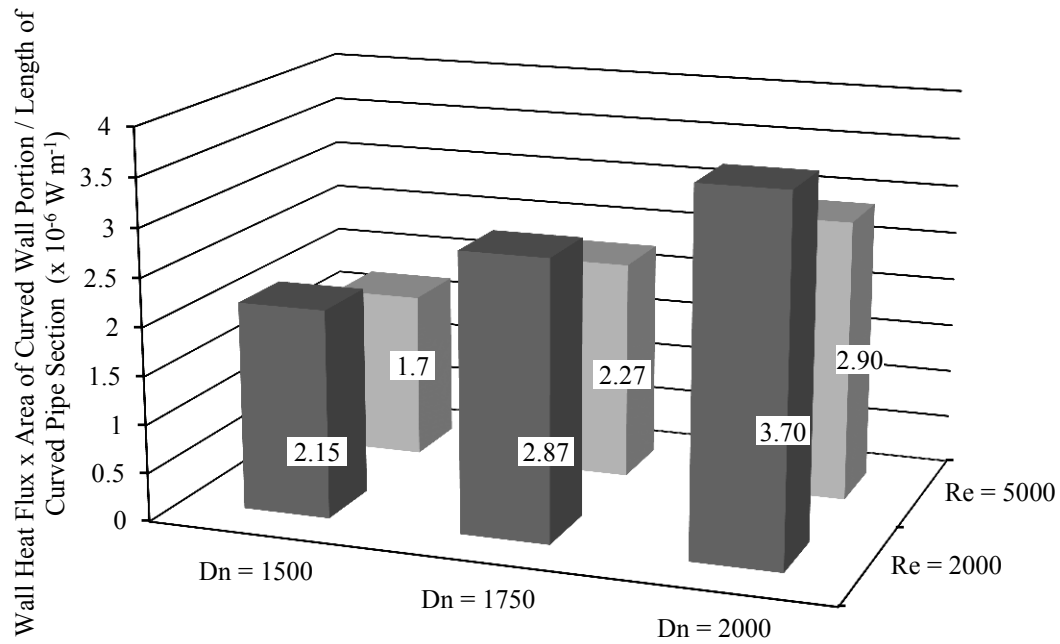
Figure 3.10: Total Heat Transferred for Curved Wall Section per Curved Wall Unit

Length

6.0 CONCLUSION

Ground source heat pumps should be studied and trends for design and implementation behaviours will prove beneficial to future industrial progression. This paper studied the effects of the Reynolds, Dean Numbers and temperature difference on U-Bend pipes specifically for the application of ground source heat pumps. Three Dean Numbers and two Reynolds Numbers were tested in the isothermal case, the heating case and the cooling case. The temperature difference between the wall and the pipe was 25 K

for both the cooling and heating case; however, one being positive and the other one being negative. The contours of the heating and cooling cases, as well as the results ultimately became equal to each other as expected, resulting in no unexpected behaviour. The Reynolds Number, when comparing the absolute heat flux at either the curved or total wall sections provides more of an impact over the fixed length. The Dean Number only has a significant effect on the heat transfer in the curved section of low turbulence, $Re = 5,000$. For all other scenarios the Dean Number destroys heat transfer in fixed length pipes as it increases. Only when the total heat flux per unit of curved area is extracted can it be realized that the Dean Number increases heat flux in fixed length pipe systems as it increases. This is due to the limitations of the test matrix in that the curved wall will decrease in area as the Dean Number increases imposing a resident time problem. In that because the curved section is shorter the fluid will not be exposed to the benefits for equal periods of time resulting in a total loss on the system heat flux. Also, the magnitude of the heat flux per unit of curved area is higher for transitionary flow than for low turbulence flow. This says that the curved section of the pipe is where most of the heat transfer takes place and the Dean Number has a greater effect than the Reynolds Number.

ACKNOWLEDGEMENTS

REFERENCES

[1]   J. Brenn, "Comparison of natural gas driven heat pumps and electrically driven heat pumps with conventional systems for building heating purposes," *Energy & Buildings*, vol. 42, no. 6, pp. 904–908, Jun. 2010.

[2]   J. Yang, *Geothermal energy, technology and geology*. New York: Nova Science Publishers, 2012.

[3]   B. Erdogmus, "Economic assessment of geothermal district heating systems: A case study of Balcova-Narlidere, Turkey," *Energy & Buildings*, vol. 38, no. 9, pp. 1053–1059, 2006.

[4]   B. Sanner, "Current status of ground source heat pumps and underground thermal energy storage in Europe," *Geothermics*, vol. 32, no. 4–6, pp. 579–588, 2003.

[5]   O. Ozgener, L. Ozgener, and J. W. Tester, "A practical approach to predict soil temperature variations for geothermal (ground) heat exchangers applications," *International Journal of Heat and Mass Transfer*, vol. 62, pp. 473–480, 2013.

[6]   T. T. Chow, "Estimation of soil temperature profile in Hong Kong from climatic variables," *Energy & Buildings*, vol. 43, no. 12, pp. 3568–3575, Dec. 2011.

[7]   N. Mattsson, "Advanced compact device for the in situ determination of geothermal characteristics of soils," *Energy & Buildings*, vol. 40, no. 7, pp. 1344–1352, 2008.

[8]   H. Zeng, N. Diao, and Z. Fang, "Heat transfer analysis of boreholes in vertical ground heat exchangers," *International Journal of Heat and Mass Transfer*, vol. 46, no. 23, pp. 4467–4481, Nov. 2003.

[9]   V. Khalajzadeh, "Parameters optimization of a vertical ground heat exchanger based on response surface methodology," *Energy & Buildings*, vol. 43, no. 6, pp. 1288–1294, Jun. 2011.

[10]   G. Florides and S. Kalogirou, "Ground heat exchangers—A review of systems, models and applications," *Renewable Energy*, vol. 32, no. 15, pp. 2461–2478, Dec. 2007.

[11]   M. Philippe, M. Bernier, and D. Marchio, "Validity ranges of three analytical solutions to heat transfer in the vicinity of single boreholes," *Geothermics*, vol. 38, no. 4, pp. 407–413, Dec. 2009.

[12]   ANSYS Inc., *Fluent Theory Guide*. ANSYS, Inc., 2009.

[13]   N. Deng, "Numerical analysis of three direct cooling systems using underground energy storage: A case study of Jinghai County, Tianjin, China," *Energy & Buildings*, vol. 47, pp. 612–618, Apr. 2012.

[14]   S. Etemad and B. Sundén, "Numerical analysis of turbulent convective heat transfer processes in a square-sectioned U-bend duct," in *15 th Australasian Fluid Mechanics Conf*, 2004.

[15] K. Y. Chung, G. Belfort, W. A. Edelstein, and X. Li, "Dean vortices in curved tube flow: 5. 3-D MRI and numerical analysis of the velocity field," *AIChE Journal*, vol. 39, no. 10, pp. 1592–1602, 1993.

[16] W. Dean, "Note on the motion of fluid in a curved pipe," *Philosophical Magazine Series 7*, vol. 4, no. 20, pp. 208–223, 1927.

[17] T. K. Seng, "Numerical study of Dean vortices in u-tubes of finite aspect ratios," M. Eng. Thesis, National University of Singapore, Singapore, 2007.

[18] W. Kays, M. Crawford, and B. Weigand, *Convective Heat and Mass Transfer*, 4th ed. McGraw-Hill, 2005.

[19] L. Ingersoll and H. Plass, "Theory of the ground heat pipe heat source for the heatpump," *Transactions of the American Society of Heating and Ventilating Engineers.*, 1948.

[20] L. Ingersoll, O. Zobel, and A. Ingersoll, "Heat conduction with engineering, geological and other applications," *Quarterly Journal of the Royal Meteorological Society*, vol. 81, no. 350, pp. 647–648, 1955.

[21] H. S. Carslaw and J. C. Jaeger, *Conduction of heat in solids*. Clarendon Press, 1959.

[22] P. Eskilson, *Thermal analysis of heat extraction boreholes*. Lund: Lund University Press, 1987.

[23] J.-K. Shin, Y.-D. Choi, and J.-S. An, "Numerical analysis of turbulent flow and heat transfer in a square sectioned U-bend duct by elliptic-blending second moment closure," *Journal of Mechanical Science and Technology*, vol. 21, no. 2, pp. 360–371, Feb. 2007.

[24] M. Di Liberto and M. Ciofalo, "A study of turbulent heat transfer in curved pipes by numerical simulation," *International Journal of Heat and Mass Transfer*, vol. 59, no. 0, pp. 112–125, Apr. 2013.

[25] S. Philippe R., "Young-person's guide to detached-eddy simulation grids," NASA Langley Technical Report Server, CR-2001-211032, 2001.

[26] T. H. Shih, W. W. Liou, A. Shabbir, Z. Yang, and J. Zhu, "A new k-ε eddy viscosity for high Reynolds Number turbulent flows - model development and validation," National Aeronautics and Space Administration, TM-106721, 1994.

[27] R. Friedrich, B. Geurts, and O. Métais, *Direct and large-eddy simulation*, 5th ed. Kluwer Academic Publishers, 2004.

[28] J. Pruvost, J. Legrand, and P. Legentilhomme, "Numerical investigation of bend and torus flows, part I : effect of swirl motion on flow structure in u-bend," *Chemical Engineering Science*, vol. 59, no. 16, pp. 3345–3357, Aug. 2004.

[29] K. Sudo, "Experimental investigation on turbulent flow through a circular-sectioned 180° bend," *Experiments in Fluids*, vol. 28, no. 1, pp. 0051–0057, 2000.

CHAPTER 4

ON SECONDARY FLOW STRUCTURES IN COAXIAL PIPE WITH AN END CAP

1.0 INTRODUCTION

Coaxial pipes are systems consists of two individual pipes, concentric to each other [1], [2] as illustrated in Figure 4.1. There are many applications of the Coaxial configuration including heat exchangers, boilers and ground source heat pumps [3]–[5]. These pipe configurations are generally used in part because of their increased performance in heat transfer applications [6], [7]. Ground source heat pumps utilize this pipe configuration with one modification. On one end of the system there is an end cap that redirects the flow from the inner pipe region to the outer pipe region [4]–[8]. This end cap will create huge disturbances in the flow and secondary flow structures in and around the end cap region will begin to develop [9].
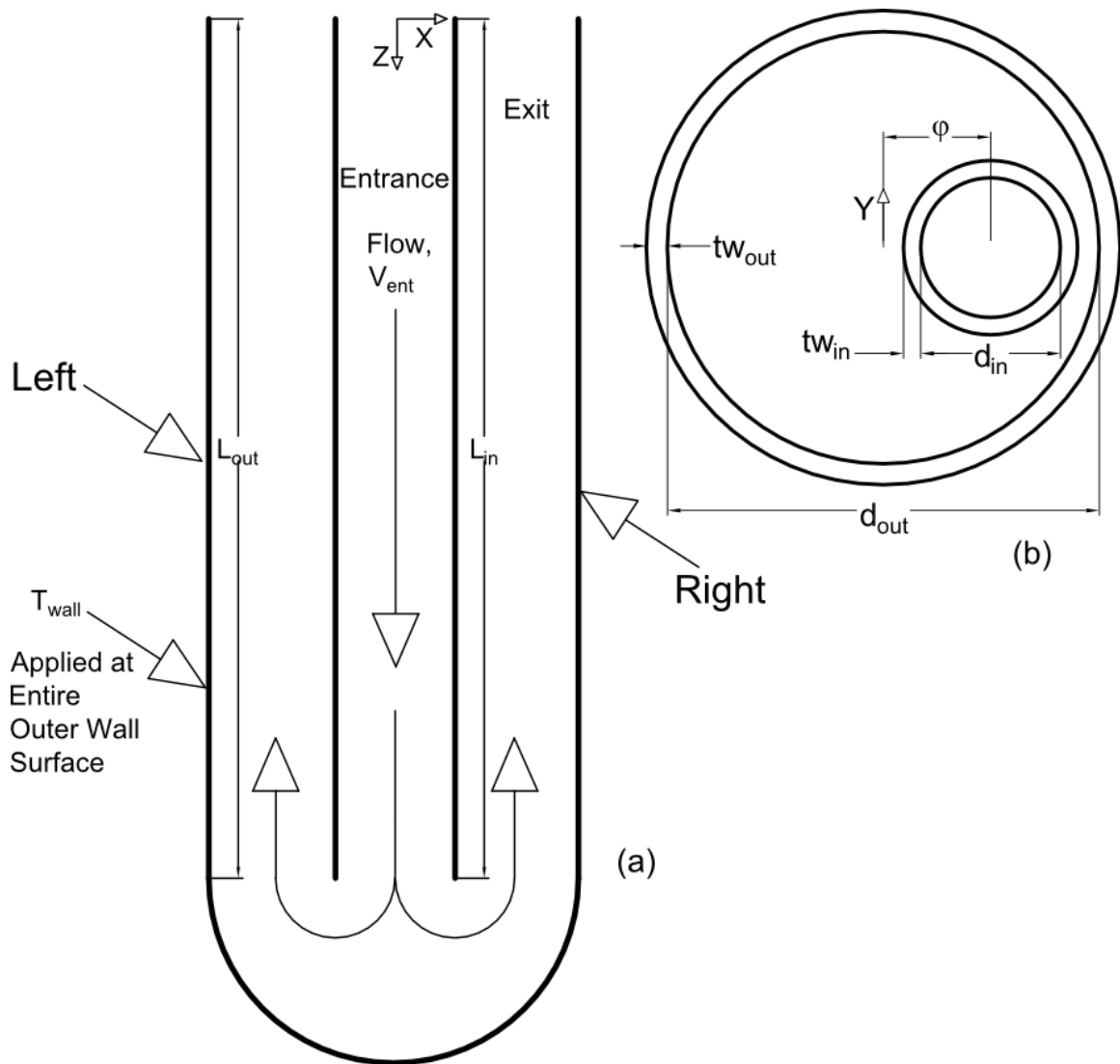
Figure 4.1: Coaxial Pipe with an End Cap (a) Side View and (b) Top View

The end cap poses an interesting situation as the flow will tend to disperse upon contact with the end cap and evenly go to the outer pipe region of the system assuming the inlet conditions are symmetric in all directions. The creation of a toroidal shaped vortex ring can occur in the end cap as a result of this even dispersal into the straight outer pipe region [10]–[14]. The vortex structures are generally defined as swirling

72

structures of flow around a central axis [15]–[17]. There are many vortex structures found in the literature that are defined as Dean [18], [19], Görtler [20], Taylor-Couette [21] and Taylor-Green [22] because the associated researchers found that those particular structures exist for a category of flows and that they can be well defined numerically. For example, Dean Vortices are defined by the Dean Number and occur in curved pipes when the curvature becomes too great and the bulk flow is converted into transverse secondary flow creating vortex structures towards the outer region of the curved section [23]–[26]. The Dean Number is a non-dimensional parameter and it is defined as the ratio between the transverse flow caused by curvature change or centrifugal forces and the longitudinal flow.

In ground source heat pump applications it is common for the inner pipe not to be structurally supported at the bottom and hence able to move freely in the outer tube in any lateral direction. This eccentricity of the inner pipe will introduce an asymmetric situation and the flow will behave as such, with more volume of fluid entering one side of pipe than the other. The vortex structures will either be enhanced or destroyed. The Coaxial pipe then goes from being symmetric in all directions to only symmetric in one direction. For ground source heat pump applications this is particularly important as the design of a system implementing this pipe configuration will need to be altered to account for this loss or gain in performance.

Coaxial pipes have been previously studied by many researchers for their applications [27]–[31]. Overall, these researchers were looking at the Coaxial system as a whole. This creates a need for expanding the work into the realm of ground source heat pumps using more detailed analysis techniques. Zanchini et al. in 2009 looked at Coaxial

73

pipes in heat exchangers. But their work is limited to assessing of the thermal performance when under varied flow direction and analyzing the thermal short circuiting troubles [1], [31] rather than focusing on ways to improve the design estimation for the optimal length of the ground loop.

This study will investigate the effects of the inner pipe offset, eccentricity, on the resulting vortex structures in the end cap region. This study will employ numerical techniques developed in FLUENT backed by limited flow visualization methods. The study will limit the simulations to the laminar flow regime, as vortex activity caused by geometry is more easily isolated from bulk turbulent flow. However, because of this parametric study, enhanced design may be implemented that can account for the eccentricity effects in the inner pipe.

2.0 EXPERIMENTAL SETUP

For limited validation of the model, an experiment was conducted to visualize the rotating flow structure with colored dye. The experimental setup is illustrated in Figure 4.2. It consists of an outer pipe with a 75 mm diameter and an inner pipe of 25 mm diameter and 6 mm wall thickness. Tap water flows through an 18 mm flexible hose to a valve acting as a flow limiter to control the flowrate. Following this the tap water flows through a flowrate monitor to capture the flowrate of the fluid through the system. Then the water enters the inner pipe of the system, is redirected by the end cap and flows through the outer pipe region. To visualize the vortex in the end cap region, blue dye will be injected via a syringe and small, 2 mm inner diameter, pipe into the outlet of the inner pipe in the end cap region.

74
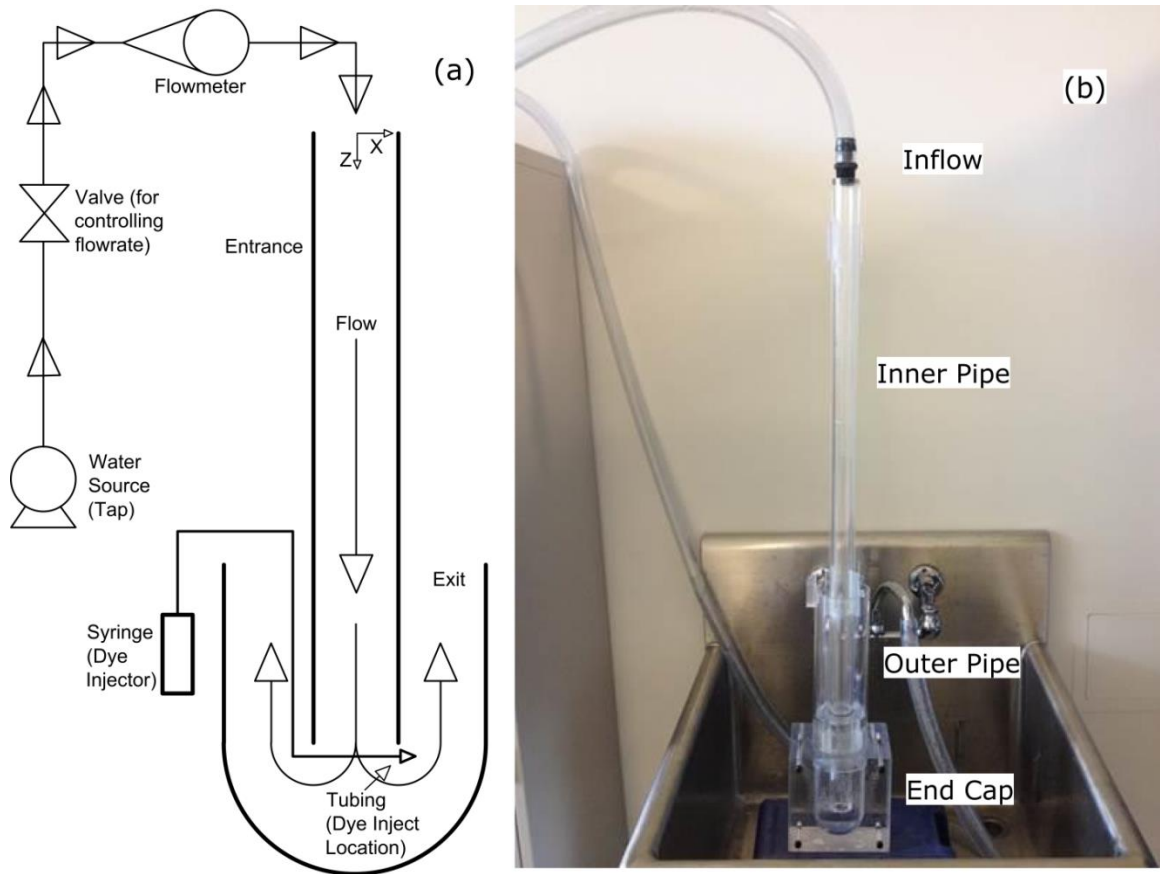
Figure 4.2: Flow through Coaxial Pipe (a) Schematic (b) Experimental Setup

3.0 NUMERICAL MODEL

This study investigates the steady state vortex structure located in the end cap region. A Reynolds Averaged Navier Stokes (RANS) model was selected for this simulation as Large Eddy Simulation (LES) and Detached Eddy Simulation (DES) are designed for transient simulations [32]–[37]. The simulations in this study are limited to steady state analysis as in practice ground source heat pumps employing Coaxial pipe

75

configurations are always in operation. In particular the Realizable k-ε model was used as it has been extensively used in the literature for pipe flow [38], [39]. Direct Numerical Simulation has also been used in literature [2], [39]–[42] although the time and resources required were to demanding and not necessary for this study. The Realizable k-ε model takes on the following form with modifications from the standard k-ε model [38]. Equations 1 and 2 show the main equations for the transportable variables, the turbulent kinetic energy, k1, and the dissipation rate, ε, respectively [38].

$$\frac{\partial}{\partial t}(\rho k_1) + \frac{\partial}{\partial x_j}(\rho k_1 u_j) = \frac{\partial}{\partial x_j}\left[\left(\mu + \frac{\mu_t}{\sigma_{k_1}}\right)\left(\frac{\partial k_1}{\partial x_j}\right)\right] + G_{k_1} + G_b - \rho\epsilon - Y_M + S_{k_1} \qquad (1)$$

$$\frac{\partial}{\partial t}(\rho\epsilon) + \frac{\partial}{\partial x_j}(\rho\epsilon u_j)$$

$$= \frac{\partial}{\partial x_j}\left[\left(\mu + \frac{\mu_t}{\sigma_\epsilon}\right)\left(\frac{\partial\epsilon}{\partial x_j}\right)\right] + \rho C_1 S\epsilon - \rho C_2\left(\frac{\epsilon^2}{k_1 + \sqrt{(\nu\epsilon)}}\right) + C_{1\epsilon}\frac{\epsilon}{k_1}C_{3\epsilon}G_b + S_\epsilon \qquad (2)$$

where,

$$\mu_t = \frac{\rho C_\mu k^2}{\epsilon} \qquad (3)$$

$$C_\mu = \frac{1}{A_0 + \frac{A_s k U^*}{\epsilon}} \qquad (4)$$

Here G_{k1} is the generation of the turbulence kinetic energy due to the mean velocity gradients, G_b is the generation of the turbulence kinetic energy due to buoyancy (forces induced by gravity and the gradient of density between the materials), Y_M is the contribution of the fluctuating dilation in compressible turbulence to the overall dissipation rate and S_{k1} and S_ε are the source terms.

There are two main differences between the Realizable k-ε and the standard k-ε model. First the eddy viscosity, μ_t, calculated in Equation 3, is not based on a constant C_μ; which is typically assumed to be equal to 0.09. Instead, C_μ is calculated by Equation 4, i.e., it is a function of the mean strain and rotation rates, turbulence fields and the angular velocity of the system rotation.

The numerical model for the tests carried out in this study was built using FLUENT [38]. It allows for selection of various turbulence models for CFD simulations [38]. The geometries were built using the default modeller of ANSYS and meshed with the default meshing module of ANSYS [38]. In the numerical model, only half the pipe was modelled as the system is symmetric across the XZ plane for all the cases.

4.0 MESH INDEPENDENCE

To verify the solution independence of mesh four mesh sizes were chosen and two parameters of the simulation were compared. First the velocity, along the outlet of the inner pipe ((-0.0254, 0, -4.925) to (0.0254, 0, -4.925)), was calculated and shown in Figure 4.3 for all the meshes tested. The velocity was chosen as a non-sensitive parameter of the simulation. The relative error between mesh 3 and 4 is very little, <1%. The second parameter is the turbulence intensity, along the inner wall of the inner pipe ((0.025, 0, 0)

77

to (0.025, 0, -4.925)), and chosen as a sensitive parameter to the simulation. The results of the study for the turbulence intensity are shown in Figure 4.4 and the discrepancy between the mesh 3 and 4 is also very small, <1%. As a result mesh 3 will be used for the test cases. Mesh 3 was developed using a maximum cell volume of 1×10^{-10} m^3.
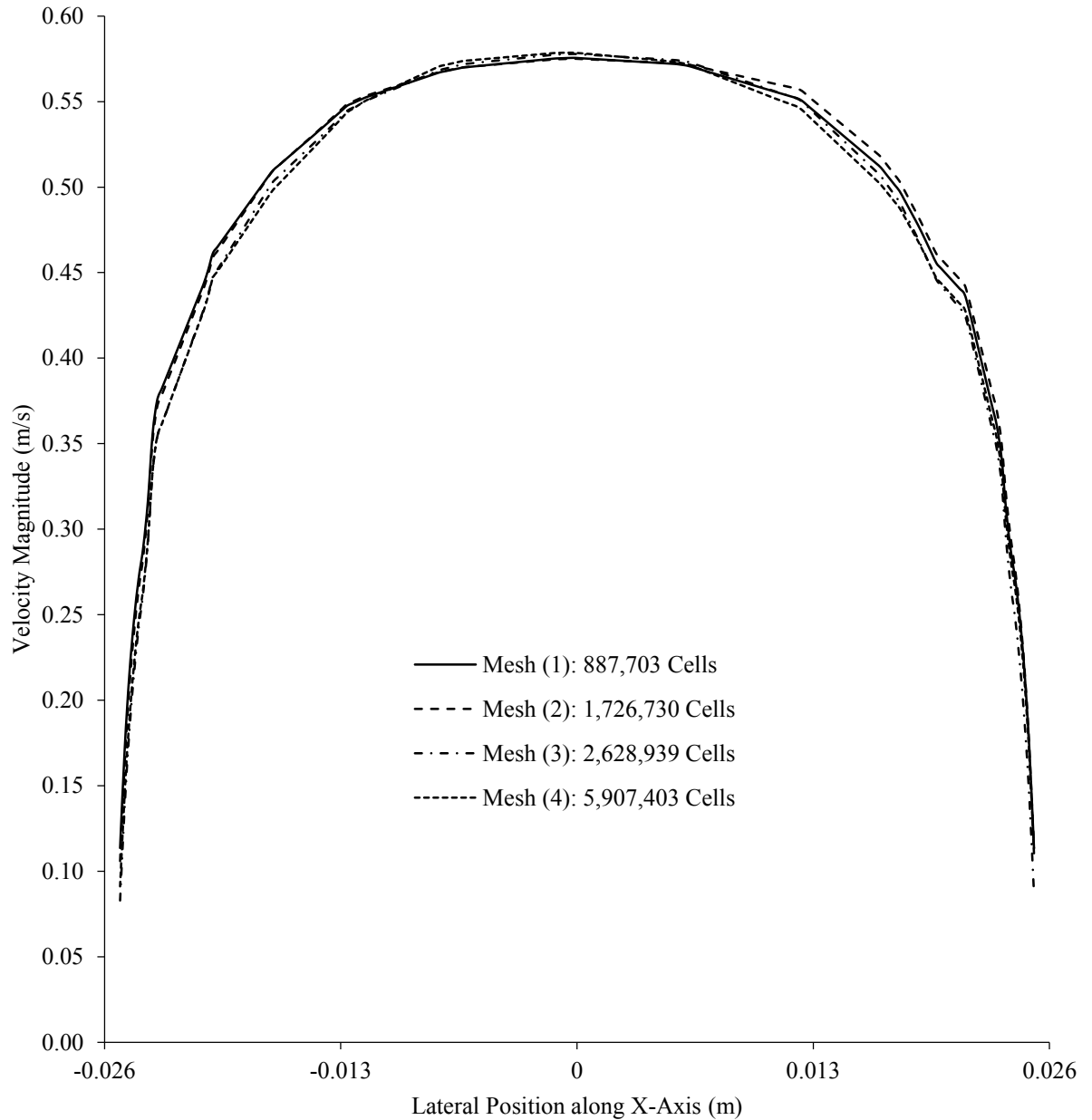
Figure 4.3: Variation of Velocity at Outlet of Inner Pipe (Y = 0 m, Z = -4.925 m) with

Mesh Densities for Coaxial Pipe with Inner Pipe of $F_{ecc} = 0$
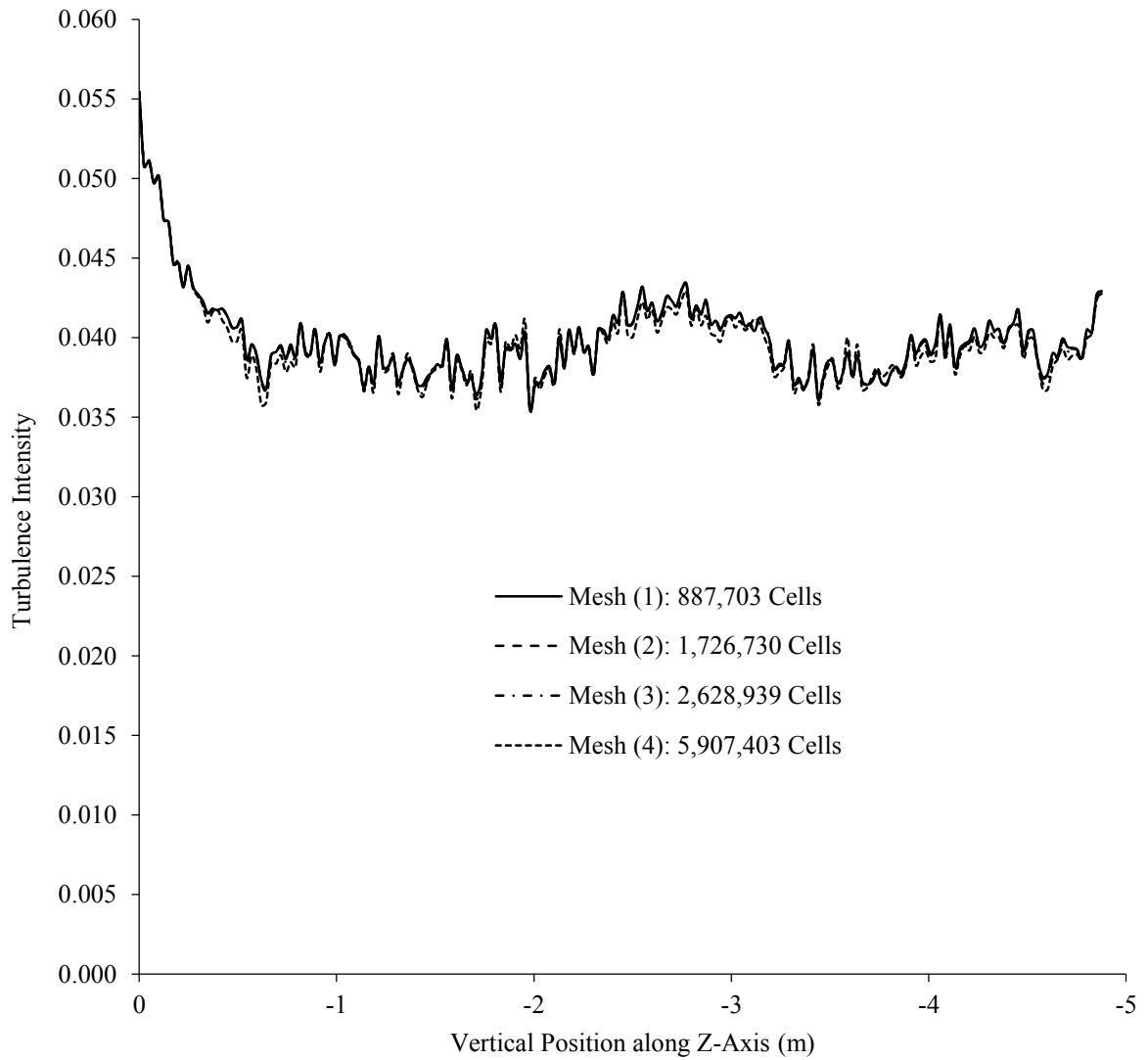
Figure 4.4: Variation of Turbulence Intensity at Wall of Inner Pipe (X = 0.025 m, Y = 0

m) with Mesh Densities for Coaxial Pipe with Inner Pipe of $F_{ecc} = 0$

79

5.0 TEST PROPERTIES

For the mathematical simulations the following section will detail the geometric and boundary conditions for the parametric study consisting of the inner pipe offset, the Reynolds Number and the operating mode. The Coaxial system and its nomenclature is illustrated in Figure 4.1. The inlet entrance is positioned at (0, 0, 0). The Coaxial configuration in this study will have the following properties. The pipe will have a straight length of 4.925 m and an outer diameter, d_{out}, of 150 mm. The inner diameter, d_{in}, is 50.8 mm with an inner wall thickness, $t_{p,in}$, being 6.35 mm and an outer wall thickness, $t_{p,out}$, of zero since it has no effect on flow simulation. The entrance velocity will be constant through all tests and equal to 0.01 m s^{-1}. The corresponding Reynolds Number of all the simulations based on this entrance velocity is 500. Thus the incoming flow into the end cap is laminar. The fluid chosen is water as that is the typical 'working fluid' of ground source heat pumps. The density is 998.2 kg m^{-3} and the dynamic viscosity is 0.001003 Pa s at a temperature of 298 K (25 ^{o}C). The walls are non-slip smooth entities with no thermal characteristics, thus creating an isothermal system. As stated earlier, five eccentricity scenarios are to be studied. The eccentricity, F_{ecc}, as defined in this paper will be equal to $\varphi/(r_{out} - (r_{in} + t_{p,in}))$ where φ is the inner pipe offset, in mm, along the X-axis, r_{in} is the inner pipe radius, r_{out} is the outer pipe radius and $t_{p,in}$ is the inner pipe wall thickness. The maximum possible eccentricity factor is one and would represent when the inner pipe is in contact with the outer pipe. The minimum value then becomes zero and is when the inner pipe is completely concentric with the outer pipe. The test cases are summarized in Table 4.1.

80

Table 4.1: Test Cases

Case	F_{ecc}	Inner Pipe Offset (φ, mm)
1	0	0
2	0.21	8.85
3	0.41	17.7
4	0.62	26.55
5	0.82	35.4

6.0 RESULTS AND DISCUSSIONS

The following sections will detail the results of this study with four main components. The first section will show the results of the experimental visualization. The second section will detail the evolution of the velocity contours and the streamlines of the bulk flow with increasing eccentricity factor. The third section will detail the change of the largest vortical structure shown with 3D imagery. The fourth section presents the results of studies on how the eccentricity of the inner pipe will either promote or destroy the total turbulent energy downstream of the end cap.

6.1 EXPERIMENTAL VISUALIZATION

For the test case with zero eccentricity an experimental visualization was accomplished. The setup is detailed in Figure 4.2. The test was performed for 12 different Reynolds Numbers but only the laminar test was easily captured. The dye immediately progressed downward toward the bottom of the end cap and progressed to continuously loop in the vortex ring as shown in Figure 4.5. Figure 4.5 is a still capture of one of the frames in a video recording. After some time, approximately one second, the dispersion takes over on the colored dye and it progresses up the straight outer pipe region. There is

81

good agreement with Figure 4.6 (a) showing the corresponding numerical plot of the associated rotating structure.

Figure 4.5: Vortex Ring Formation in End Cap Region
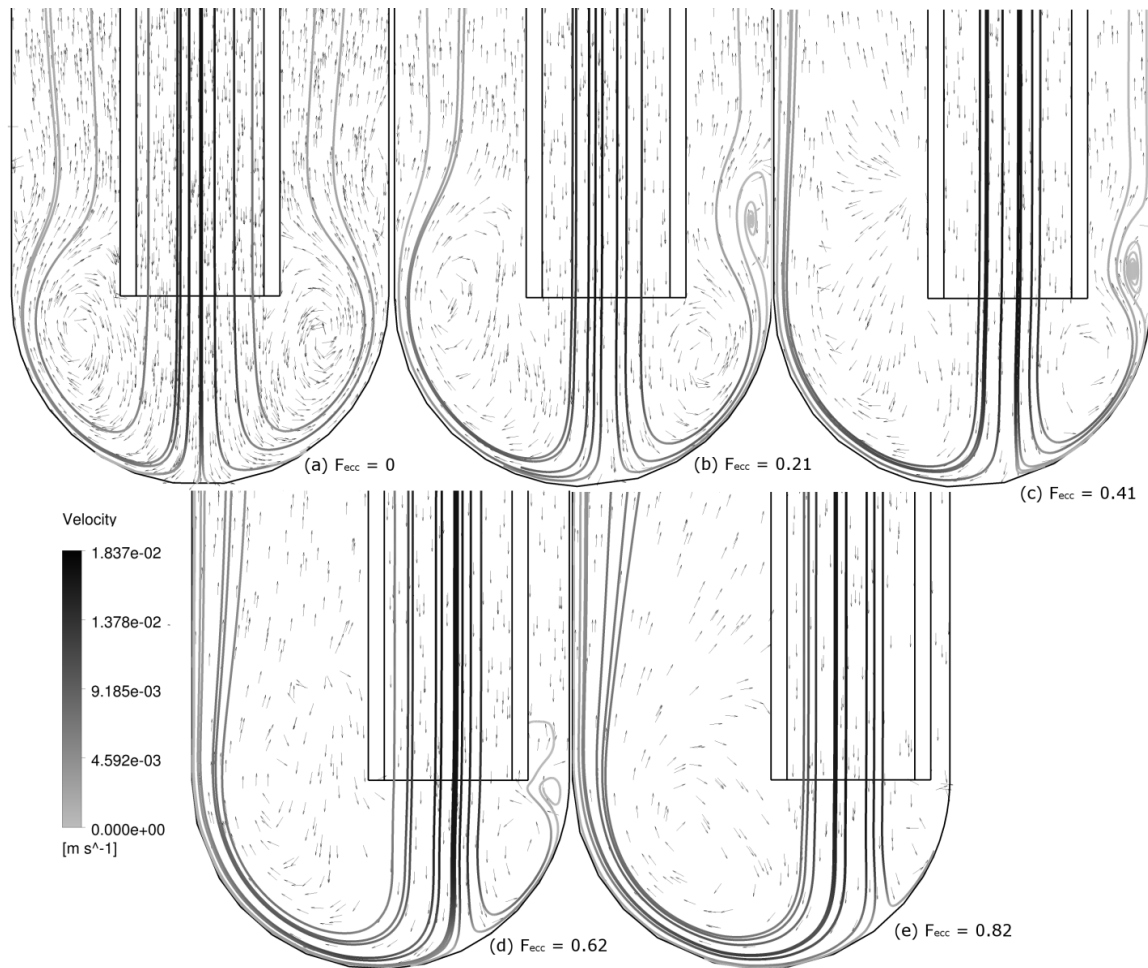
Figure 4.6: Velocity Arrow and Streamline Plot across Plane of Symmetry for End Cap

There are a couple of reasons why this ring forms in the location it does. First, the simplest reason is that because the flow generally goes from the inner pipe to the outer wall and progresses up the wall at high speeds there is a region of lower pressure that exists at the centre of this structure. This lower pressure sucks the fluid from the outer wall at the edge of the end cap in the outer pipe and brings it toward its centre. The flow will tend towards this centre orbiting around creating this structure that not only helps the fluid pass through the end cap region more efficiently but also increases the turbulence

83

levels in this area. The second is similar but it can be reasoned that as the flow loops around the outer wall of the end cap to the outer pipe centrifugal forces pull the fluid to the inside creating pseudo-Dean- vortex structures at the inner wall of the flow. However, since this flow situation does not directly resemble that of a curved pipe quantifying the magnitude of the vortex with respect to a Dean Number is not possible.

6.2 VELOCITY AND STREAMLINES

In this section the numerical arrow plots combined with streamline plots of the velocity are shown for all the simulations tested. These are plotted for various eccentricities including $F_{ecc} = 0$ to $F_{ecc} = 0.82$. An $F_{ecc} = 0.21$ means that the inner pipe is displaced 21% from center, where the full range of motion is considered as being from the center of the outer pipe to where the inner pipe would be in contact with the outer pipe. Figure 4.6 (a) shows the arrow plot of the case of $F_{ecc} = 0$ that also corresponds with the experimental visualization. It can be seen in the figure that there are two large counter-rotating structures that exist in the end cap region as a result of the interaction with the end cap and the redirection into the outer pipe. The bulk flow, indicated by the streamlines mainly flows around these two structures indicating that these structures exist to separate the flow and redirect the bulk flow into the outer pipe more efficiently.

Figure 4.6 (b) shows the same streamlines and velocity arrows for the case of $F_{ecc} = 0.21$. In this figure the inner pipe begins to move closer to the 'right' wall. The rotating structure in this region starts to shrink and the bulk flow starts to be influenced at about 0.33D (50 mm) downstream of the end cap by a second rotating structure. On the 'left' side the rotating structure starts to grow and manifest itself in the end cap region and

84

slightly downstream of it, at about 0.2D (30 mm). Studies into vortex activity and turbulence levels in fluids traversing in pipes show that larger vortex structures will increase heat transfer efficiency in the regions of the higher activity, thus if the eccentricity can increase this activity it can increase heat transfer [43].

The streamlines and velocity arrow plot as shown in Figure 4.6 (c) are for the case of F_{ecc} = 0.41. In this flow simulation the 'right' structure continues to shrink and more bulk flow starts to be consumed by the developed flow structure on the 'right' side downstream of the end cap (0.2D or 30 mm). This flow structure also starts to move closer to the end cap region. The 'left' structure starts to be destroyed with the effects of the centrifugal forces pushing all the flow to the outside wall. Similarly, for the case when F_{ecc} = 0.62 as shown in Figure 4.6 (d). The 'right' structure has become very small (about 20% of the size when F_{ecc} = 0). The 'left' structure starts to form again from the larger influence of the centrifugal forces imposed when F_{ecc} increases.

Figure 4.6 (e) shows the streamlines and the velocity arrow plot for F_{ecc} = 0.82. This is the maximum F_{ecc} tested and corresponds to when the inner pipe is almost touching the outer pipe wall. The 'right' structure is now in the path of incoming flow from the outlet of the inner pipe and looking at the arrow plot does not give a clear picture of its existence. The 'left' structure has grown in size (110% of the size when F_{ecc} = 0.62) and it is clear that the centrifugal forces are heavily influencing the flow as the streamlines show the flow staying close to the outer wall for some time downstream of the end cap.

Dean vortices are created because of sharp curvature change and it can be seen in Figure 4.6 (e) that the bulk of the flow follows a simple 180º flow pattern. Because of this simple flow pattern it can be reasoned that the flow will undergo large centrifugal forces and the formation of the well-defined Dean Vortex structures will occur [16]. However, because of the geometry it would be difficult to numerically quantify with any confidence the Dean Number [18] of the flow for that eccentricity scenario.

Overall, for the plane of symmetry for all the factors of eccentricity simulated it can be said that the flows where $F_{ecc} = 0$ and $F_{ecc} = 0.82$ are the most uniform. When $F_{ecc} = 0$ the flow equally distributes into all directions of the outer pipe region and when $F_{ecc} = 0.82$ the flow mostly enters the outer pipe region through one side mimicking the flow conditions of that a curved pipe where there exists large vortex structures occurring at the inner wall. However, for the F_{ecc} in between 0.21 and 0.82 they do not follow conventional patterns but they do show in these figures that they do induce more disturbances in the flow. This would imply that the eccentricity would enhance the chaotic nature of the turbulent flow and induce more mixing and energy transfer. However, as the eccentricity increases, the volume of flow to one side of the inner pipe grows. Downstream of the end cap this could pose a problem in heat transfer applications as the volume of this body of fluid would destroy heat transfer efficiency within the pipe.

6.3 LARGE VORTICAL STRUCTURE

The largest rotating structure induced by the end cap exists in the end cap region. The present section expands on the two-dimensional visualization of the arrow plots and streamlines presented in the last section. To visualize this structure a surface was created

in FLUENT corresponding to 0.1 s^{-1} swirl strength, that is, the frequency at which a particular particle will rotate around a central axis. This is important as the larger this surface becomes the stronger and more influential to the flow this vortex will become. The isometric view of the contour plots of the Y coordinate of the particles are shown in Figure 4.7. These plots are for the surface of particles corresponding to 0.1 s^{-1} swirl strength for the eccentricities investigated in the previous section.
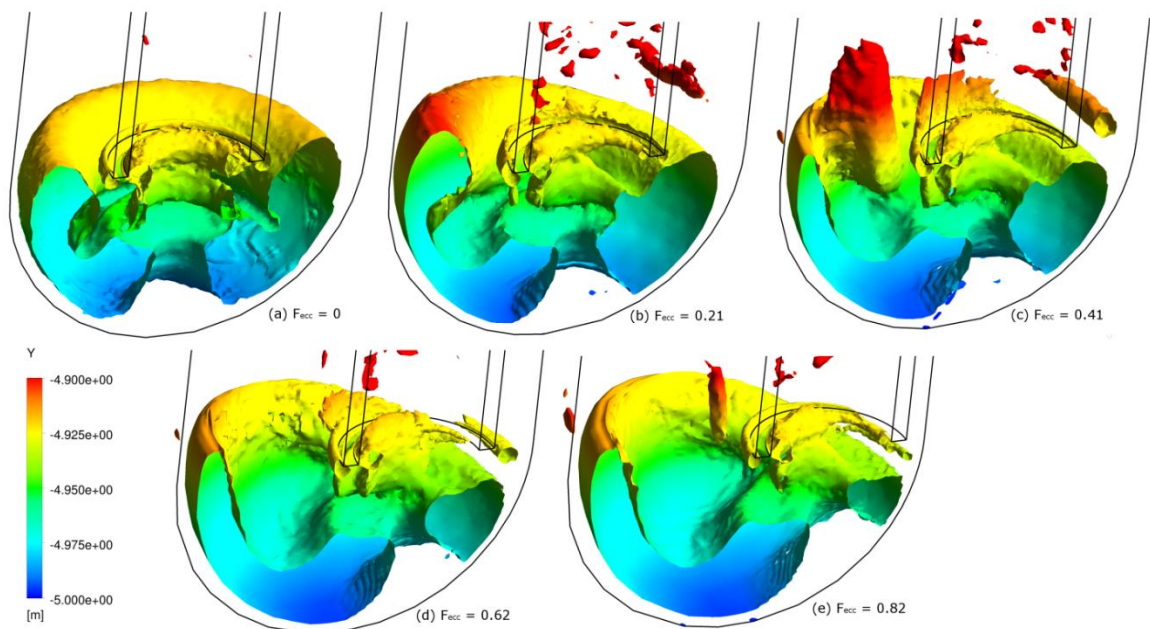
Figure 4.7: Surface of flow with Swirling Strength = 0.1 s^{-1} at End Cap

Figure 4.7 (a) shows the 0.1 s^{-1} swirl strength surface for the case of $F_{ecc} = 0$. This is the case corresponding to the inner and outer pipe being concentric to each other. The figure illustrates the large horseshoe structure that exists outside of the central rotating structure highlighted in Figure 4.6 (a). This region is symmetrical for both the 'right' and 'left' structures.

www.manaraa.com

For the case pertaining to $F_{ecc} = 0.21$ the aforementioned swirl strength can be found in Figure 4.7 (b). The horseshoe shaped structure on the 'left' gets larger when the eccentricity is increased to 0.21. The separation of the two legs increases as the structure seen in Figure 4.7 (a) gets larger. The 'right' structure becomes more of a circular shape and flow loses its symmetric nature as the eccentricity is introduced.

The surface associated with the eccentricity of 0.41 is shown in Figure 4.7 (c). The 'left' structure in this figure separates more as F_{ecc} increases. The structure starts to traverse downstream of eth end cap with a second structure of equal strength manifests itself between about 0D (0 mm downstream of end cap) and 0.5D (75 mm downstream of end cap). The 'right' structure continues its shrinkage as it is about two-thirds of its original size in Figure 4.7 (b).

Figure 4.7 (d) shows the 0.1 s^{-1} swirl strength surface for the case of $F_{ecc} = 0.62$. The 'left' structure shows even more growth as the rotating structure traverse further up the outer pipe (0.2D compared to 0.1D). The 'right' structure shrinks even further, about one half of its size in Figure 4.7 (c). The structure begins to be influenced by the incoming flow from the inner pipe but does not appear to be destroyed completely by the flow but rather influences that incoming flow to travel other paths. Similarly, Figure 4.7 (e) presents the surface for the case of $F_{ecc} = 0.82$. This case represents the maximum F_{ecc} simulated. The 'left' structure does not change significantly with the increasing F_{ecc}, however, the 'right' structure shrinks to about half of its size from Figure 7 (d) or about 17% of its original size as in Figure 4. 7 (b) when $F_{ecc} = 0.21$.

The preceding figures represent the outer limits of the rotating structure illustrated in the previous section with the arrow plots and streamlines. When $F_{ecc} = 0$ the kidney shaped surface can be seen to stretch, thin and elongate on the 'left' side as the F_{ecc} increases and shrink and become circular on the 'right' side. As the F_{ecc} increases more of the flow will direct itself to the 'left' side where this uniform kidney stretches and thins as F_{ecc} increases, due to a higher volume of flow. This stretching extends the vortex activity into the outer cap region increasing the turbulence activity for length after the end cap region while keeping the activity in the end cap region itself relatively constant. This will generally increase the dispersion and mixing activity in the flow allowing for higher rates of heat and energy transfer throughout the flow [44]. For applications where heat transfer is important this could be beneficial.

6.4 TURBULENT ENERGY DISSIPATION WITH FLOW EXITING END CAP

The turbulent kinetic energy is the energy per unit of the flow associated with eddies and turbulence. This parameter is important because it represents the flows ability to transfer heat and other energies through the flow domain via the turbulent eddies. In particular, where there is increased turbulence, there will typically be higher heat transfer rates for ground source heat pumps or other heat exchanger type applications. As seen in the previous section, changing the F_{ecc} can change how the turbulent activities and vortex structures behave downstream of the end cap. Looking at cross-sections will give a better visual for comparing the ideal F_{ecc} for turbulent activity downstream of the end cap.
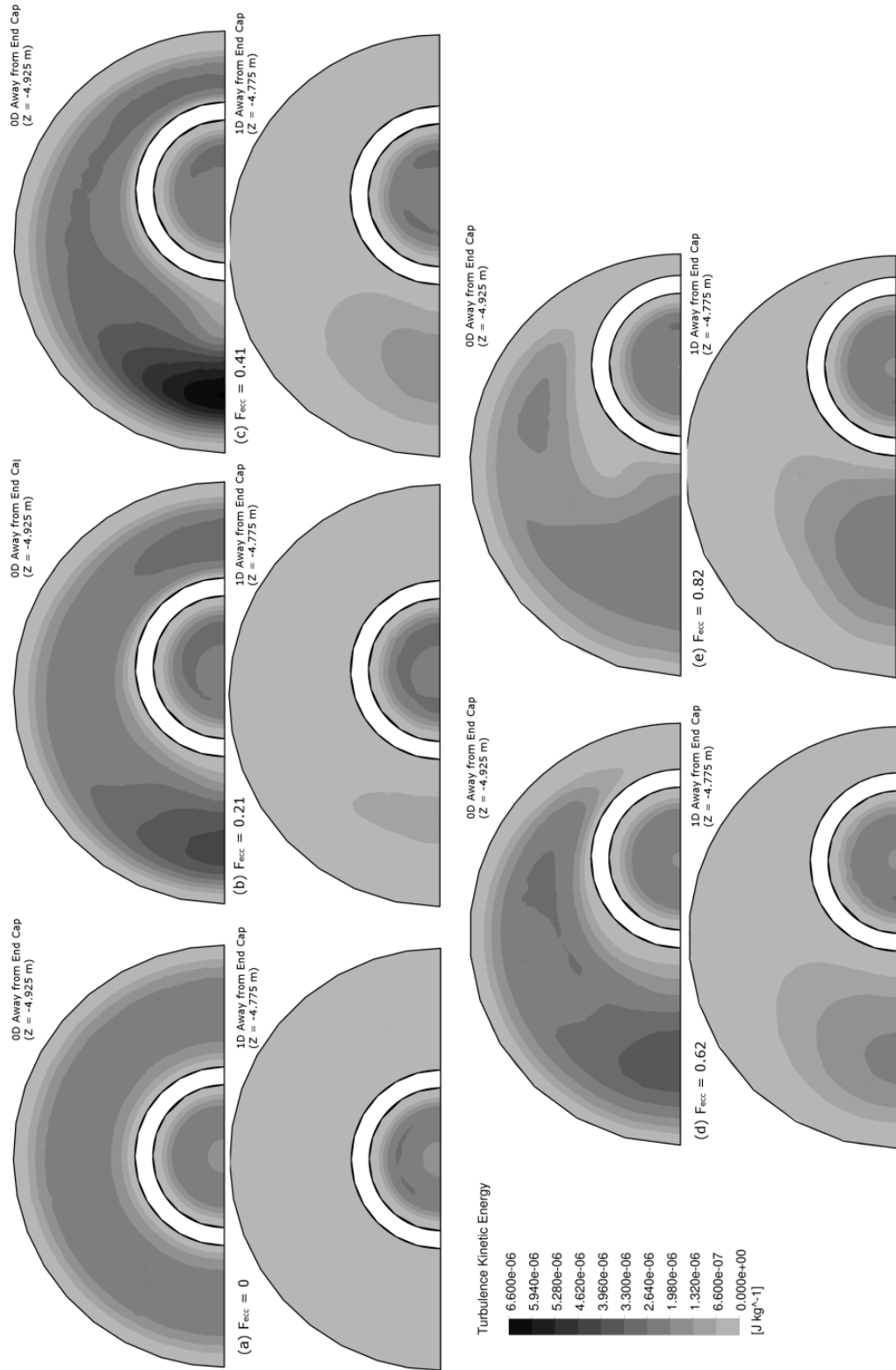
Figure 4.8: Turbulent Kinetic Energy at 0D and 1D away from End Cap Region

90

Figure 4.8 (a) shows the turbulent kinetic energy contours at 0D (0 mm from end cap region, Y = -4.925 m) and 1D (150 mm from end cap region, Y = -4.775 m) for F_{ecc} = 0. The turbulent kinetic energy maximum is 1.98 x 10^{-6} J kg^{-1} at 0D and 0.66 x 10^{-6} J kg^{-1} at 1D. This represents a 66% dissipation of the maximum over 1D (150 mm) of flow. Similarly, Figures 4.8 (b) shows the turbulent kinetic energy contours for F_{ecc} = 0.21. The turbulent kinetic energy maximum is 3.96 x 10^{-6} J kg^{-1} at 0D and 1.32 x 10^{-6} J kg^{-1} at 1D. This represents a 66% dissipation of the maximum over 1D (150 mm) of flow. It can be seen that as the inner pipe offset is first introduced there is a significant increase in the maximum of the turbulent kinetic energy as the turbulence is enhanced by the changing flow pattern. It can be seen how the changing flow structures modify the vortex structures and provide increased mixing potential in the end cap region.

In Figure 4.8 (c) is the turbulent kinetic energy contours at 0D (0 mm from end cap region, Y = -4.925 m) and 1D (150 mm from end cap region, Y = -4.775 m) for F_{ecc} = 0.41. The turbulent kinetic energy maximum is 6.60 x 10^{-6} J kg^{-1} at 0D and 1.98 x 10^{-6} J kg^{-1} at 1D. This represents a 70% dissipation of the maximum over 1D (150 mm) of flow. As well as in Figure 4.8 (d), it is shown the turbulent kinetic energy contours at 0D (0 mm from end cap region, Y = -4.925 m) and 1D (150 mm from end cap region, Y = -4.775 m) for F_{ecc} = 0.62. The turbulent kinetic energy maximum is 3.30 x 10^{-6} J kg^{-1} at 0D and 2.64 x 10^{-6} J kg^{-1} at 1D. This represents a 20% dissipation of the maximum over 1D (150 mm) of flow. The maximum of the turbulent kinetic energy can be seen to exist when the inner pipe eccentricity is 41%. Finally, Figure 4.8 (e) shows the turbulent kinetic energy contours at 0D (0 mm from end cap region, Y = -4.925 m) and 1D (150 mm from end cap region, Y = -4.775 m) for F_{ecc} = 0.82. The turbulent kinetic energy

91

maximum is 1.98 x 10^{-6} J kg^{-1} at 0D and 1.98 x 10^{-6} J kg^{-1} at 1D. This represents a ~0% dissipation of the maximum over 1D (150 mm) of flow.

The preceding figures show the fluids ability to sustain turbulence levels downstream of the end cap for varying F_{ecc}. When F_{ecc} = 0 the uniformity of the symmetrical system can be seen but also that the systems turbulence levels are not sustained very well through 1D. When F_{ecc} = 0.41 the maximum energy levels are seen at the edge of the end cap but are dissipated rather quickly indicating that the offset will generate turbulence more rapidly but it may not be able to sustain it for any purposeful length. When F_{ecc} = 0.82 the turbulence level of the flow is not at its maximum at the edge of the end cap over the range of F_{ecc} simulated but it is the highest over the range at the 1D location. Also, The maximum energy levels in that specific case do not actually disappear but only exist in less of the flow indicating that the highest energy levels exhibited actually last longer. F_{ecc} = 0.82 is the case when the flow most resembles a curved pipe flow with one large vortex structure to the 'left' of the domain. From the literature Dean Number quantifiable flows have been extensively studied as able to create and sustain turbulence levels in and downstream of the curved section. A similar pattern is happening in this pseudo-Dean vortex flow pattern.

7.0 CONCLUSION

The vortex structures in the end cap are very important for heat transfer applications. The offset of the inner pipe has a very influential effect on these rotating structures. The study drew the following conclusions:

- The symmetric (around the central axis of the inner pipe, Z-axis) rotating structure is destroyed once eccentricity is introduced and subsequently becomes two independent structures at 0.41 F_{ecc} (17.7 mm).

- The portion of the rotating structure on the side that the inner pipe is moving towards the outer wall and shrinks with increasing eccentricity but is never completely destroyed as per Figure 4.6 (e).

- When the eccentricity is greater than $F_{ecc} = 0.62$, the flow starts to resemble that of a curved pipe as the bulk flow starts to exhibit the effects of centrifugal forces creating low structures at the outer wall typically known as Dean vortices.

- The turbulence kinetic energy at the edge of the end cap (0D away from end cap) exists at a maximum 6.6 x 10^{-6} J kg^{-1} when the factor of eccentricity is 0.41 (17.7 mm).

- The turbulence kinetic energy dissipates the least (~0%) through 1D (150 mm) downstream of the end cap when the eccentricity is 0.82 (35.4 mm) and the most (70%) when the eccentricity factor is 0.41 (17.7 mm).

ACKNOWEDGEMENTS

REFERENCES

[1]   E. Zanchini, S. Lazzari, A. Priarone, Improving the thermal performance of Coaxial borehole heat exchangers, Energy. 35 (2010) 657–666. doi:10.1016/j.energy.2009.10.038.

[2]   S.Y. Chung, G.H. Rhee, H.J. Sung, Direct numerical simulation of turbulent concentric annular pipe flow: Part 1: Flow field, International Journal of Heat and Fluid Flow. 23 (2002) 426–440. doi:10.1016/S0142-727X(02)00140-6.

[3]   D.J. Ryley, Geothermal energy — problems in heat and fluid flow, International Journal of Heat and Fluid Flow. 3 (1982) 115–123. doi:10.1016/0142-727X(82)90051-0.

[4]   J.W. Lund, Direct utilization of geothermal energy 2010 worldwide review, Geothermics. 40 (2011) 159–180.

[5]   A. Capozza, Design of borehole heat exchangers for ground-source heat pumps: A literature review, methodology comparison and analysis on the penalty temperature, Energy & Buildings. 55 (2012) 369–379.

[6]   A. Bejan, The thermodynamic design of heat and mass transfer processes and devices, International Journal of Heat and Fluid Flow. 8 (1987) 258–276. doi:10.1016/0142-727X(87)90062-2.

[7]   C.J. Wood, H. Liu, S.B. Riffat, Comparative performance of "U-tube" and "Coaxial" loop designs for use with a ground source heat pump, Applied Thermal Engineering. 37 (2012) 190–195. doi:10.1016/j.applthermaleng.2011.11.015.

[8]   B. Sanner, Current status of ground source heat pumps and underground thermal energy storage in Europe, Geothermics. 32 (2003) 579–588. doi:10.1016/S0375-6505(03)00060-9.

[9]   W.C. Reynolds, Fundamentals of turbulence for turbulence modeling and simulation, in: Modern Theoretical and Experimental Approaches to Turbulent Flow Structure and Its Modelling, 1987.

[10]   V. Di Sarli, A. Di Benedetto, E.J. Long, G.K. Hargrave, Time-Resolved Particle Image Velocimetry of dynamic interactions between hydrogen-enriched methane/air premixed flames and toroidal vortex structures, International Journal of Hydrogen Energy. 37 (2012) 16201–16213. doi:10.1016/j.ijhydene.2012.08.061.

[11]   J. Ruostekoski, J.R. Anglin, Creating vortex rings and three-dimensional skyrmions in Bose-Einstein condensates, Physical Review Letters. 86 (2001) 3934.

[12]   T.S. Lundgren, N.N. Mansour, Vortex ring bubbles, Journal of Fluid Mechanics. 224 (1991) 177–196.

[13]   D.I. Pullin, Vortex ring formation at tube and orifice openings, Physics of Fluids (1958-1988). 22 (2008) 401–403. doi:10.1063/1.862606.

[14]   P.N. Shankar, M. Kumar, Toroidal vortex rings, Current Science Bangalore. 66 (1994) 151–151.

[15]   S. Muntean, A. Ruprecht, R. Susan-Resiga, A numerical investigation of the 3d swirling flow in a pipe with constant diameter. part 1: inviscid computation, in: Proceedings of the Workshop on Vortex Dominated Flows-Achievements and Open Problems, 2005: pp. 77–86.

[16]   K.Y. Chung, G. Belfort, W.A. Edelstein, X. Li, Dean vortices in curved tube flow: 5. 3-D MRI and numerical analysis of the velocity field, AIChE Journal. 39 (1993) 1592–1602. doi:10.1002/aic.690391003.

[17]   A. Kalpakli, R. Örlü, P.H. Alfredsson, Vortical patterns in turbulent flow downstream a 90° curved pipe at high Womersley numbers, International Journal of Heat and Fluid Flow. 44 (2013) 692–699. doi:10.1016/j.ijheatfluidflow.2013.09.008.

[18]   W. Dean, Note on the motion of fluid in a curved pipe, Philosophical Magazine Series 7. 4 (1927) 208–223. doi:10.1080/14786440708564324.

[19]   T.K. Seng, Numerical study of Dean vortices in u-tubes of finite aspect ratios, M. Eng. Thesis, National University of Singapore, 2007.

[20]   P. Hall, Taylor—Gortler vortices in fully developed or boundary-layer flows: linear theory, Journal of Fluid Mechanics. 124 (1982) 475–494. doi:10.1017/S0022112082002596.

97

[21]   P. Chossat, G. Iooss, Taylor Vortices, Spirals and Ribbons, in: The Couette-Taylor Problem, Springer New York, 1994: pp. 35–58.

[22]   G.I. Taylor, A.E. Green, Mechanism of the Production of Small Eddies from Large Ones, Proc. R. Soc. Lond. A. 158 (1937) 499–521. doi:10.1098/rspa.1937.0036.

[23]   J. Eustice, Flow of water in curved pipes, Proceedings of the Royal Society A: Mathematical, Physical and Engineering Sciences. 84 (1910) 107–118. doi:10.1098/rspa.1910.0061.

[24]   S.A. Berger, L. Talbot, L.S. Yao, Flow in curved pipes, Annual Review of Fluid Mechanics. 15 (1983) 461–512.

[25]   S.V. Patankar, V.S. Pratap, D.B. Spalding, Prediction of turbulent flow in curved pipes, Journal of Fluid Mechanics. 67 (1975) 583–595.

[26]   A. Noorani, G.K. El Khoury, P. Schlatter, Evolution of turbulence characteristics from straight to curved pipes, International Journal of Heat and Fluid Flow. 41 (2013) 16–26. doi:10.1016/j.ijheatfluidflow.2013.03.005.

[27]   M. Futakawa, K. Kikuchi, Vibrational characteristics of a Coaxial double-pipe, Nuclear Engineering and Design. 94 (1986) 115–123. doi:10.1016/0029-5493(86)90138-X.

98

[28]   A. Giannadakis, K. Perrakis, T. Panidis, A swirling jet under the influence of a Coaxial flow, Experimental Thermal and Fluid Science. 32 (2008) 1548–1563. doi:10.1016/j.expthermflusci.2008.04.010.

[29]   H. Han, J.T. Kim, H.T. Ahn, S.J. Lee, A three-dimensional performance analysis of all-glass vacuum tubes with Coaxial fluid conduit, International Communications in Heat and Mass Transfer. 35 (2008) 589–596. doi:10.1016/j.icheatmasstransfer.2007.11.006.

[30]   M. Hatami, D.D. Ganji, Heat transfer and flow analysis for SA-TiO2 non-Newtonian nanofluid passing through the porous media between two Coaxial cylinders, Journal of Molecular Liquids. 188 (2013) 155–161. doi:10.1016/j.molliq.2013.10.009.

[31]   E. Zanchini, S. Lazzari, A. Priarone, Effects of flow direction and thermal short-circuiting on the performance of small Coaxial ground heat exchangers, Renewable Energy. 35 (2010) 1255–1265. doi:10.1016/j.renene.2009.11.043.

[32]   C. Heschl, K. Inthavong, W. Sanz, J. Tu, Evaluation and improvements of RANS turbulence models for linear diffuser flows, Computers & Fluids. 71 (2013) 272–282. doi:10.1016/j.compfluid.2012.10.015.

[33]   J.L. Lumley, Computational modeling of turbulent flows, Advances in Applied Mechanics. 18 (1978) 123–176.

[34]   S. Philippe R., Young-person's guide to detached-eddy simulation grids, NASA Langley Technical Report Server, CR-2001-211032, 2001.

[35]   T.H. Shih, W.W. Liou, A. Shabbir, Z. Yang, J. Zhu, A new k-ε eddy viscosity for high reynolds number turbulent flows - model development and validation, National Aeronautics and Space Adminitration, TM-106721, 1994.

[36]   C. Lian, G. Xia, C.L. Merkle, Impact of source terms on reliability of CFD algorithms, Computers & Fluids. 39 (2010) 1909–1922. doi:10.1016/j.compfluid.2010.06.021.

[37]   S. Gorji, M. Seddighi, C. Ariyaratne, A.E. Vardy, T. O'Donoghue, D. Pokrajac, et al., A comparative study of turbulence models in a transient channel flow, Computers & Fluids. 89 (2014) 111–123. doi:10.1016/j.compfluid.2013.10.037.

[38]   ANSYS Inc., Fluent Theory Guide, ANSYS, Inc., 2009.

[39]   M. Nikjooy, K.C. Karki, H.C. Mongia, V.G. McDonell, G.S. Samuelsen, A numerical and experimental study of Coaxial jets, International Journal of Heat and Fluid Flow. 10 (1989) 253–261. doi:10.1016/0142-727X(89)90044-1.

[40]   J. Ahn, J.H. Lee, S.J. Jang, H.J. Sung, Direct numerical simulations of fully developed turbulent pipe flows for Reτ = 180, 544 and 934, International Journal of Heat and Fluid Flow. 44 (2013) 222–228. doi:10.1016/j.ijheatfluidflow.2013.05.022.

[41]   L. Redjem-Saad, M. Ould-Rouiss, G. Lauriat, Direct numerical simulation of turbulent heat transfer in pipe flows: Effect of Prandtl number, International Journal of Heat and Fluid Flow. 28 (2007) 847–861. doi:10.1016/j.ijheatfluidflow.2007.02.003.

[42]   A. Kalpakli, R. Örlü, Turbulent pipe flow downstream a 90° pipe bend with and without superimposed swirl, International Journal of Heat and Fluid Flow. 41 (2013) 103–111. doi:10.1016/j.ijheatfluidflow.2013.01.003.

[43]   M. Fiebig, Vortices and Heat Transfer, ZAMM - Journal of Applied Mathematics and Mechanics / Zeitschrift Für Angewandte Mathematik Und Mechanik. 77 (1997) 3–18. doi:10.1002/zamm.19970770103.

[44]   R. Benzi, G. Paladin, G. Parisi, A. Vulpiani, On the multifractal nature of fully developed turbulence and chaotic systems, Journal of Physics A: Mathematical and General. 17 (1984) 3521.

CHAPTER 5

THE EFFECTS OF INNER PIPE OFFSET ON COAXIAL GROUND SOURCE HEAT EXCHANGERS

1.0 INTRODUCTION

Ground source heat pumps provide an efficient and cost effective way to heat and cool commercial structures or residential buildings [1]. The earth acts as the heat source or the sink depending on whether it is operating in the heating cycle and the cooling cycle. A schematic of a typical GSHP is shown in Figure 5.1. In the heating cycle the ground is used as a heat source, i.e., colder fluid is pumped through a pipe loop in the earth and is pre-heated for the surface heat exchanger. Whereas in the cooling cycle, the ground is the heat sink, i.e., the ground acts to pre-cool the fluid for more efficient heat removal from the building [2]. While there are many methods of employing ground source heat pumps, the most common setup encountered in practice is the vertical ground source heat pump configuration [3]. In this configuration specifically, the ground loop is of a vertical configuration that reaches depths of up to 250 m. This configuration maintains many advantages over the alternatives [4]. Disadvantages to the vertical ground source heat pump configuration is the extensive drilling and pipe costs that are needed to meet the thermal requirement of the establishment on the surface [5].

102
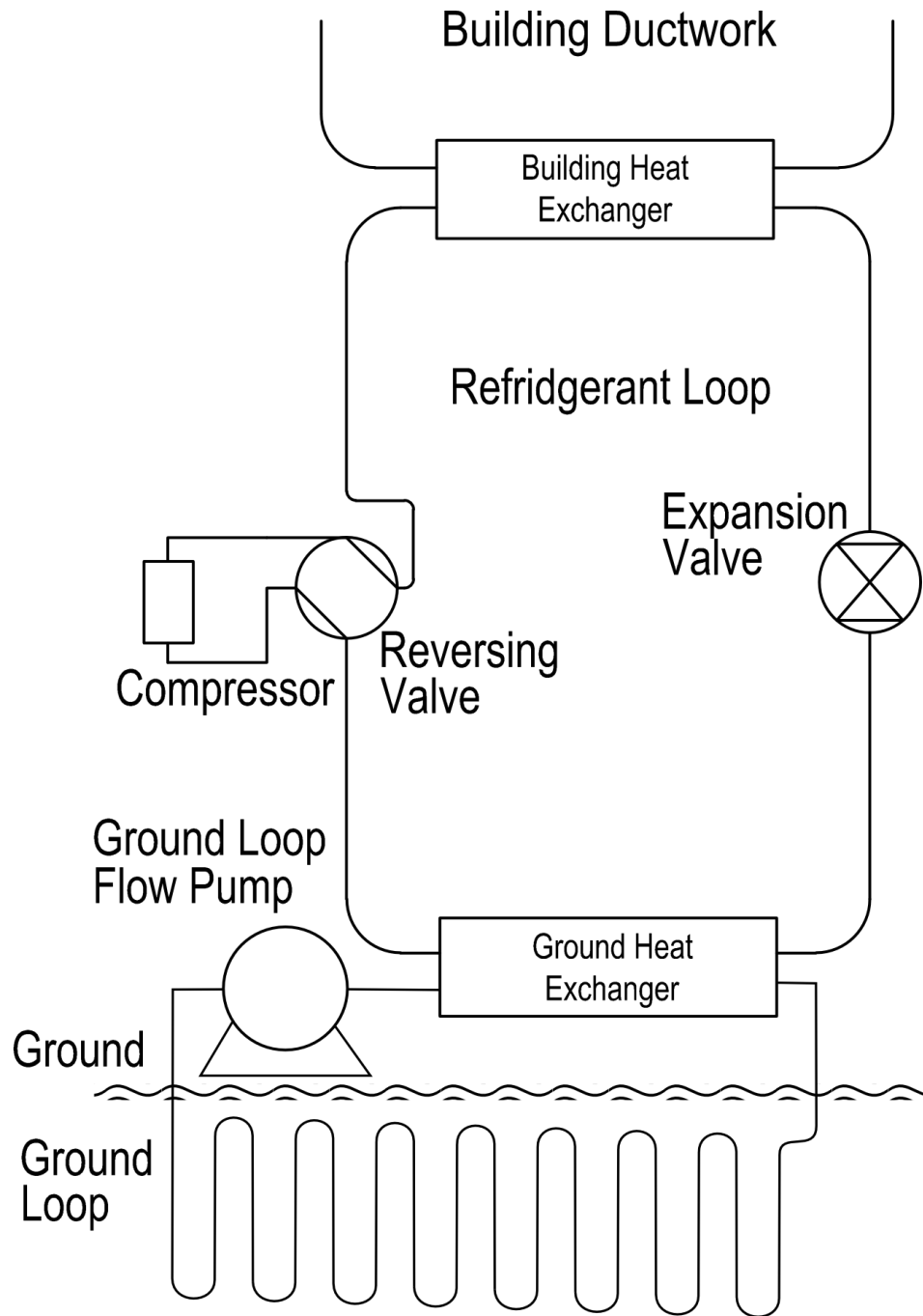
Figure 5.1: Typical Ground Source Heat Pump System

There are many types of vertical ground loop configurations; they include, the vertical Single U-Bend and the Coaxial pipe systems. The focus of this paper will be the Coaxial pipe loop configuration. A schematic of this pipe loop is shown in Figure 5.2, showing the top and side views of the essential components. Essentially a smaller radius pipe is installed in a larger radius pipe creating what is known as a Coaxial configuration as the central axes of both the inner and outer pipes are the same [6]. Shown in Figure 5.2, it can be seen that the fluid will enter the loop through the inner pipe and be redirected to the surface through the larger, outer pipe that encases the smaller inner pipe [6]. It has shown to improve thermal performance over the more traditional pipe loop configurations such as the Single U-Bend setup. Coaxial ground loop configurations show lower pressure drops over U-Bends [7], which means reduced power requirements for its operation.
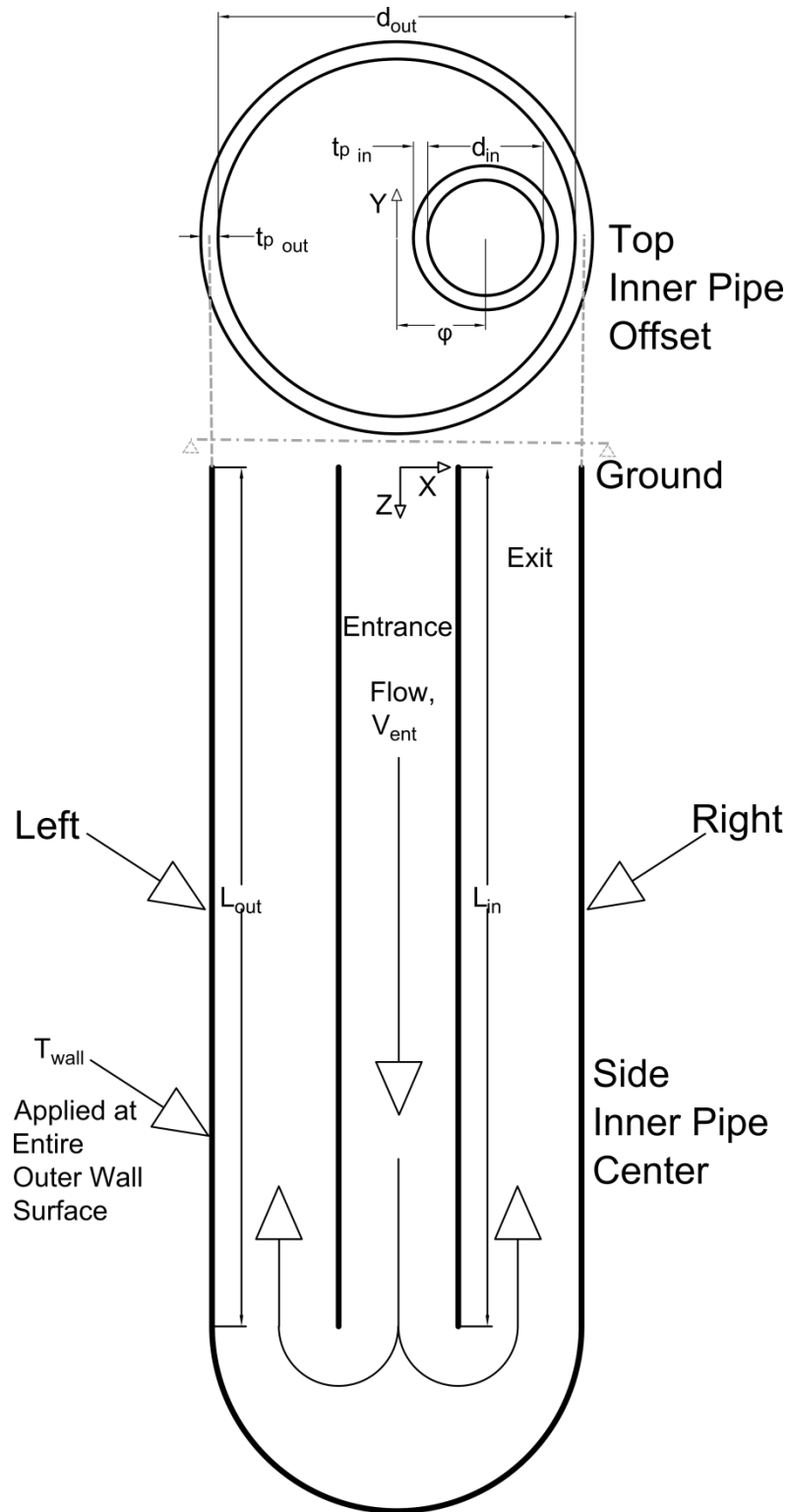
Figure 5.2: Top/Side View of Coaxial Ground Loop

The potential for offset of the inner pipe from the concentric axis is a very real problem and creates uncertainty in the design process. Especially the question how the working fluid will interact with the end cap after this offset takes place is very important. The end cap that redirects the flow to the outer ring for delivery to the surface will unintentionally create turbulence [5]. Since the inner pipe offset will greatly affect the flow into the end cap the inner pipe offset has a great influence on the turbulence in the system in and around the end cap region.

From literature review it is very clear to see that turbulence will enhance heat transfer [7], [8] through a few mechanisms. Turbulent flows are diffusive and dispersive [12], these processes will promote mixing and increase energy and heat transport. This is particularly useful in heat transfer as that heat energy can be quickly transferred through the flow domain from the wall to the bulk of the flow. The domain characteristics can make the flow more chaotic and sensitive leading to increased turbulence and mixing behaviour. This makes the flow more chaotic than it would otherwise be with fully developed turbulence flow alone [8], [9].

In pipe flow, heat transfer is generally convective from the wall to the fluid bulk. If the bulk of the flow is laminar then the boundary layer will exhibit a conductive heat transfer scenario mitigating the transfer process until the convective behaviour is realized between the boundary layer and the bulk. For flows with turbulent behaviours the boundary layer conductive heat transfer is nullified and the convective heat transfer extends itself between the boundary layer and the wall of the domain. For ground source heat pump applications where the fluid is generally a water and glycol mix. The fluid does not change throughout operation so the main parameter that can be adjusted in the

106

design phase is factors contributing to the calculation of the Reynolds Number, namely the flow inlet velocity. This indicates a direct relationship between the Reynolds Number and the magnitude of convective heat transfer in ground source heat pump applications.

This leaves two specific problems unique to Coaxial pipes that should be studied to, first, understand how the Reynolds Number enhances the heat transfer and discover regions of increased turbulence, and second, parametrically study the effects of the Reynolds Number and geometric variances on heat transfer efficiency in this complex geometry.

The effect of the end cap can be studied with a range of tests on the inner pipe location as the fluid can either be directed into a relatively flat symmetrical wall or directed into the much more curved section where the wall is not actually orthogonal to the incoming flow. The convection process can be studied with a range of Reynolds Number tests to determine whether the Reynolds Number should be increased to maximum as indicated by its effect on the convection or if a balance should be obtained as to not interfere with the diffusion and subtle eddy structures.

The objective of this paper is to study the effects of the Reynolds Number and the location of the inner pipe with respect to the outer pipe on the heat transfer efficiency of the system. This paper will investigate the isolated effects of the inner pipe displacement, the Reynolds Number and the ΔT of the system on the heat transfer performance. This will be done with a numerical model developed in FLUENT; a case of the simulated results will be verified by experimental measurements.

107

2.0 TEST MATRIX

The test matrix for this study can be detailed in Table 5.1. The Reynolds Number will be calculated based on the inlet flow and the associated velocity will be used at the inlet boundary condition, there will be three tested to cover the laminar, transitional and turbulent flow regimes. The properties of the flow and the surrounding pipe can be found in Table 5.2. Five different eccentricities are chosen to model varying degrees of offset in the inner pipe. The factor of eccentricity, F_{ecc}, is defined as $\varphi/(r_{out} - r_{in})$ where φ is the difference in the central axis of the two pipes. Three ΔT's are used to model heating, cooling, and isothermal cases. To understand where high regions of heat transfer are a difference in temperature is needed throughout the domain even close to the outlet. The resulting number of simulations tested will be 45.

Table 5.1: Test Matrix

Case #	ΔT (°K)	Re	F_{ecc}	Case #	ΔT (°K)	Re	F_{ecc}
1			0	31			0
2			0.21	32			0.21
3		500	0.41	33		500	0.41
4			0.62	34			0.62
5			0.82	35			0.82
6			0	36			0
7	-50		0.21	37	50		0.21
8	(Heating)	3,000	0.41	38	(Cooling)	3,000	0.41
9			0.62	39			0.62
10			0.82	40			0.82
11			0	41			0
12			0.21	42			0.21
13		5,000	0.41	43		5,000	0.41
14			0.62	44			0.62
15			0.82	45			0.82
16			0				
17			0.21				
18		500	0.41				
19			0.62				
20			0.82				
21			0				
22			0.21				
23	0	3,000	0.41				
24			0.62				
25			0.82				
26			0				
27			0.21				
28		5,000	0.41				
29			0.62				
30			0.82				

Table 5.2: Material Properties

Material	Density (kg m^{-3})	Specific Heat (J kg^{-1} K^{-1})	Thermal Conductivity (W m^{-1} K^{-1})	Viscosity (kg m^{-1} s^{-1})
Water	998.2	4182	0.6	1.003 x 10^{-3}
Pipe	950	2300	0.44	N/A

109

The constant parameters for these simulations will be as follows. The wall temperature will be a constant 250 K. Therefore, the ΔT will result from changing the inlet boundary condition. The walls will be non-slip entities with the convection heat transfer option selected for the faces that meet flow. The outlet will have the outflow condition ensuring all flow exits the simulation as intended. The inner diameter of the inner pipe, d_{in}, will be 0.0508 m and have a wall thickness, $t_{p,in}$, of 0.00635 m. The outer pipe will have a $d_{out} = 0.15$ m and without a thickness, $t_{p,out} = 0$, computationally as it is the heat source for these studies and computing conduction through the wall will result in wasted computer resources. The overall system will be 5 m long with the inner pipe only spanning 4.925 m.

3.0 EXPERIMENTAL SETUP

Due to a lack of available data on Coaxial fluid flow in the literature, a limited set of experiments were conducted for the isothermal case, $\Delta T = 0$. To invoke proper turbulence flow characterization with the available Dantec hot wire anemometer the Coaxial loop was experimentally modelled three times on different days to ensure replicability and repeatability of the observation. In general, hot wire anemometry was employed to gather point velocity measurements and the mean velocity across a line in the outer tube and its associated turbulence intensity was used to validate the numerical model proposed in this paper for the parametric analysis. Detailed velocity measurements were carried out using air as the medium.

The setup is portrayed in Figure 5.3. The RIGID 4,474 W Blower is connected to a Variable AC Unit, enabling the flow rate to be varied to the desired value, 0.0022 m^3 s^{-1}

corresponding to 4.5 m s^{-1} through the inner pipe. Right after the blower is a KING Rotameter (Range: 3.8 - 38.7 x 10^{-4} m^3/s. Accuracy +/- 3%) used to monitor the flow rate and calculate the corresponding velocity. The KING Rotameter is connected to the inlet of the system via an 18 mm inner diameter flexible hosing. The inlet of the system is a 25.4 mm inner diameter 914 mm long acrylic pipe. At the outlet of the inner pipe is a custom machined Acrylic block shown in Figure 5.4. The outer Acrylic pipe is connected to the Acrylic block and is 76 mm inner diameter and 340 mm long. The hotwire setup consists of 55P11 Probe and 55H21 Probe Support for 1D velocity measurements.

1: RIGID 4,474 W Vacuum/Blower
2: KING Rotameter (3.8 - 38.7 x 10^{-4} m^3/s)
3: 18 mm Flexible Plastic Hosing
4: Acrylic Tube (25.4 mm ID; 38.1 mm OD)
5: Acrylic Tube (150 mm ID; 157 mm OD)
6: Acrylic Block Machined for Dimensions Shown
7: DANTEC 55P11 and 55H21 Hot-Wire Probe
   and Probe Support

Figure 5.3: Experimental Setup
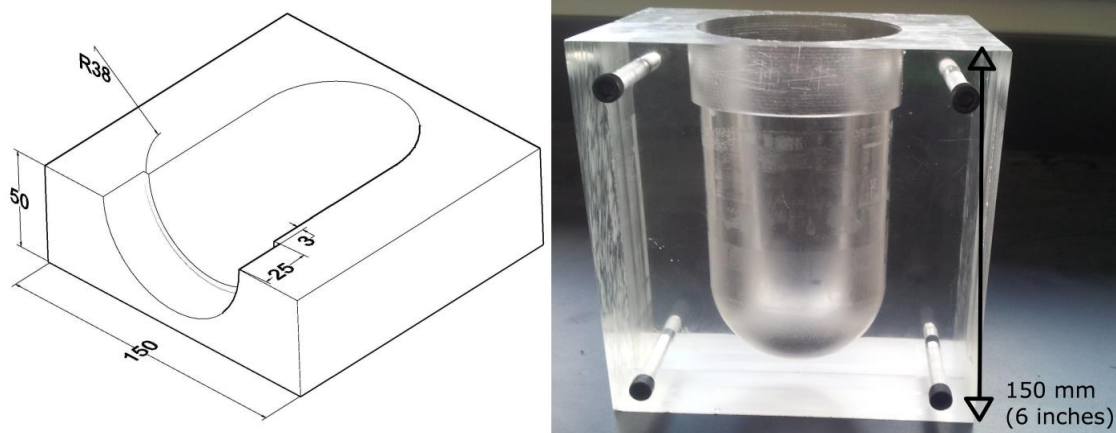
Figure 5.4: Isometric View and Photo of End Cap (Dimensions in mm)

The hotwire setup includes two stages. Before each series of measurements a detailed calibration was performed utilizing the StreamWare software. The software automatically generated the curve fit for a set of ten data points. The curve fit coefficients were generated along with the associated calibration errors. The calibration data and curve coefficients were used to reduce the voltage readings from the probe into velocity measurements. The average error of the calibration coefficients were roughly 0.3-0.5% for all calibrations. Default settings were employed for the automatic calibration to occur [10], [11].

For the experiment, the sampling rate was set at 80 kHz over a 1s sampling time resulting in 80,000 samples for each point. The lateral position of the probe was deduced with a Micrometer Model No. CD-8" CSX with a resolution of three decimal places (0.001 mm). The procedure of each test can be summarized as:

1. Calibration using the auto-calibration features of StreamWare.

113

2. Remove the probe from the calibration nozzle and place it in the Coaxial pipe.

3. Turn on the blower and adjust the flowrate to meet desired Re.

4. Position the probe and record the x-location.

5. Running data acquisition using StreamWare with 80 kHz sampling rate for one second.

6. Reposition probe and repeat step 5 until complete.

The above procedure was run 3 times on different days all with approximately the same flowrate.

4.0 MATHEMATICAL MODEL

The k-ε model is used based on literature review [12]–[17]. The k- ε model has a vast history when used for similar flow situations and in particular when macroscopic fluid properties are to be extracted and analyzed. A modification of the standard k-ε model known as the realizable k-ε model was implemented because of the modifications imposed by the RANS model [12].

The realizable k-ε model takes the following form as found commonly in the literature [8], [12]. Equations 2 and 3 show the main equations for the transportable variables, the turbulent kinetic energy, k1, and the dissipation rate, ε, respectively.

$$\frac{\partial}{\partial t}(\rho k_1) + \frac{\partial}{\partial x_j}(\rho k_1 u_j) = \frac{\partial}{\partial x_j}\left[\left(\mu + \frac{\mu_t}{\sigma_{k_1}}\right)\left(\frac{\partial k_1}{\partial x_j}\right)\right] + G_{k_1} + G_b - \rho\epsilon - Y_M + S_{k_1} \quad (2)$$

$$\frac{\partial}{\partial t}(\rho\epsilon) + \frac{\partial}{\partial x_j}(\rho\epsilon u_j)$$

$$= \frac{\partial}{\partial x_j}\left[\left(\mu + \frac{\mu_t}{\sigma_\epsilon}\right)\left(\frac{\partial\epsilon}{\partial x_j}\right)\right] + \rho C_1 S\epsilon - \rho C_2\left(\frac{\epsilon^2}{k_1 + \sqrt{(\nu\epsilon)}}\right) + C_{1\epsilon}\frac{\epsilon}{k_1}C_{3\epsilon}G_b \quad (3)$$

$$+ S_\epsilon$$

where,

$$\mu_t = \frac{\rho C_\mu k^2}{\epsilon} \quad (4)$$

$$C_\mu = \frac{1}{A_0 + \frac{A_8 k U^*}{\epsilon}} \quad (5)$$

The term G_{k1} and G_b refer to the generation of the turbulent kinetic energy due to the mean velocity gradients and due to buoyancy (forces induced by gravity and the gradient of density between the materials), respectively. Whereas Y_M is the contribution of the fluctuating dilation in compressible turbulence to the overall dissipation rate and S_{k1} and S_ϵ are the source terms.

There are two main differences between the realizable k-ε and the standard k-ε model. First the eddy viscosity, μ_t, calculated in Equation 4, is not based on a constant C_μ; which is typically assumed to be equal to 0.09. Instead, C_μ is calculated by Equation

115

5, i.e., it is a function of the mean strain and rotation rates, turbulence fields and the angular velocity of the system rotation.

The numerical model was set up using the commercially available software package provided by ANSYS Inc. The default modeller and meshing program was used and FLUENT was the solver. Both transient and steady state simulations were performed limiting our turbulence model to RANS based solvers. Transient analysis was performed for a flow time of 50 s and a time step of 0.001 s. The steady state simulation was run until convergence was reached using the default convergence criteria of FLUENT [18].

To run these simulations the Shared Hierarchical Academic Research Computing Network, SHARCNET, available to Canadian research intuitions was utilized to provide for relatively quick numerical solving of the tests cases submitted.

5.0 MESH INDEPENDENCE

Numerical model results are commonly influenced by the selection of suitable mesh. Therefore, mesh independence study was carried out to ensure proper realization of the involved physics and to eliminate the spatial effects of the cell size from the simulation. The geometry used for the mesh study is the one where $F_{ecc} = 0$. In addition, no cell should be larger than the length scale of interest. The turbulence length scale as formulated by FLUENT is 7% of the pipe diameter in fully developed flow cases [18].

Four mesh sizes were chosen and one parameter of the simulation was compared to complete the mesh study. The parameter chosen is the turbulence intensity, along the inner wall of the inner pipe ((0.025, 0, 0) to (0.025, 0, -4.925)), and chosen as a sensitive

116

parameter to the simulation. The results of the study for the turbulence intensity are shown in Figure 5.5 and the discrepancy between the mesh 3 and 4 is <1%. As a result mesh 3 will be used for the test cases. Mesh 3 was developed using a maximum cell volume of 1×10^{-10} m^3.
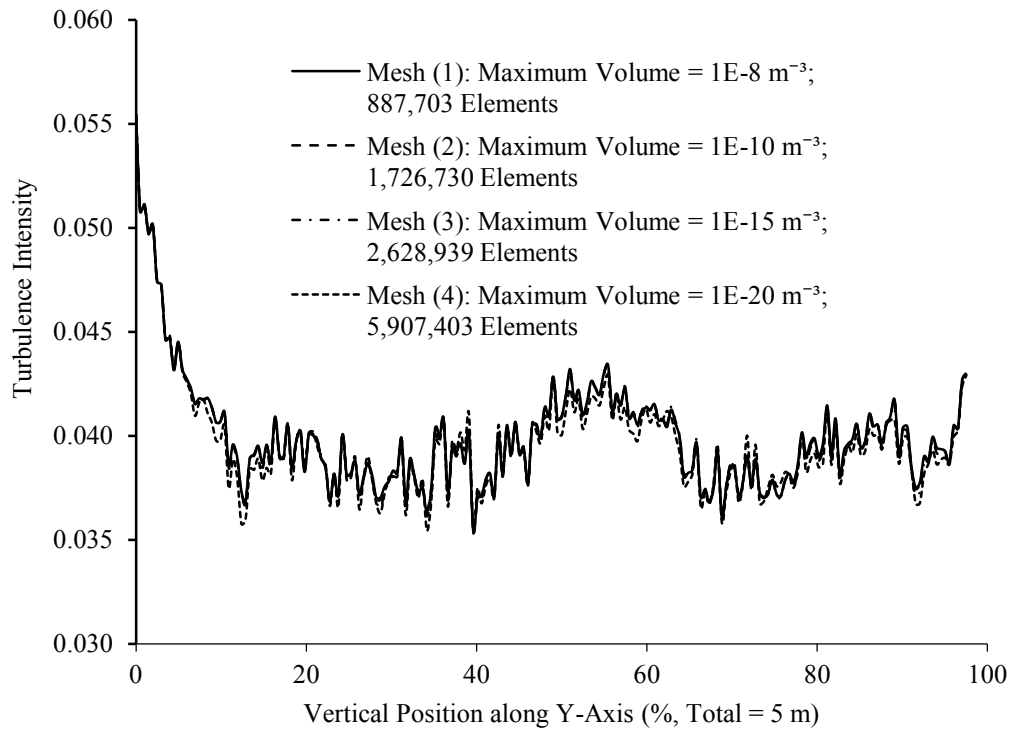
Figure 5.5: The Effect of Mesh Density on the Turbulence Intensity at X = 0.025 m, Y = 0 m for $F_{ecc} = 0$

6.0 RESULTS AND DISCUSSIONS

The results will be broken down into four main sections. First the simulated results will be validated against the experimental measurements. Second, the transient simulation results will be compared against the results obtained from steady state simulation. Third the isothermal flow characteristics will be looked at for varying Reynolds Numbers and F_{ecc}. Finally the heat flux along opposite walls of the system will be analyzed for both varying Reynolds Numbers and F_{ecc}.

6.1 EXPERIMENTAL RESULTS

The experimental setup and measurement procedures are discussed in the earlier section. The present section discusses the results obtained from the measurements. The point velocity measurements were taken at 13 locations across a line at 335 mm from the outlet of the system. The line was oriented to be orthogonal to the flow spanning the shortest distance from the outer wall of the inner pipe to the inner wall of the outer pipe. The results of the experimental velocity profile are displayed in Figure 5.6. The velocity profile shows two regions of interest. Close to the inner wall there is a region of negative velocity and close to the outer wall there is a region of positive velocity. This indicates that there is a large rotating structure at this location that forces the bulk of the flow going up at the outer wall to come back down near the inner wall and be pushed back into the end cap region.
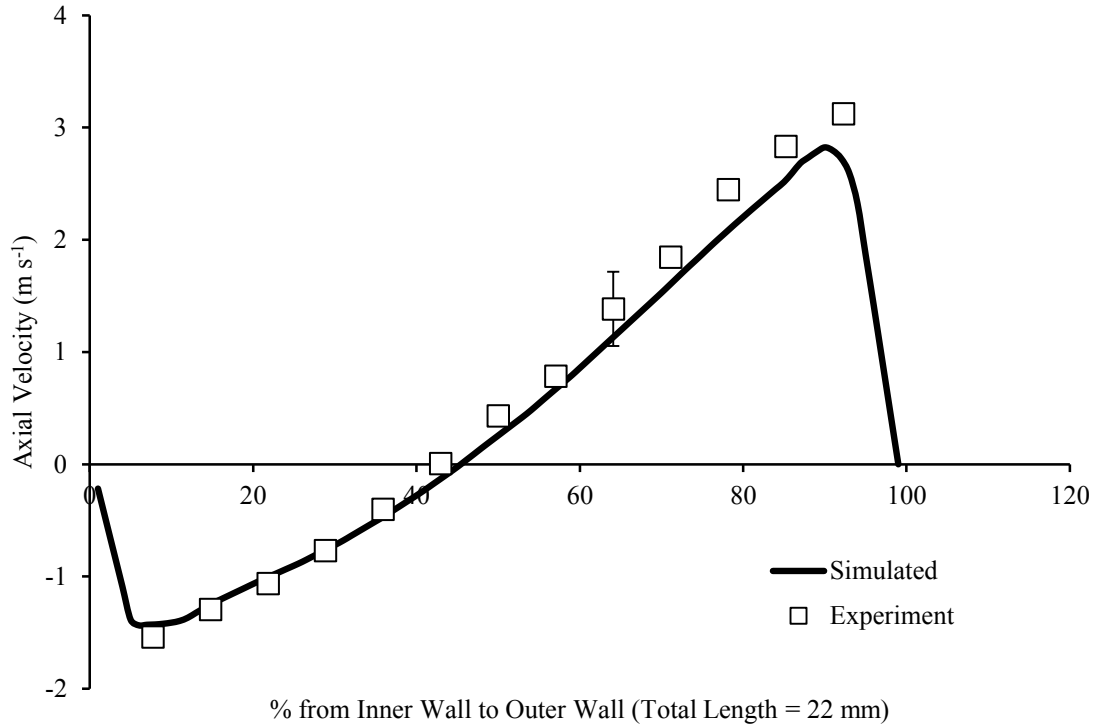
Figure 5.6: Measured Axial Velocity along line (orthogonal to inner wall) centred at Z = -330 m from the outlet

The calculated turbulence intensity using the fluctuations of the velocity and the mean velocity was determined and is shown in Figure 5.7. The turbulence intensity shows a maximum near the center of the region measured. Considering the velocity and the fluctuations at this location the point of maximum turbulence intensity would be near the centre of this rotating structure where the velocities would be constantly changing as opposed to the outer edges of the structure where it is more consistent.

119
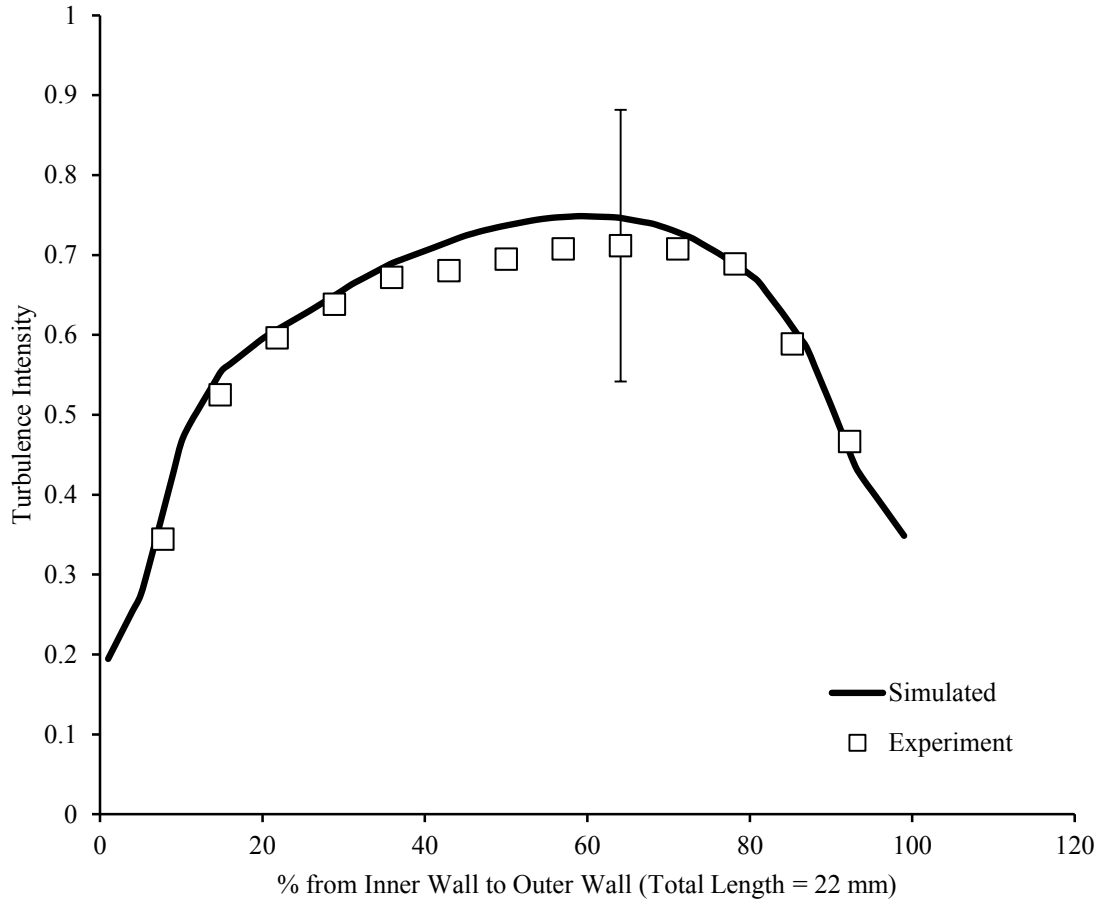
Figure 5.7: Comparison of Experimental and Simulated Turbulence Intensities along line

(orthogonal to inner wall) centred at $Z = -330$ m from the outlet

The uncertainty in the velocity measurements is a combination of the uncertainty

is the calibration measurement and the repetitions. With three replications, the

uncertainty in the resulting flow velocity was estimated to be around 0.33 m s^{-1} [11], [19],

shown in Figure 5.6, indicated by the error bar.

The uncertainty in the calculated turbulence intensity is defined as the partial

derivative of the turbulence intensity equation multiplied by the uncertainty of the

120

velocity. The uncertainty then becomes the uncertainty of the velocity multiplied by the root-mean square of the velocity fluctuations divided by the velocity squared [19],

$$E_I = \sqrt{\frac{\partial I}{\partial \overline{u}} E_{\overline{u}}^2 + \frac{\partial I}{\partial u'_{rms}} E_{u'_{rms}}^2}$$

$$= \sqrt{-\frac{u'_{rms}}{\overline{u}^2} E_{\overline{u}}^2 + \overline{u}^{-1} E_{u'_{rms}}^2} \tag{6}$$

That is, the value of the typical uncertainty is 0.17 as shown in Figure 5.7 by the indicated error bar.

The uncertainty in the horizontal direction is measured by the uncertainty in the measuring device used to calculate the horizontal position. The uncertainty in this direction is typically 0.5 mm or 2% of the measured area.

6.2 COMPARISON OF SIMULATED AND EXPERIMENTAL RESULTS

The chosen mathematical model was simulated for both a transient and steady state case. In the transient case the time step used was 0.001 and was simulated for 50 s flow time and the steady state case was simulated until convergence was reached. The inlet conditions were Re = 5,000, F_{ecc} = 0, and ΔT = 0. Both transient and steady state simulations were completed to test the validity of assuming a steady state scenario.

121

Figure 5.6 shows the axial velocity as measured in the experiment and calculated in the mathematical model. There is good agreement and the uncertainty of the experimental measurements covers the simulated values. Figure 5.7 shows the calculated turbulence intensity based on the fluctuations along that line. There is a good agreement and the uncertainty of the calculated measurements from the experiment covers the simulated values. Figure 5.8 shows the axial velocity contours of the mathematical model with a line indicating the position at which the experimental values were recorded.
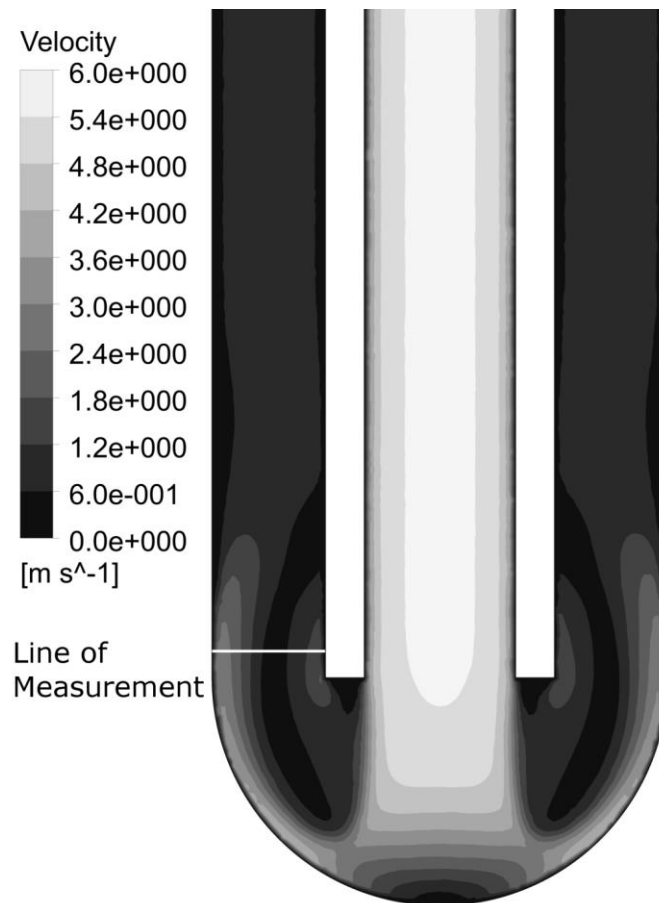
Figure 5.8: Simulated Axial Velocity Contours

6.3 STEADY STATE RESULTS AND TRANSIENT RESULTS

The transient simulation proved to be lengthy to calculate even on high end computing machines and for a parametric study of this magnitude a faster solution was desired. Further comparison to steady state simulations was deemed necessary as the flow conditions allowed for steady state analysis. One specific case was used to do the comparison, Re = 0, F_{ecc} = 0, and ΔT = 0. The turbulent kinetic energy was chosen to compare the two simulations. The turbulent kinetic energy it is a transportable variable in the k-ε model, thus signifying its importance in comparing the steady state and transient simulations. Figure 5.9 shows the turbulent kinetic energy and is the first of the transportable variables in the k-ε model that were analyzed in this comparison. The turbulent kinetic energy can give further insight to the eddies' energy level. Eddies with high energy will fluctuate around their mean velocity at a greater rate and thus will have higher turbulence intensity values, leading to higher heat transfer in those regions.

123
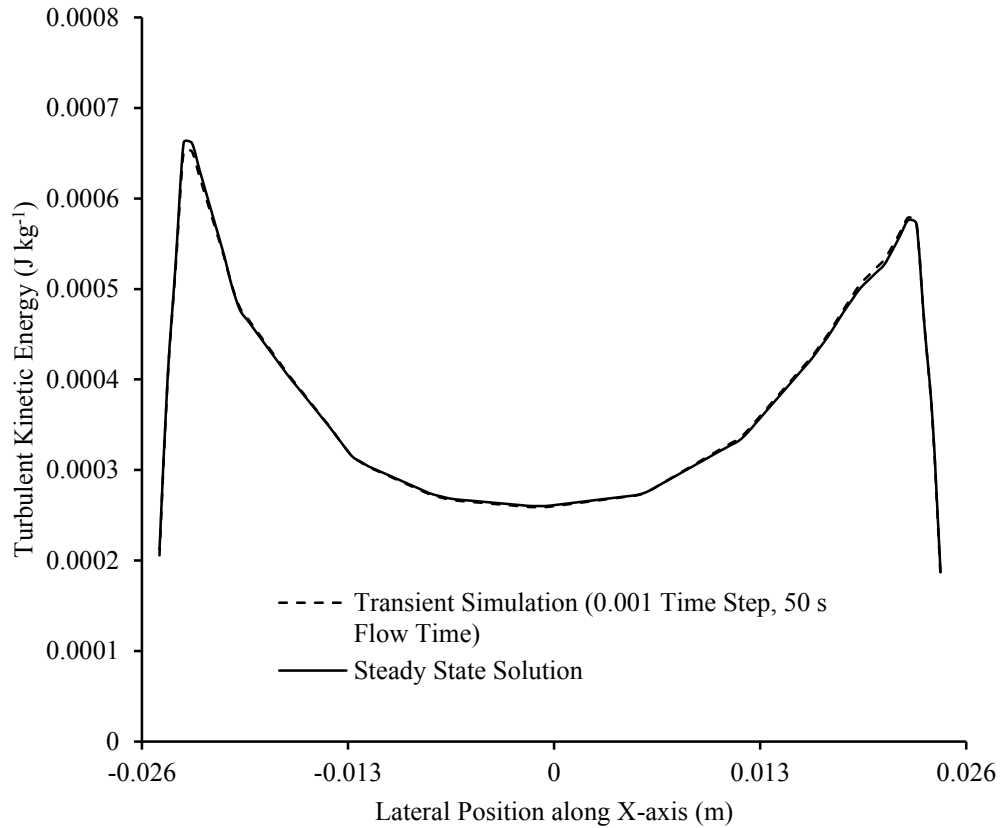
Figure 5.9: Steady State versus Transient, Their Effect on the Turbulent Kinetic Energy

at Y = 0 m, Z = -4.925 m for $F_{ecc} = 0$

6.4 ISOTHERMAL MODE

This section will detail the effects of the Reynolds Number on the eddy viscosity to gain insight on where the regions of higher heat transfer will be as the Reynolds Number is increased for the idealized case alone, $F_{ecc} = 0$.

The eddy viscosity contour plot of the three isothermal test cases with $F_{ecc} = 0$ are shown in Figure 5.10. It can be seen how the maximum shifts downstream of the end cap more with increasing Reynolds Number. For Re = 500, the maximum occurs in the end

124

cap region, the maximum for Re = 3,000 occurs at 50 mm, $0.33D_{out}$, downstream of the end cap with high value regions extending 200 mm, $1.33D_{out}$, downstream of the end cap. For Re = 5,000, the maximum eddy viscosity occurs at 70 mm, $0.46D_{out}$, downstream of the end cap with the high value regions extending beyond 300 mm, $2D_{out}$, away from the end cap.
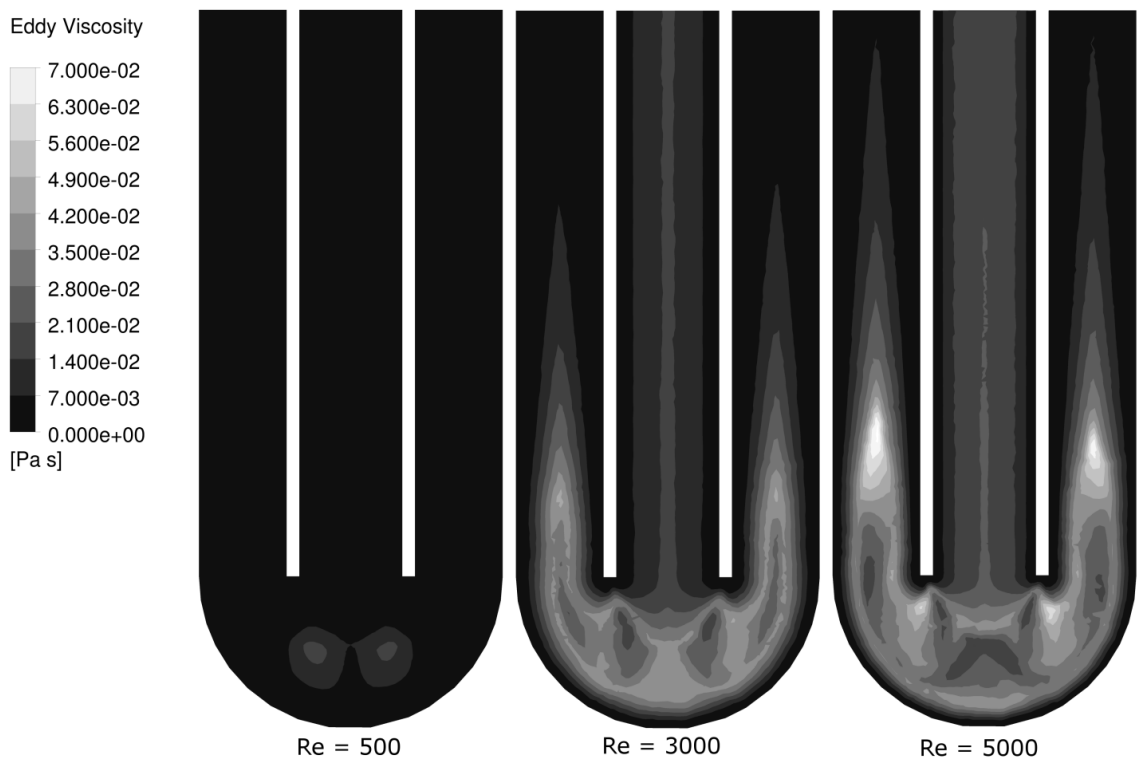
Figure 5.10: Eddy Viscosity Contours along Plane of Symmetry for $\Delta T = 0$, $F_{ecc} = 0$

The preceding parameter supports the conclusion that the higher the Reynolds Number is for a specific F_{ecc} the stronger and further downstream of the end cap the high regions of turbulence will be. This is important to know as ultimately the heat flux and

high heat transfer coefficients will improve the performance of Coaxial heat pipe systems.

6.5 THERMAL PERFORMANCE

The heat flux will be used to compare across test cases as it is an area rate metric and will normalize results across Reynolds Numbers and temperature differences. The heat flux can be used to determine where and how much more efficient one region of flow is than another for heat transfer. From the previous insights on the regions closer to the end cap displays a higher heat flux values and these high values should last longer through the outer pipe when the Reynolds Number is increased. This section will look at the heat transfer along two lines, corresponding to opposite sides of the offsetting inner pipe. As F_{ecc} increases the inner pipe will move away from the 'left' wall and closer to the 'right' wall as detailed in Figure 5.2. The 'left' line will be the line connecting the point (-0.075, 0, 0) to (-0.075, -5, 0) and the 'right' line will be the line connecting the point (0.075, 0, 0) to (0.075, -5, 0).

Figure 5.11 shows the variation of the heat flux along line 'left' through the length of the pipe for select Reynolds Numbers of F_{ecc} equal to 0, 0.21, 0.41, 0.62, and 0.82, respectively. For all F_{ecc} the Reynolds Number increases the heat flux throughout the outer pipe but more so when F_{ecc} is lower, such as $F_{ecc} = 0$. The heat flux decreases with increasing F_{ecc} but the heat flux at the end cap (Y = -5 m to Y = -4.925 m) increases with increasing F_{ecc} and Reynolds Number. However, the overall heat flux is the highest when $F_{ecc} = 0$ and Re = 5,000. This is because when $F_{ecc} = 0$ the inner pipe is positioned directly over the end cap so the flow will disperse into the outer region evenly with even

126

turbulence. This is unlike when $F_{ecc} > 0$ where the flow is initially met with a curved wall and is pushed more so in one direction than the other creating more turbulence in one region of the flow over the other.

Figure 5.11: Simulated Heat Flux along Line 'left' for Different Re of Select F_{ecc}

Figure 5.12 shows the heat flux along line 'left' for varying F_{ecc} of Re = 500, Re = 3,000 and Re = 5,000, respectively. The heat flux can be seen to decrease with increasing F_{ecc} but less so after F_{ecc}, i.e. the difference in the heat flux from $F_{ecc} = 0$ to $F_{ecc} = 0.21$ is about 50% where the total difference between $F_{ecc} = 0.21$ and $F_{ecc} = 0.82$ is only about 10%. This indicates for all Reynolds Number flow regimes that once offset is introduced the heat flux is generally destroyed on the 'left' side of the system but the relative difference of higher offsets is small.
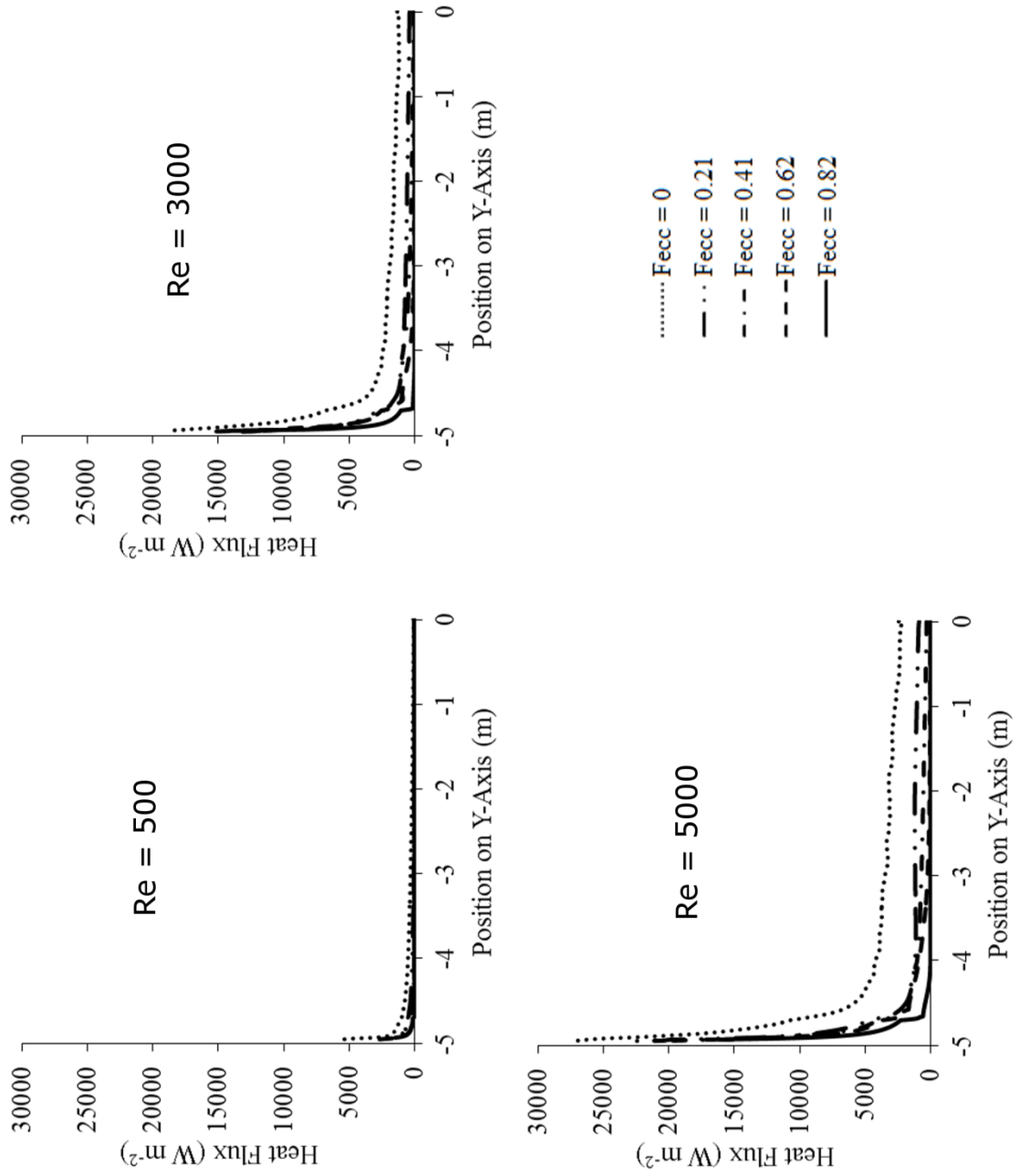
Figure 5.12: Simulated Heat Flux along Line 'left' for different F_{ecc} of select Re

Figure 5.13 shows the corresponding heat flux along line 'right' for varying Reynolds Numbers of F_{ecc} equal to 0, 0.21, 0.41, 0.62, and 0.82, respectively. For all F_{ecc} the increase in Reynolds Number results in an increase in the heat flux throughout the outer pipe. Figure 5.14 shows the heat flux along line 'right' for varying F_{ecc} of Re = 500, Re = 3,000 and Re = 5,000, respectively. The negative slope of the heat flux between Y = -5 m and Y = -4 meters also decreases in magnitude for increasing F_{ecc} at each Reynolds Number but less so for Re = 5,000. This indicates that as the inner pipe moves closer to this side of the wall the heat flux will remain higher for longer distances downstream of the inner pipe. As the gap between the inner pipe and the outer pipe becomes smaller with increasing F_{ecc} the velocity will increase because the relative volume will decrease in this region. As the velocity increases the local Re increases which, as proven in this study and in others [20] will increase the heat flux as well as the turbulence activity.
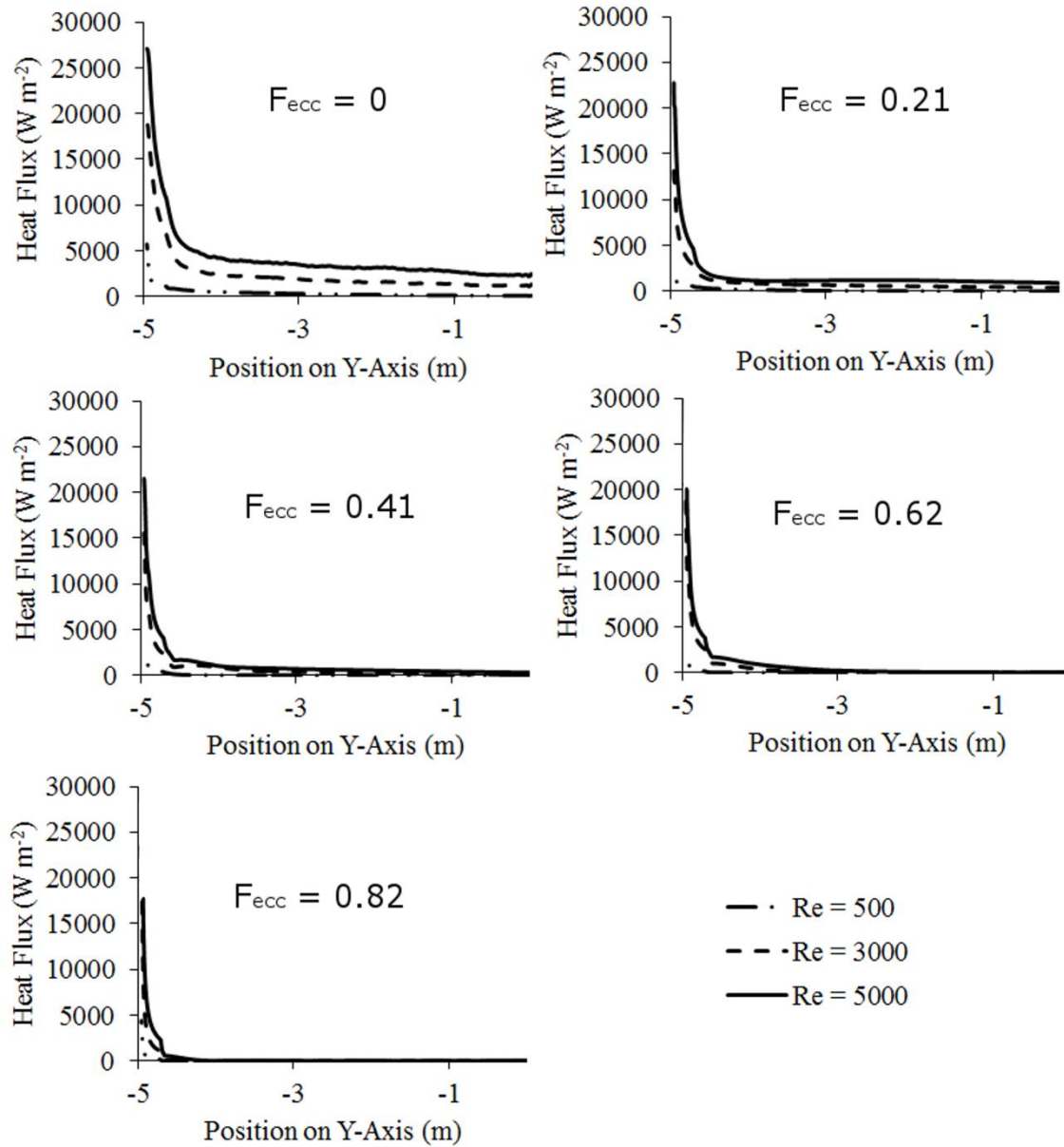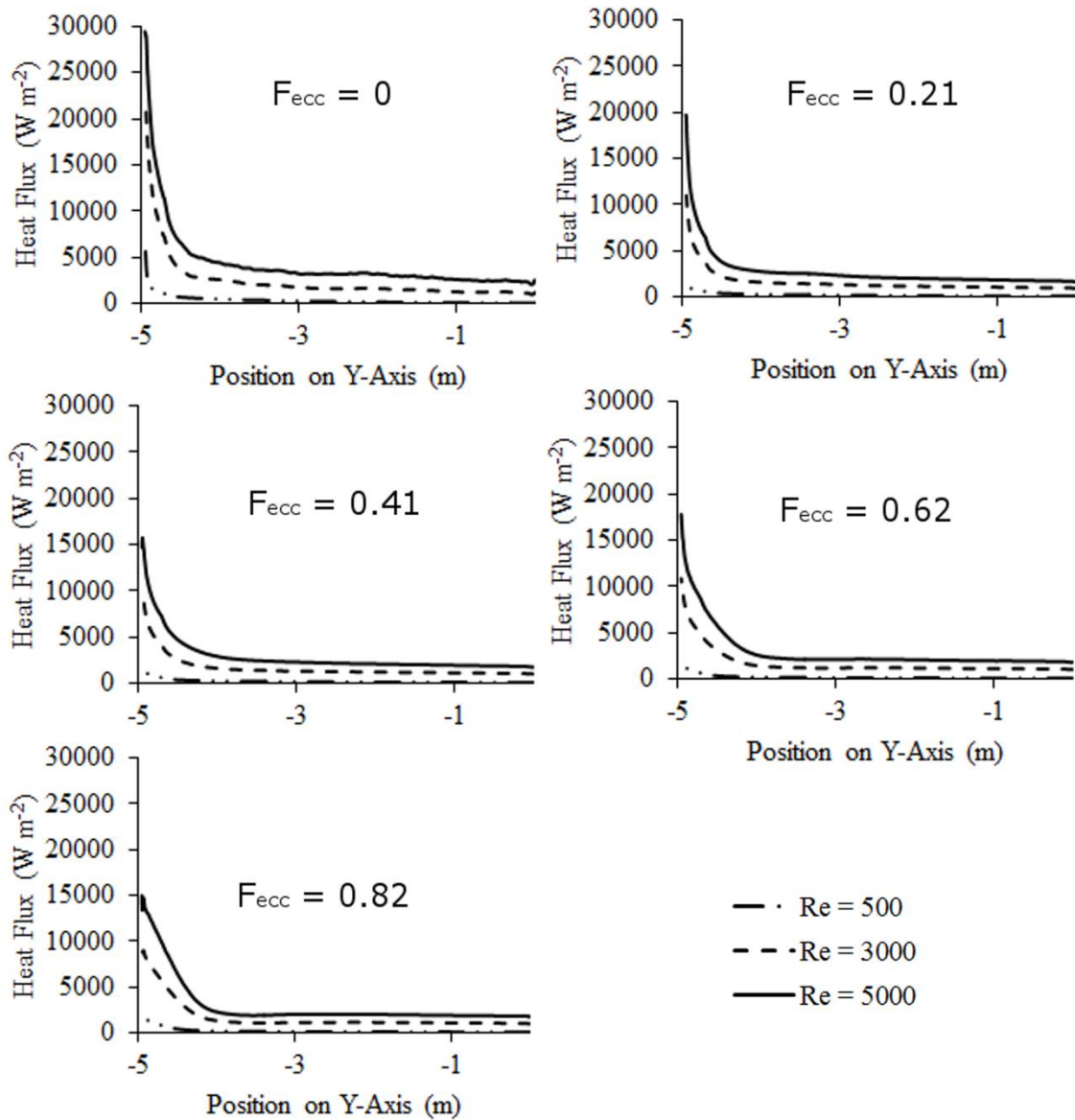
Figure 5.13: Simulated Heat Flux along Line 'right' for Different Re of Select F_{ecc}
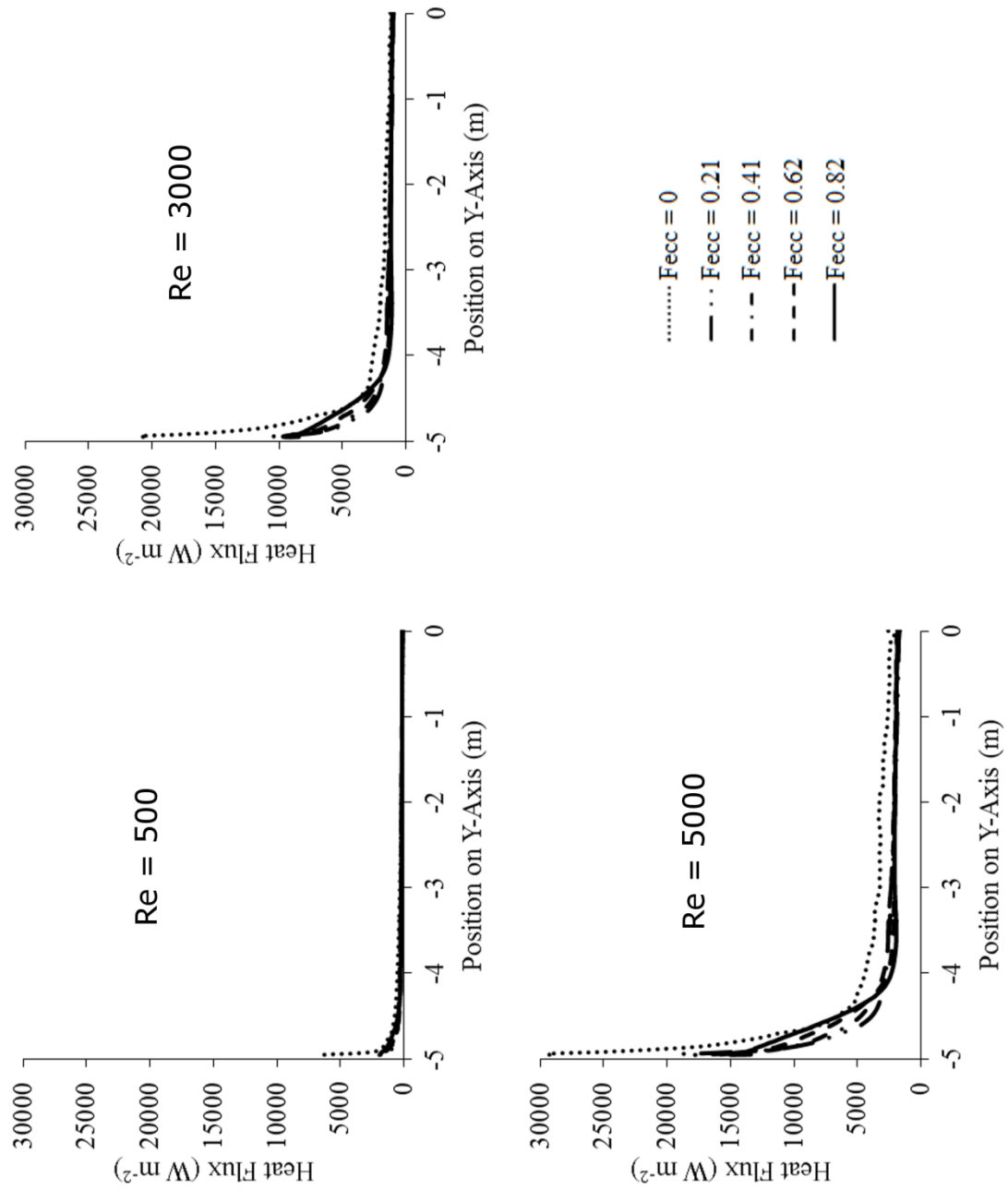
Figure 5.14: Simulated Heat Flux along Line 'right' for different F_{ecc} of select Re

7.0 CONCLUSIONS

This study employed mathematical models to study the effects of the inner pipe offset and the Reynolds Number on the heat flux through the length of the pipe downstream of the end cap. The following conclusions can be made.

- The heat flux will increase regardless of eccentricity with increasing Reynolds Number based on incoming flow.

- The heat flux will decrease along the wall portion where the inner pipe is moving away from it with increasing eccentricity. About 50% reduction in the heat flux is observed when the offset ($F_{ecc} > 0$) is introduced and a further 10% reduction in overall heat flux afterwards (from $F_{ecc} = 0.21$ to $F_{ecc} = 0.82$) is observed.

- The overall heat flux will increase slightly along the wall portion where the inner pipe is moving closer to it with increasing eccentricity. The higher heat flux that exists at the end cap will last longer downstream of the end cap as F_{ecc} increases (less negative slope with increasing F_{ecc}).

- The areas of maximum turbulent eddy flow characteristics, the turbulent kinetic energy and eddy viscosity, occur further downstream and have higher magnitudes as the Reynolds Number is increased.

133

ACKNOWLEDGEMENTS

REFERENCES

[1]   J.W. Lund, Direct utilization of geothermal energy 2010 worldwide review, Geothermics. 40 (2011) 159–180.

[2]   A.M. Omer, Ground-source heat pumps systems and applications, Renewable and Sustainable Energy Reviews. 12 (2008) 344–371.

[3]   S.J. Self, Geothermal heat pump systems: Status review and comparison with other heating options, Applied Energy. 101 (2013) 341–348.

[4]   H. Benli, A performance comparison between a horizontal source and a vertical source heat pump systems for a greenhouse heating in the mild climate Elaziğ, Turkey, Applied Thermal Engineering. 50 (2013) 197–206.

[5]   J. Lund, B. Sanner, L. Rybach, R. Curtis, G. Hellström, Geothermal (ground-source) heat pumps: a world overview, GHC Bulletin. 25 (2004) 1–10.

[6]   L. Rybach, W.J. Eugster, Sustainability aspects of geothermal heat pump operation, with experience from Switzerland, Geothermics. 39 (2010) 365–369.

[7]   E. Zanchini, S. Lazzari, A. Priarone, Improving the thermal performance of Coaxial borehole heat exchangers, Energy. 35 (2010) 657–666.

[8]   W.C. Reynolds, Fundamentals of Turbulence for Turbulence Modeling and Simulation, Defense Technical Information Center, 1987.

[9] R. Benzi, G. Paladin, G. Parisi, A. Vulpiani, On the multifractal nature of fully developed turbulence and chaotic systems, Journal of Physics A: Mathematical and General. 17 (1984) 3521.

[10] Dantec, MiniCTA Anemometer Package How to Get Started a Basic Guide, (2002).

[11] Dantec Dynamics, StreamLine/StreamWare Installation and User Guide, (2000).

[12] T.H. Shih, W.W. Liou, A. Shabbir, Z. Yang, J. Zhu, A new k-ε eddy viscosity for high reynolds number turbulent flows - model development and validation, National Aeronautics and Space Adminitration, TM-106721, 1994.

[13] B. Andersson, R. Andersson, L. Håkansson, Computational Fluid Dynamics for Engineers, Cambridge University Press, 2012.

[14] T.J. Chung, Computational Fluid Dynamics, Cambridge University Press, 2002.

[15] C. Lian, G. Xia, C.L. Merkle, Impact of source terms on reliability of CFD algorithms, Computers & Fluids. 39 (2010) 1909–1922.

[16] S. Gorji et al., A comparative study of turbulence models in a transient channel flow, Computers & Fluids. 89 (2014) 111–123.

[17] C. Heschl, K. Inthavong, W. Sanz, J. Tu, Evaluation and improvements of RANS turbulence models for linear diffuser flows, Computers & Fluids. 71 (2013) 272–282.

[18] ANSYS Inc., Fluent Theory Guide, ANSYS, Inc., 2009.

[19]   H.W. Coleman, W.G. Steele, Experimentation and uncertainty analysis for engineers, John Wiley & Sons, New York, 1989.

[20]   H. Sugiyama, D. Hitomi, Numerical analysis of developing turbulent flow in a 180° bend tube by an algebraic Reynolds stress model, International Journal for Numerical Methods in Fluids. 47 (2005) 1431–1449.

CHAPTER 6

SINGLE U-BEND VERSUS COAXIAL GROUND EXCHANGER LOOPS

1.0 INTRODUCTION

Ground source heat pump (GSHP) is a means to exploit environmentally sustainable geothermal energy especially for space heating and cooling. The working principle is simple. It consists primarily of a reversible heat pump and a loop which exchanges thermal energy between the earth and the building [1]. The heat pump itself acts as a reversible vapor-compression refrigeration loop [2]. A pump delivers a working fluid through a ground pipe loop absorbing or rejecting heat, depending on the season of operation. The pretreated working fluid acts as a catalyst for the heat exchanger [2]. In the heating mode the goal is to heat up the building by gathering thermal energy from the earth and pumping it through the HVAC systems. In the cooling mode the thermal energy is taken away from the building and deposited into the earth for future use. A group of ground source heat pumps can be linked together to form what is known as geothermal energy fields for buildings of larger demand.

There are two main types of GSHP installation, the open loops and the closed loops. The closed loops recycle the working fluid through a closed loop of pipes buried within the earth while open loops directly use a pond or an aquifer water to meet the thermal demand. Among the closed loop systems, there are horizontal and vertical configurations, each with its own set of advantages and design constraints. The horizontal system employs underground pipe loops laid horizontally a few metres in the ground

www.manaraa.com

throughout a big field. The vertical system uses vertical pipe loops installed in boreholes and sometimes connected in series. This makes the vertical system more expensive due to the increased digging cost. However, the smaller surface area requirement of vertical implementations makes it much more applicable for consumers [3]. With the relatively constant ground temperature [4] the vertical ground loops provide an advantage with a more predictable performance in the heat transfer process [5], [6]. This has spawned research into using different configurations of vertical pipe loop configurations. The conventional type of vertical pipe loop is called a Single U-Bend. A schematic of this type of pipe loop is shown in Figure 6.1. A working fluid traverses the system down the inlet pipe (left side in Figure 6.1), through the bend and up the return pipe gathering or rejecting thermal energy through the process.
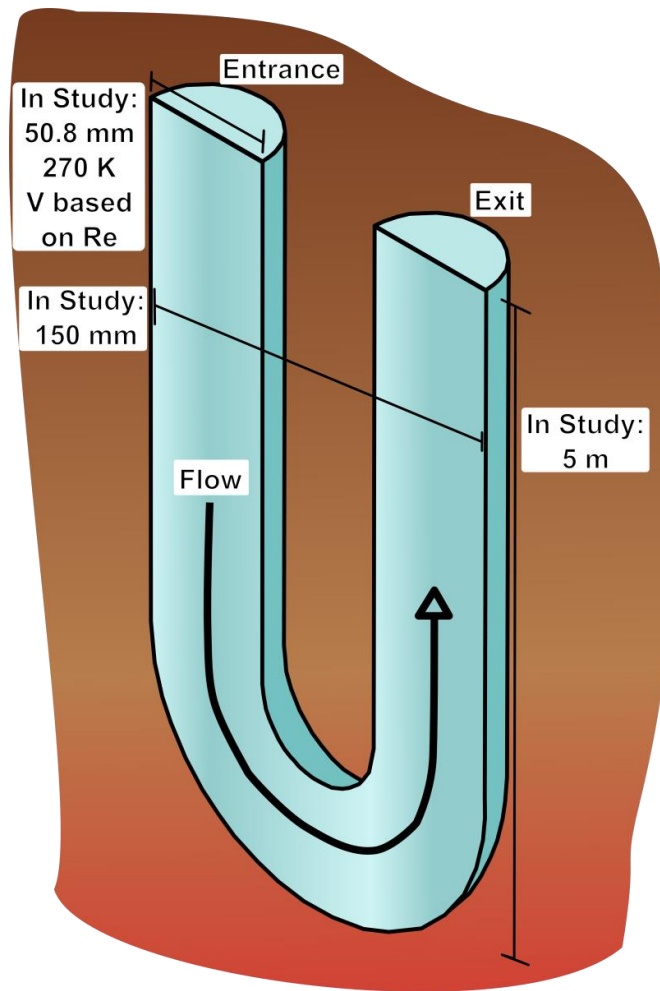
Figure 6.1: Schematic of U-Bend

The emerging competitor to this established technology is the Coaxial system. A schematic of this system is shown in Figure 6.2. This system consists of an inner pipe installed concentric within an outer pipe [6]. Under ideal condition, the system is perfectly symmetric. The working fluid traverses the system through the inner pipe to the bottom, and is redirected via an end cap into the outer pipe and returned to the surface heat pump.
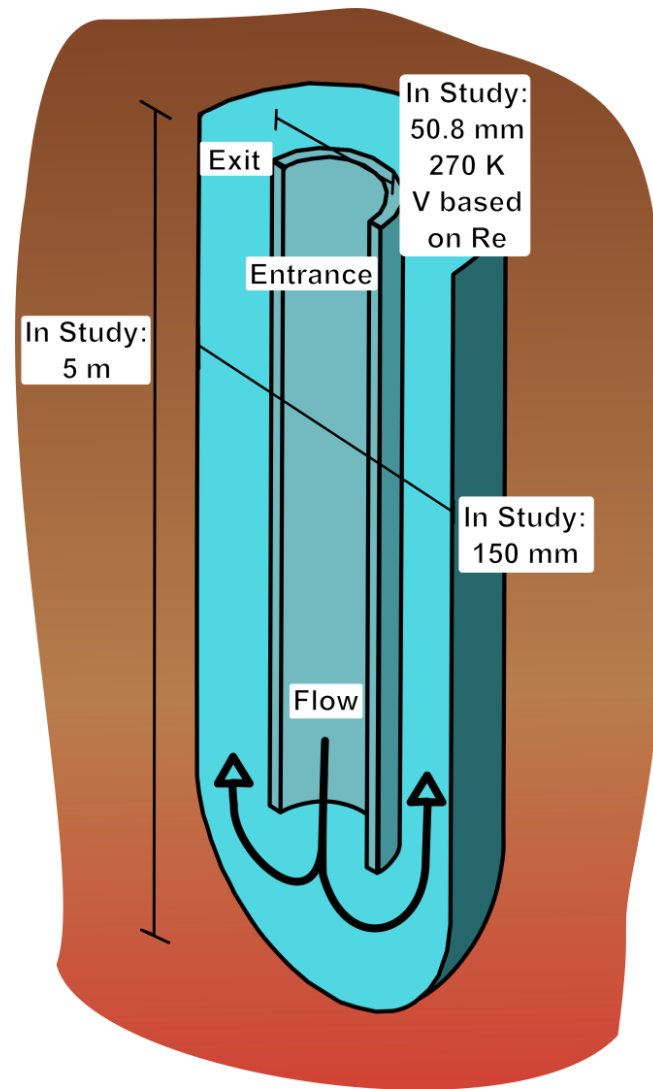
Figure 6.2: Schematic of Coaxial

These two systems have varying performance. Wood et al. [7] studied the comparative performance of the single U-Bend and the Coaxial ground loop configuration. Experimental tests on 72 m long ground loops were conducted for a U-Bend of 20 mm diameter and a Coaxial of 20 mm inner pipe diameter and 40 mm outer pipe diameter. The researchers concluded varying results. When looking at rates of heat

transfer the U-Bend performed better with a higher average heat transfer coefficient. They attributed this to the consistently turbulent flow in the U-Bend. For their tested Coaxial system, the much larger outer cross section resulted in a lower Reynolds Number laminar flow. However, with that being said the higher velocities in the U-Bend also lead to a lower residence time. This lessens the time available for heating or cooling of the working fluid. The final conclusion was that the Coaxial system will perform better over equivalent lengths due to the longer resident time and the larger surface area available on the outer pipe volume of flow exposed to the heat source. The other benefits of the Coaxial system were also found to include a reduced pressure loss over equivalent lengths, reducing operational costs. This study was limited to the said pipe dimensions and a single inlet conditions.

Industrial metrics point to the Coaxial system being twice as efficient, or only needing half of the pipe compared to the U-Bend to achieve similar thermal performance. Anecdotally, it can be stated that the Coaxial system will improve the efficiency in gathering thermal resources from the earth but from the literature the notion that laminar flow exists indicates that the system is not quite optimized for heat transfer applications.

ASHRAE has a geothermal division with many publications on the implementation and design of geothermal systems, both large and small scale. Nonetheless, this free energy technology is underutilized in many parts of the world. To move forward, there is a need to systematically compare the U-Bend and the Coaxial under both laminar and turbulent flows. Efficient, affordable, and robust numerical techniques can enable this to be realised. As such, this study is a step toward elucidating the underlying differences in Coaxial and single U-Bend systems under different

operating conditions, i.e., inlet velocity or Reynolds Number. Numerical simulation using a commercially available software, FLUENT, is employed and normalization techniques are used to analyse the flow conditions through the U-Bend and Coaxial pipes and the corresponding heat transfer rates from the adjacent earth.

2.0 MATHEMATICAL FORMULATION

Mathematical models employ either analytical or numerical solution that can be invoked to analyze the physical problem under consideration. While analytical solutions are easier to apply, they are usually restricted to the simplest of cases [8]. Hence, numerical turbulence modelling is chosen because it has the ability to look at more details. In general there are Reynolds Averaged Navier-Stokes models (RANS), Large Eddy Simulation (LES) models, and Detached Eddy Simulation models (DES) for simulating turbulent flow. The choice is typically a balance between computation time and accuracy. Though LES will more accurately model the large scale eddies, it tends to underperform at the boundary layers of which are very influential in this type of flow with heat convection. The RANS approach is chosen as it outperforms at the boundary layer [9]. The RANS model selected is the realizable k-ε model [10].

3.0 MODEL SETUP AND COMPUTER FRAMEWORK

The single U-Bend and the Coaxial configurations are chosen to fit in an equivalent 5 m deep (for numerical feasibility) borehole with a diameter of 150 mm. Also, the inlet diameter of both test specimens will be equal. Two Reynolds Numbers are chosen to study the performance difference of these two systems for a low Reynolds

143

Number and a high Reynolds Number condition. Table 6.1 shows the testing matrix along with key parameters.

Table 6.1: Parameter Combination Matrix

Case	Type	Re	Length (m)	T_{inlet} (K)
1	U-Bend	500	5	270 (Heating)
2	Coaxial	500	5	270 (Heating)
3	U-Bend	5,000	5	270 (Heating)
4	Coaxial	5,000	5	270 (Heating)

The geometry of the simulated pipes is illustrated in Figures 6.1 and 6.2. The U-Bend configuration consists of a pipe diameter of 50 mm with an outer pipe spacing of 50 mm between the two arms of the loop. The length of the pipe is 5 m and the radius of curvature of the bend is 50 mm. With the pipe diameter being 50 mm and the spacing being 50 mm then the overall dimension at the surface will equate to 150 mm, fitting within the virtual borehole. The Coaxial dimensions are an inner pipe diameter of 50 mm, consistent with the U-Bend, and an outer pipe diameter of 150 mm. The length of the pipe is 5 m.

For both simulated tests the wall temperatures are configured to be a constant 280 K and the inlet fluid temperature is 270 K during the heating mode of operation. The inlet velocity is set based on the Reynolds Number of the specific test and water is used as the working fluid. The inlet flow is uniform with no perturbations and no applied pressure, resulting in negative pressure at the outlet being numerically equivalent to the pressure loss of the system. The turbulence condition of the velocity inlet is set with a turbulence intensity of 0% and a hydraulic diameter of 0.508 m. The outlet is set as an outflow with a flow rating of one, i.e., all the fluid is exiting across this boundary. The thermal and

144

flow properties of the materials used in the model are given in Table 6.2.   To save computational resources only half of the pipe is modeled and the symmetry boundary condition is taken advantage of.   Uniform velocity flow enters the pipe through the inlet and is exposed to non-slip wall entities held at a constant temperature. The flow is directed through the system and exits the pipe through the outlet.

Table 6.2: Material Thermal Properties

Material	ρ (kg m^{-3})	C_p (J kg^{-1} K^{-1})	k (W m^{-1} K^{-1})	μ (Pa s)
Water	998.2	4182	0.6	1.00×10^{-3}
Pipe	950	2300	0.44	N/A

Spatial discretization of the parameters in the flow is very important and with FLUENT, there are many options to select. The most appropriate options for this flow scenario, based on literature review, are as follows. The Semi-Implicit Method for Pressure-Linked Equations (SIMPLE), algorithm is selected for the pressure-velocity coupling [11]. Pressure Staggering Option (PRESTO!), is selected as the pressure interpolation scheme. The energy and momentum is discretized based on second order upwind algorithms and all flow parameters are relaxed with a 0.75 relaxation factor [4]. FLUENT is chosen for this study [12] because of the aforementioned flexibility.

To ensure model accuracy, verification, which ensures that the equations are being solved in the intended way (mesh/grid independency), and validation, which ensures that the phenomenon is being simulated close to reality, were performed. Sudo et al.'s [13] experimental air flow in a U-Bend arrangement was used to validate the current

145

model, prior to running the studied cases on SHARCNET (a high performance computing facility set up by a consortium of Canadian academic institutions).

4.0 RESULTS AND DISCUSSION

4.1 FLOW AND TURBULENCE CHARACTERISTICS

The turbulence kinetic energy, wall heat flux and pressure loss for the U-Bend and the Coaxial will be looked at and compared for both Reynolds Number flows simulated. The turbulence kinetic energy contours is a valid comparison as it highlights the regions of high turbulence in the flow resulting in the ability to identify which regions will provide the most thermal energy transfer. The pressure loss is a metric utilized throughout literature as a means to evaluate the operational efficiency of the system, that is, for a higher pressure loss there is more pumping power required for the system to operate.

The flow pattern in these two types of systems can be reasonably predicted. The U-Bend is a standard pipe flow situation. There exists a straight portion, a 180^0 bend and a subsequent straight portion. The velocity profile in the straight portions will be relatively parabolic before the 180^0 bend disturbance and after some distance from the 180° bend. In the U-Bend the flow profile will push itself outwards, that is the maximum velocity will manifest itself closer to the outer wall, as it is influenced by the centrifugal forces of the bend. The flow close to the inner wall will be moving slower than the outer wall creating longitudinal vortex structures. This phenomenon is described in the literature as Dean flow in curved pipes [14]. The flow pattern in the Coaxial is more

146

symmetric. The flow incoming from the inner pipe into the end cap region is of higher velocity. As the flow makes contact with the end cap wall it disperses into the outer pipe annulus. This flow is relatively fast and as it travels it creates a low pressure region at the inner pipe wall of the annulus close to the end cap region. The flow redirects into this area and a large rotating structure is formed helping in transferring kinetic and thermal energy through the flow. The flow then proceeds to eventually redirect itself past the disturbances and become more uniform at a distance proportional to the Reynolds Number.

Figure 6.3 shows the turbulence kinetic energy contours. The turbulence kinetic energy which signifies the fluctuations in velocity that grant flow more diffusiveness [15] increases with Re. The Coaxial pipe for the case when Re = 500 shows two areas in the end cap region where the turbulent levels are the highest; but relatively insignificant when contrasted with the turbulence levels encountered at Re = 5,000, and hence, not visible in Figure 6.3. When the Re is increased to 5,000 the patterns of the kinetic energy are much more visible. The turbulent kinetic energy in this case is at maximum just at the outset of the inner pipe and it lasts for about one diameter or two downstream of the end cap. For the U-Bend, the relative levels of the turbulent kinetic energy are negligible before and after the U-Bend when the flow Reynolds Number is 500. When Re = 5,000 the levels are much greater than that associated with the Coaxial system. The regions with the highest kinetic energy occur at the outer wall at approximately the 135º position of the bend and at about one diameter downstream of the U-Bend near the inside wall. Also, the high turbulent kinetic energy levels extend to a few diameters downstream of the U-Bend.
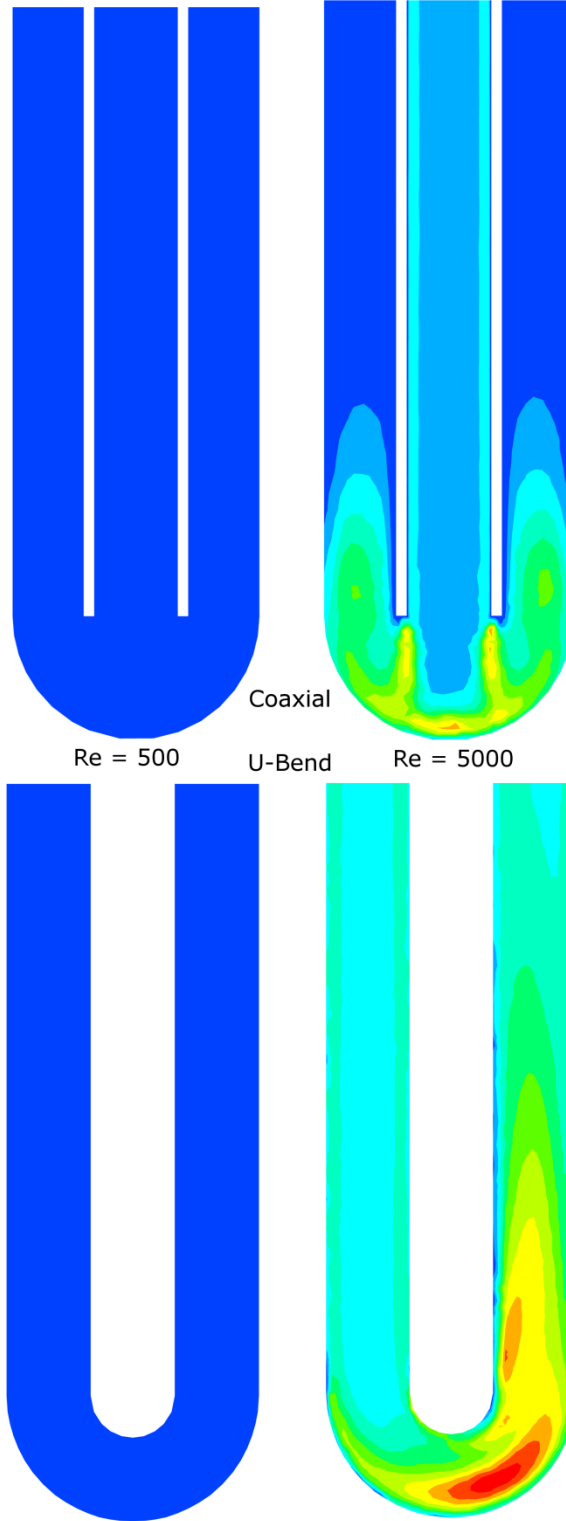
Figure 6.3: Turbulence Kinetic Energy Contours of Simulated Results

The pressure loss lends an insight into the operational pumping costs. Figure 6.4 clearly shows that the pressure loss is lower for the Coaxial system at both low and high Reynolds Numbers. Furthermore, the pressure loss increases more with the Reynolds Number for the U-Bend, presumably due to higher velocity (and thus, friction) over the entire pipe length. In short, the Coaxial loops will be cheaper to operate.
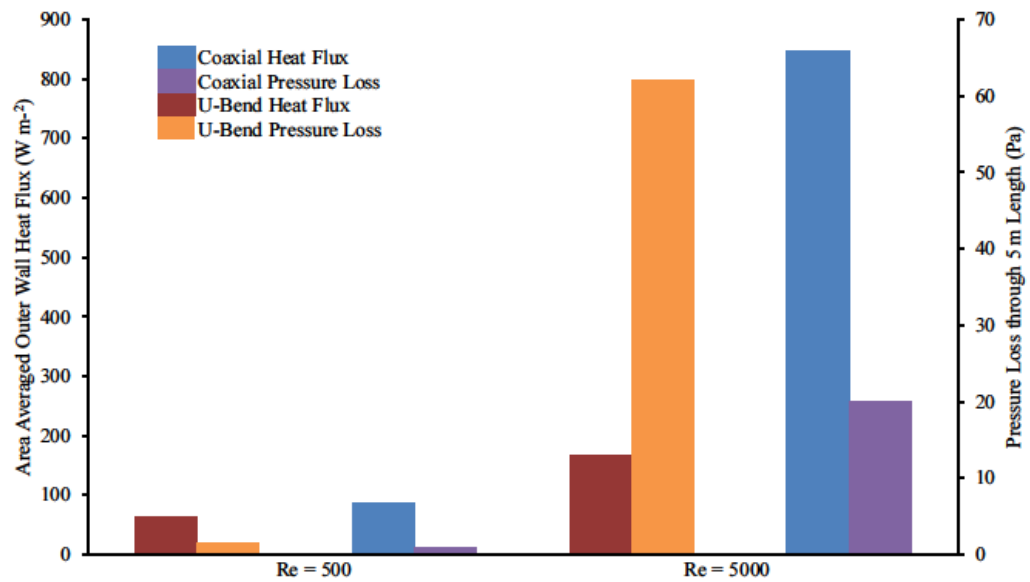
Figure 6.4: Wall Averaged Heat Flux and Pressure Loss of Simulated Results

4.2 THERMAL ANALYSIS

The average heat flux at the outer walls gives an indication of the overall systems efficiency. A temperature difference of 10° K is used to more clearly illustrate the heat transfer differences. In general, the Coaxial system's wall that will be exposed to the grout or soil is much larger for an equivalent system, i.e., identical virtual boreholes of equal length and diameter. Moreover, Figure 6.4 shows that the average heat flux values for the Coaxial system are higher than the U-Bend, especially for Re = 5,000. Table 6.3 shows the total energy transferred in each simulation in Joules. It can be seen that the energy transferred generally drops with the Reynolds Number as is indicative of shortening residence time effect, that is, the time the fluid is exposed to the heat source plays a large effect in the amount of heat actually transferred. This is particularly true for the U-Bend system where approximately two orders of magnitude decrease in the total amount of heat transferred is observed when increasing Re from 500 to 5,000. The significantly less contacting surface area, compared to the Coaxial counterpart, is the main reason behind this serious decrease. With the much larger outer contact area for the Coaxial system the total heat energy transferred is not as affected by the residence time compared to the U-Bend, over the range of conditions considered.

Table 6.3: Energy Transferred in Joules of Simulations

Type\Re	Re = 500 (J)	Re = 5,000 (J)
U-Bend	1.00×10^5	2.63×10^3
Coaxial	8.14×10^5	7.98×10^5

150

5.0 CONCLUDING REMARKS

This preliminary study indicates some promising features of the emerging Coaxial system. It can provide significantly better heat exchange while simultaneously lowering the pumping requirement. For the limited range of studied conditions, the following concluding remarks can be made.

The turbulence in the U-Bend system is higher and is more significantly enhanced by the U-Bend and the enhanced turbulence lasts longer as compared to the corresponding turbulence level in the Coaxial system. Nevertheless, this higher turbulence level over a larger region alone does not result in higher heat transfer. A proper balance between flow turbulence and residence time is needed for maximum heat transfer. The outer pipe cross sectional area of the tested Coaxial system is much larger than the inner pipe region (and the corresponding U-Bend) leading to much lower Reynolds Numbers and turbulence levels. This increase in cross-sectional area slows down the flowing fluid, resulting in more time for effective heat transfer. The heat flux averaged over the entire wall for the Coaxial is much larger and it increases more with the Reynolds Number than the U-Bend. The larger cross-sectional area of the outer pipe in the Coaxial system also resulted in significantly less pressure loss and hence, lowered operating costs. The Coaxial system is also less prone to residence time effects than the U-Bend system, presumably due to the much larger outer returning flow passage. Thus, it appears that once the flow enters into the turbulence regime any further increase in Reynolds Number is undesirable; that is, its enhancement in heat transfer can be overcome by the corresponding negative effect caused by decrease in residence time. The

151

ideal system should be one that operates just in the turbulent flow regime, allowing maximum residence time for effective turbulence heat convection. As importantly, having a larger area of contact is critical. For a real system where the length is much longer than that considered in this study, the sensitivity to some decrease in residence time with moderate increase in Reynolds Number is expected to be less.

The Coaxial system utilizes more borehole real estate when using an overall system dimension constraint. This can result in less grout usage and promise a reduced thermal (conduction) resistance along with much larger area of contact. It could also lead to easier installation as the system can be encased within itself as opposed to the U-Bend that will require more grout and structural support at installation.

ACKNOWLEDGEMENTS

153

REFERENCES

[1]   A. Cooperman, J. Dieckmann, J. Brodrick, Residential GSHPs, ASHRAE Journal. 54 (2012) 72–79.

[2]   J. Yang, Geothermal energy, technology and geology, Nova Science Publishers, New York, 2012.

[3]   B. Sanner, Current status of ground source heat pumps and underground thermal energy storage in Europe, Geothermics. 32 (2003) 579–588. doi:10.1016/S0375-6505(03)00060-9.

[4]   O. Ozgener, L. Ozgener, J.W. Tester, A practical approach to predict soil temperature variations for geothermal (ground) heat exchangers applications, International Journal of Heat and Mass Transfer. 62 (2013) 473–480. doi:10.1016/j.ijheatmasstransfer.2013.03.031.

[5]   H. Zeng, N. Diao, Z. Fang, Heat transfer analysis of boreholes in vertical ground heat exchangers, International Journal of Heat and Mass Transfer. 46 (2003) 4467–4481. doi:10.1016/S0017-9310(03)00270-9.

[6]   V. Khalajzadeh, Parameters optimization of a vertical ground heat exchanger based on response surface methodology, Energy & Buildings. 43 (2011) 1288–1294.

[7]   C.J. Wood, H. Liu, S.B. Riffat, Comparative performance of "U-tube" and "Coaxial" loop designs for use with a ground source heat pump, Applied Thermal Engineering. 37 (2012) 190–195. doi:10.1016/j.applthermaleng.2011.11.015.

[8]   M. Philippe, M. Bernier, D. Marchio, Validity ranges of three analytical solutions to heat transfer in the vicinity of single boreholes, Geothermics. 38 (2009) 407–413. doi:10.1016/j.geothermics.2009.07.002.

[9]   B. Andersson, R. Andersson, L. Håkansson, Computational Fluid Dynamics for Engineers, Cambridge University Press, 2012.

[10]   J. Pruvost, J. Legrand, P. Legentilhomme, Numerical investigation of bend and torus flows, part I : effect of swirl motion on flow structure in u-bend, Chemical Engineering Science. 59 (2004) 3345–3357. doi:10.1016/j.ces.2004.03.040.

[11]   T.H. Shih, W.W. Liou, A. Shabbir, Z. Yang, J. Zhu, A new k-ε eddy viscosity for high reynolds number turbulent flows - model development and validation, National Aeronautics and Space Adminitration, TM-106721, 1994.

[12]   ANSYS Inc., Fluent Theory Guide, ANSYS, Inc., 2009.

[13]   K. Sudo, Experimental investigation on turbulent flow through a circular-sectioned 180° bend, Experiments in Fluids. 28 (2000) 0051–0057.

[14]   W. Dean, Note on the motion of fluid in a curved pipe, Philosophical Magazine Series 7. 4 (1927) 208–223. doi:10.1080/14786440708564324.

[15]   R. Benzi, G. Paladin, G. Parisi, A. Vulpiani, On the multifractal nature of fully developed turbulence and chaotic systems, Journal of Physics A: Mathematical and General. 17 (1984) 3521.

CHAPTER 7

CONCLUSION

1.0 GENERAL

Ground source heat pumps, in particular the U-Bend or Coaxial type, can be improved to benefit the entire system. For example, if the length of the system can be reduced to 90% of the original length then that means 10% less drilling must occur. With the exponential cost function of drilling boreholes any depth cut will result in large amounts of capital saved. The first step to this minimization is to understand the driving parameters of the heat transfer, as that is the goal, enhancing the heat transfer to reduce the length. The following sections will detail the conclusions of the U-Bend study and the Coaxial study independently, illustrating the key design parameters and the factors that destroy or enhance the heat transfer. Following this, the conclusions from the comparative analysis, based on equivalent systems (installation size) will be summarized.

2.0 U-BEND

Chapters 2 and 3 cover the work completed on the U-Bend system. The focus of the paper included in Chapter 2 was to develop a transient, CFD, model for the U-Bend pipe without inclusion of the ground formation. The focus of the model for the U-Bend pipe flow is to gain insight on how turbulence levels can play a massive role in the heat transfer rate of the pipe. Chapter 2 concluded that the Dean Number, the measure of the severity of the bend curvature can play a massive role in the heat transfer process as it creates vortex structures that increase mixing and energy transfer. It was also concluded

157

that the Reynolds Number can decrease the resident time of the flow in the pipe, as in this study the pipe was a fixed length, so increasing the velocity of the flow will decrease the time at which it is exposed to the heat source.

The focus of the submitted manuscript in Chapter 3 is to answer the questions raised by the shortcomings of the conference paper. The study included flow in all turbulence regimes and parametrically studied the Dean Number and the Reynolds Number, rather than only fixing Reynolds Number in Chapter 2. This study found that the level of the Reynolds Number greatly affects the rate of heat transfer as evident by the jump in heat flux as the Reynolds Number changes from 2,000 to 5,000. However, the influence indicated by the Dean Number in the previous study is only seen to appear when the flow is turbulent. When the flow is laminar the Dean Number has a negligent effect, and actually has a negative effect in some cases. This study showed that the Reynolds Number, realized by the changing inlet velocity is the driving parameter of the system performance. The Dean Number only enhances the flow if the flow is already turbulent. This study also shows how the effect of the Dean Number diminishes when the length of the system increases. As the Dean Number enhances the flow at the curved pipe or shortly thereafter when that length becomes fractions of the total system length the flow will be primarily influenced by the Reynolds Number.

3.0 COAXIAL

Chapters 4 and 5 cover the work completed on the Coaxial system. The focus of the manuscript included in Chapter 4 was to develop a CFD model, in FLUENT, that would simulate the inherent physics of a Coaxial system accurately. This chapter focused

on the vortex structures at the end cap of the Coaxial system. The vortex structures in the end cap are very important for heat transfer applications. The offset of the inner pipe has a very influential effect on these rotating structures. It was found that simply by introducing the initial offset of the inner pipe the large symmetric rotating structure completely loses shape, leading to a rather complex pattern of mixing and energy momentum. The structure splits into two independent structures at approximately 41% offset. The structure on the side of the end cap region that shrinks with increasing eccentricity is never completely destroyed although at high eccentricities the flow completely intersects with the structure. The turbulence kinetic energy at the edge of the end cap (0D away from end cap) exists at a maximum 6.6 x 10-6 J kg-1 when the factor of eccentricity is 0.41 (17.7 mm). The turbulence kinetic energy dissipates the least (~0%) through 1D (150 mm) downstream of the end cap when the eccentricity is 0.82 (35.4 mm) and the most (70%) when the eccentricity factor is 0.41 (17.7 mm).

The focus of Chapter 5 was the effect of the inner pipe offset. As the inner pipe of a Coaxial system is typically unsupported and free to move it displaces itself from the centre. This causes local changes in the volume of flow and changes in the inner pipe distance of the outer wall and the inner pipe wall. This local volumetric change can significantly change the effective heat transfer of the Coaxial system. The heat flux will increase regardless of eccentricity with increasing Reynolds Number based on incoming flow. The heat flux will decrease along the wall portion where the inner pipe is moving away from it with increasing eccentricity. About 50% reduction in the heat flux is observed when the offset ($F_{ecc} > 0$) is introduced and a further 10% reduction in overall heat flux afterwards (from $F_{ecc} = 0.21$ to $F_{ecc} = 0.82$) is observed. The overall heat flux

159

will increase slightly along the wall portion where the inner pipe is moving closer to it with increasing eccentricity. The higher heat flux that exists at the end cap will last longer downstream of the end cap as F_{ecc} increases (less negative slope with increasing F_{ecc}). The areas of maximum turbulent eddy flow characteristics, the turbulent kinetic energy and eddy viscosity, occur further downstream and have higher magnitudes as the Reynolds Number is increased.

4.0 COMPARISON OF U-BEND AND COAXIAL

This preliminary study indicates some promising features of the emerging Coaxial system. It can provide better heat exchange while lowering the pumping requirement. For the limited range of studied conditions, the following remarks can be made.

- The Coaxial system utilizes more borehole real estate when using an overall system dimension constraint.

- The Coaxial system will be easier to install as the system is generally encased within itself as opposed to the U-Bend that will require more grout and structural support at installation.

- The turbulence metrics of the U-Bend last long, after the main disturbance, i.e. the 180° bend or the end cap respectively.

- The pressure loss in the Coaxial system is less than that of the U-Bend system. Leading to lower operational costs.

- The Coaxial system has a much larger contact area between the pipe and the borehole than the U-Bend.

160

- The outer pipe region of the Coaxial system is much larger than the inner pipe region leading to much lower Reynolds Numbers and turbulence levels. This leads to more time for effective heat transfer.

- The heat flux averaged over the entire wall for the Coaxial is much larger and increases more with the Reynolds Number than the U-Bend.

- The Coaxial pipe is less prone to resident time effects than the U-Bend pipe.

5.0 RECCOMENDATIONS

To continue the study of this topic and enhance the understanding of specifically the Coaxial ground loop, the following steps in research should be followed:

- Analysis on 2D Coaxial systems should be explored to cut down computational time since it is an axisymmetric system (for 50 - 120 m systems).

- The addition of grout and a soil body should be explored to more realistically model the heat transfer so that comparisons with the field measurements could be made rather than comparisons among systems.

- Field data should be explored to add area specific temperatures and thermal properties in the grout and soils.

- The inner pipe offset problem of the Coaxial should be incorporated into a 3D system to include two dimensional eccentricities to further understand its complex effects on the potential heat flux.

- For existing pipes, modification to the pump to induce a pulse-like inlet flow condition could be used to create turbulent situations in the entire pipe.

APPENDIX A

PERMISSION STATEMENT FOR CHAPTER 2

The following is a copy of the E-Mail granting permission for the publication used in

Chapter 2:

Beth Darchi <DarchiB@asme.org>
Wed, Mar 5, 2014 at 4:48 PM
To: Chris Cvetkovski <cvetkovc@uwindsor.ca>
Dear Mr. Cvetkovski:

It is our pleasure to grant you permission to use ASME paper "On Fluid Flow and Heat Transfer in a Pipe With a U-Bend," by Christopher G. Cvetkovski; Hoda S. Mozaffari; Stanley Reitsma; Tirupati Bolisetti; David S.-K. Ting, Proc. ASME. 55478; Volume 1: Heat Transfer in Energy Systems; Thermophysical Properties; Theory and Fundamental Research in Heat Transfer, Paper number HT2013-17209, as cited in your letter for inclusion in a Master Thesis entitled Enhancing Ground Source Heat Pump Performance to be published by University of Windsor.

Permission is granted for the specific use as stated herein and does not permit further use of the materials without proper authorization. Proper attribution must be made to the author(s) of the materials. PLEASE NOTE: if any or all of the figures and/or Tables are of another source, permission should be granted from that outside source or include the reference of the original source. ASME does not grant permission for outside source material that may be referenced in the ASME works.

As is customary, we request that you ensure full acknowledgment of this material, the author(s), source and ASME as original publisher. Acknowledgment must be retained on all pages printed and distributed.

Many thanks for your interest in ASME publications.

Sincerely,

Beth Darchi
Publishing Administrator, ASME
2 Park Avenue, 6th Floor
New York, NY 10016-5990
Tel 1.212.591.7700
darchib@asme.org

www.manaraa.com

APPENDIX B

VALIDATION AND VERIFICATION SECTIONS FOR CHAPTER 6

The manuscript included in Chapter 6, submitted to the ASHRAE Trade Journal, is missing some key validation and verification sections that prove the viability of the simulated results but are required to be removed as the scope of the trade journal is limited.

VERIFICATION AND VALIDATION

There are two steps, verification and validation, to ensuring model accuracy in the CFD realm. While both have the same goal, they are very unique processes. Verification is essentially ensures that the equations that are proposed are in fact being solved in the intended way. When using established software, there is an abundance of literature support for the verification of FLUENT's solver [1]. To validate the model is to compare the results with that of established experimental or numerical findings, preferably experimental. In the validation stage this study will also perform a mesh analysis study to determine that the numerical grid does not interfere with the results that are outputted from the simulations.

The mesh study consisted of four progressively denser meshes. The meshes were constructed identically using tetrahedron elements with a maximum volume constraint that was varied to obtain denser meshes. Figure 1 shows the result of this study. Mesh 1

163

uses a maximum volume constraint of 1×10^{-8}, Mesh 2 uses a maximum volume constraint of 1×10^{-10}, Mesh 3 uses a maximum volume constraint of 1×10^{-15} and Mesh 1 uses a maximum volume constraint of 1×10^{-20}. The optimum mesh is the mesh that shows a relative error of less than 1% from that of a denser mesh. The third mesh, with a maximum volume of 1×10^{-15}, was selected. The relative error of this was 0.8%.
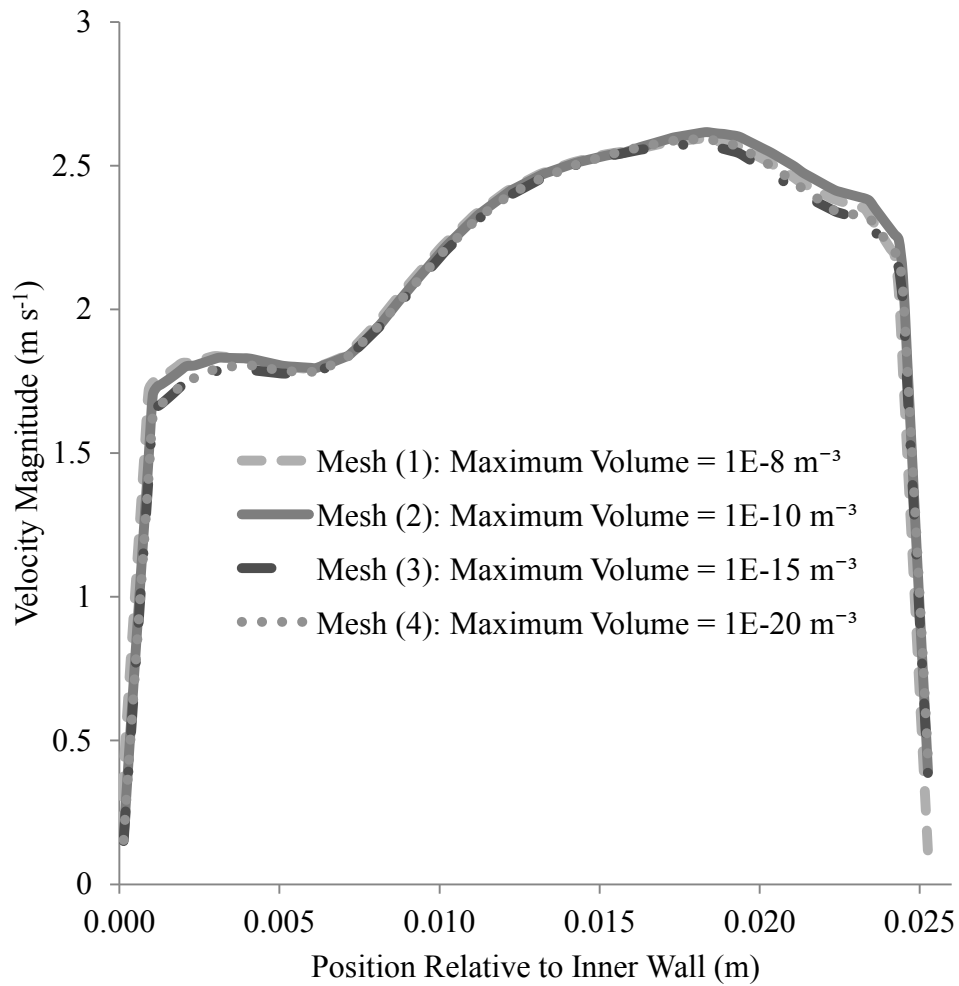

Figure 1: Variation of Velocity Magnitude across Centerline at $\varphi = 90^{\circ}$ of U-Bend with

Varying Mesh Densities

164

The second stage of the validation is the comparison with existing studies. An experimental work done by Sudo et al. [2] is used in the present study. In the experiment a U-Bend arrangement was constructed with air being blown into one end. The diameter of the pipe was 104 mm. The air would travel through a straight pipe of 100 diameters before traversing through the U-Bend with a radius of curvature of 2 diameters and then exit through a straight pipe of 40 diameter length. To compare all non-dimensionless parameters were created equal and an identical geometrical configuration was constructed. The Reynolds Number of the flow was 6.0×10^4 which created a mean velocity of 8.7 m/s. The results of the comparison are shown in Figure 2 where the line-work (the results of Sudo et al.) is overlaid onto the contour map (the results of the present study's model. Good agreement was determined to exist and along with the proven models for this type of flow and FLUENT's consistency in mathematical calculations it was decided to run the cases on SHARCNET.
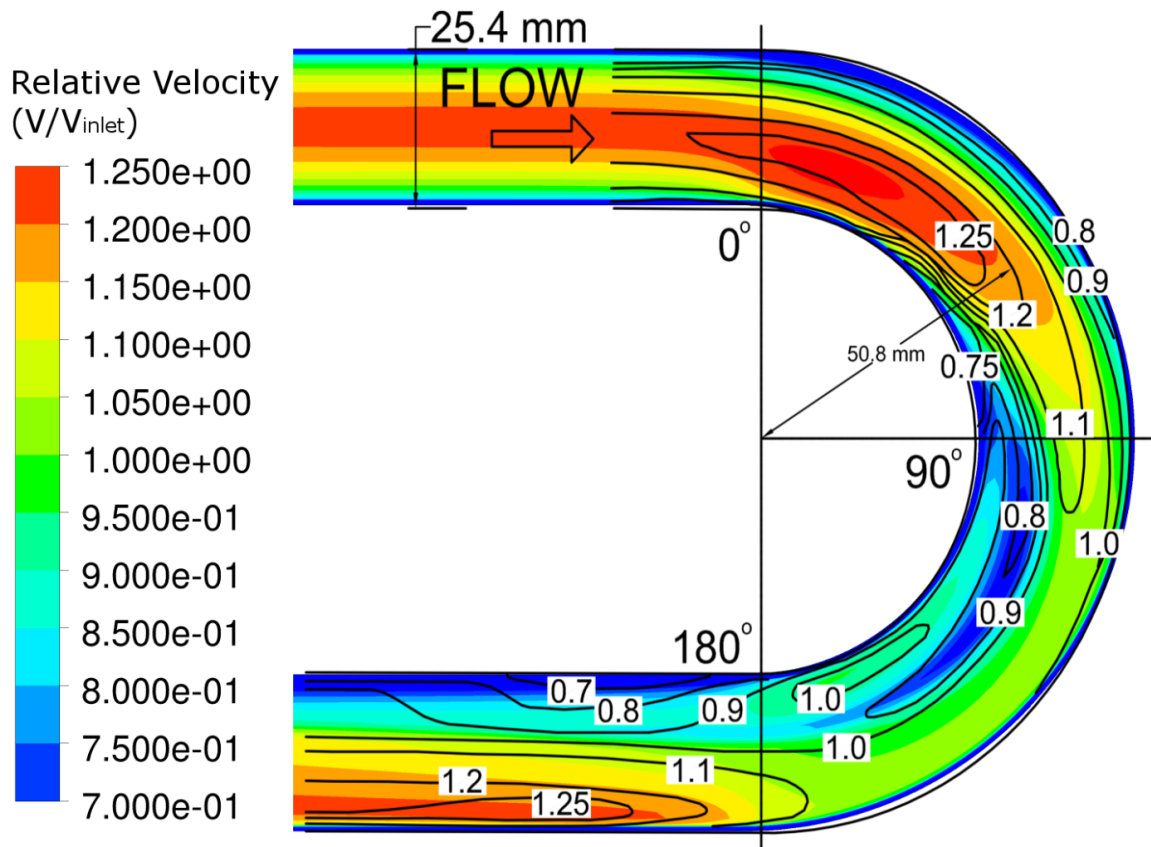
Figure 2: Experimental (Linework)/Numerical (Colour Map) Velocity Contours, Sudo et

al. [18], Re = 60,000, Dn = 30,000, ΔT = 0

[1]   ANSYS Inc., Fluent Theory Guide, ANSYS, Inc., 2009.

[2]   K. Sudo, Experimental investigation on turbulent flow through a circular-

sectioned 180° bend, Experiments in Fluids. 28 (2000) 0051–0057.

VITA AUCTORIS

NAME: Christopher G. Cvetkovski

PLACE OF BIRTH: Garden City, Michigan, U.S.A

YEAR OF BIRTH: 1990

EDUCATION: Holy Names High School, Windsor, Canada
                            2004 - 2008
                            University of Windsor, Windsor, Canada
                            2008 - 2012, B.A.Sc